POWER FACTOR IMPROVEMENT BY THYRISTOR CONTROL IN TRACTION AND INDUSTRIAL POWER SUPPLY SYSTEMS

A Thesis Submitted
in Partial Fulfilment of the Requirements
for the Degree of
MASTER OF TECHNOLOGY

By
BINOY K. PATEL

to the
DEPARTMENT OF ELECTRICAL ENGINEERING
INDIAN INSTITUTE OF TECHNOLOGY, KANPUR

DECEMBER 1979

T O

M Y P A R E N T S

EE-1979-M-PAT-POW

CERTIFICATE

It is certified that this work entitled "Power Factor Improvement by Thyristor Control in Traction and Industrial Power Supply Systems" by Binoy Krishna Patel has been carried out under my supervision and that this work has not been submitted elsewhere for a degree.

(Dr. S.R. Doradla)
Assistant Professor,
Department of Electrical Engineering,
Indian Institute of Technology,
Kanpur.

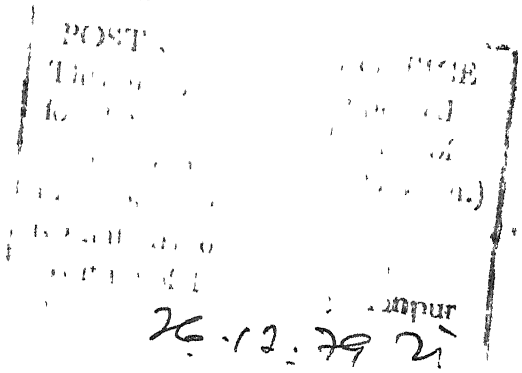

ACKNOWLEDGEMENT

I take this opportunity to express my deep sense of gratitude to Dr. S.R. Doradla who had initiated me into the problem. His sincere advice, valuable suggestion and keen interest throughout the course of this work has been a source of constant encouragement.

I am grateful to my friends especially Nalin, Sachchidanand, Ashok, Anil, Chaubey, Goyal, Binod, Sinha, Bendale, Jayant, Debu and Om for their helps rendered to me throughout the programme.

Mr. B.B. Srivastava who, inspite of his busy schedule, readily prepared the drawings deserve special thanks. Thanks are also due to Mr. V.K. Dadwal and Mr. R. Prasad for carrying out the typing and cyclostyling works of the thesis respectively with great care and interest.

The help rendered by Mr. N.D. Sharma, Mr. S.V. Gorpade, Mr. V.S. Yadav and others in the concerned laboratories of IIT/K are gratefully acknowledged.

(B.K. PATEL)

CONTENTS

LIST OF TABLES

LIST OF FIGURES

NOMENCLATURE

a_n , b_n : Fourier coefficients

c_n : peak value of nth harmonic

C : capacitance

DSP : displacement factor

E : load EMF , volts

f : supply frequency , Hz

i_S : instantaneous value of supply current , amp

i_L : instantaneous value of load current , amp

i_{LN} : instantaneous value of normalised load current , amp

i_C : instantaneous value of capacitor current , amp

i_{TCR} : instantaneous value of TCR current , amp

I : rms value of current , amp

I_{SRMS} : rms value of source current , amp

I_{nRMS} : rms value of nth harmonic component in the source current , amp

I_L : rms value of load current , amp

I_C : rms value of capacitor current , amp

I_{TCR} : rms value of TCR current , amp

I_{TCRF} : rms value of fundamental component in TCR current , amp

L : inductance

m	: normalised value of load EMF
R	: resistance
t	: time , sec.
Z	: impedance
α , ϕ	: triggering angles
β	: extinction angle
γ	: time instant at which instantaneous ac supply voltage equals load EMF
θ	: power factor angle
ψ_n	: phase angle of nth harmonic
ω	: angular frequency of ac supply voltage , rad/sec.

ABSTRACT

This thesis is concerned with the study of improvement of power factor in (1) ac-fed traction systems (2) industrial power supply systems.

A comparative study of the external performance characteristics of the following converter circuit configurations is made assuming continuous and constant load current : Fully controlled converter with optional freewheeling, Fully controlled converter, Forced commutated converter with symmetrical single pulse-width control. The performance characteristics of the fully controlled converter with optional freewheel are also verified experimentally. Furthermore, the different possible modes of operation are recognised with various load circuit parameters under rectification and inversion operations. These modes are identifed on the operating diagrams of the converter. A graphical procedure for estimating the minimum inductance for continuous current operation is presented.

Different methods of reactive power compensation are briefly reviewed. The thyristor phase-controlled reactor for dynamic VAR compensation in industrial power

systems is explained in detail. A single-phase thyristor controlled reactive power compensator is built and experimental results are obtained with the compensator under steady state and transient operating conditions.

CHAPTER I

INTRODUCTION

1.1 INTRODUCTION

Power factor is an important performance quantity in ac power system. It is defined as the ratio of active power input to the apparent power input from the ac supply. Thus, large reactive power requirement causes the system to operate at low power factor. Almost all major loads connected to the power supply system consume large amount of lagging reactive power. Induction motors which constitute nearly about seventy percent of industrial load operate at lagging power factor. Induction and arc furnaces widely used in metallurgical industries (mainly steel plants) draw large amount of reactive power. The domestic consumers also consume considerable amount of lagging current due to extensive use of arc and fluorescent lamps and also pump drives used for irrigation purposes. With the advent of high power semiconductor switches, the static thyristor power converters are fast replacing conventional M - G sets for the control of dc drives. Phase angle control [1 - 3] is commonly used in these ac to dc thyristor power converters to obtain vari-

able dc output. The power factor on the ac side deteriorates considerably with large phase angle delays at light load conditions. The thyristor converters have gained much popularity specially in electric traction system, paper and textile mills, and in rolling mills in steel industries. With an increasing number of such drives operating on an ac supply, there is ever increasing demand for reactive power from the supply system.

All these above requirements add up to a very large lagging reactive power demand from the power supply system thus causing the system to operate at considerably low power factor. Supply power factor is vital for an economical design and efficient, reliable and quality operation of the system. There are many disadvantages [4] if the supply power factor is poor. Some of them are as follows :

(1) It causes large I^2R loss in the system, i.e., in the generators and transmission lines because of the large current. This causes unnecessary heating of the system components.

(2) It causes the source generators to operate at decreased power factor thus increasing the kVA loading on the source generators and circuits to cause an over-

loaded condition and prevents capacity for additional load growth.

(3) By increasing kVA load on the generators, it prevents any possibility of additional kW loading which may be placed on the generators if prime-mover capacity is available.

(4) It causes poor voltage regulation at the load. Particularly in HVAC systems with long transmission lines, the resultant over-voltages due to load rejection affect insulation co-ordination.

(5) It decreases voltage level at the load thus lowering the power transfer capability.

(6) The cross-sectional area of bus bars and the contacts of the switchgears have to be increased since they have to be designed for the maximum current which would correspond to the minimum power factor for the same kW to be transferred in the ac supply system.

(7) Low power factor results in an overall increased investment in system facilities per kW of load supplied.

Hence, the utility authorities as well as the consumers have always given due attention to devise means to improve the power factor for reliable and economic operation of the system.

1.2 OUTLINE OF THESIS

1.2.1 Improvement of power factor in ac traction power supply system

The problem of reactive power has always been given much attention in the field of single-phase ac traction where thyristor converters are used for the control of the dc traction motors. The railway power systems are weaker having low short-circuit capacity than industrial power systems [5]. Furthermore, it is highly uneconomical to compensate reactive power externally because the traction system is fed by sub-stations located at short intervals. It is also not desirable to compensate reactive power by capacitor banks housed in the locomotive from the standpoint of space and weight. Besides, a fixed bank of capacitors may not be able to achieve perfect compensation as the load is fluctuating. It is advantageous to achieve improvement in power factor by modification of the converter circuit rather than by external compensation. Broadly two classes of converters have emerged [1, 2] using line commutation and forced commutation. The converters employing forced commutation are complex while those employing line commutation are relatively simple. Half-controlled converters are generally employed in ac traction since they provide better supply power factor

compared to fully controlled converters [3]. However, the half-controlled bridge circuit provides only unidirectional output voltage. It cannot provide at its output terminals dc voltage of negative polarity which is essential for regeneration. This is a serious limitation, especially in traction applications where regeneration of load energy to the supply line might result in substantial economy. W. Farrer and D.W. Andrew [6] developed a novel control strategy for the full bridge thyristor converter circuit which has given characteristics identical in form to those of a half-controlled thyristor bridge without sacrificing regenerative capability. In chapter II, the input and output characteristics assuming constant load current are obtained for (i) conventional fully controlled converter, (ii) fully controlled converter with facility for freewheeling control [6], and (iii) forced commutated converter with single symmetrical pulse-width modulation control [8] and compared among these three control schemes. Experimental results with large inductance in the load circuit are obtained to corroborate the theoretical results. Details of the control circuit are also given.

The operating diagrams [1, 13] showing different modes of operation with actual load circuit

parameters for a fully controlled converter circuit with freewheel facility are discussed thoroughly in chapter III. Continuous current operation of the converter is desirable [14] . Estimation of minimum inductance to be connected in the load circuit to achieve continuous current operation of the fully controlled converter with optional freewheeling is also carried out in chapter III.

1.2.2 Improvement of power factor in utility systems

The problem of power factor improvement in ac loads is very wellknown since the inception of ac transmission and distribution. This is, in fact, attempted at various stages in the power system network ; domestic consumers, bulk power consumers, industrial power systems and HVAC network. The domestic consumer derives maximum benefit if he operates his equipments at maximum power factor. The bulk consumers are also usually charged tariffs for the kVA installed in addition to the actual kW consumed. This would mean that there is a considerable saving if the power factor of the bulk load is improved. In the case of large industrial power systems, where the loads are normally concentrated in one plant and served from one network terminal, the reactive power demand of large, and fluctuating industrial loads is either reduced or cancelled resulting in improved power factor at the

supply network feeding the industrial load. In the HVAC network, the magnitude of the voltage at a bus is very much dependent on the balance of reactive power at the bus. The objective in this case is, therefore, not to view in terms of power factor improvement since the loads are not localised, but to regulate the voltage at the bus in the event of planned and unplanned disturbances of both loads and generation.

Chapter IV of this thesis clearly enumerates chronologically different methods of power factor improvement in industrial power systems. The relative merits and demerits of the different types of external compensators are also outlined. The different reactive power compensators used for the improvement of power factor are,

(1) Fixed capacitors

(2) Switched capacitors

(3) Synchronous condensers

(4) Static reactor compensators

In case of static reactor compensators, the different methods of realizing a variable inductor are outlined.

In chapter V , description of a practical static reactive compensator using a fixed capacitor and a

thyristor phase-controlled reactor (inductor) used to continuously improve the power factor of single-phase loads is given. The control circuit details are explained and experimental results showing steady-state and transient behaviour of the system are thoroughly discussed. Some modifications required in the control circuit to improve its response are clearly mentioned.

In chapter VI , overall conclusions are drawn and guidelines for further research work are mentioned.

CHAPTER II

CONVERTER CIRCUITS FOR POWER FACTOR IMPROVEMENT IN TRACTION POWER SUPPLY

2.1. INTRODUCTION

Solid-state thyristor control of dc drives is playing an important role in the variable speed drive system and also in traction systems. The replacement of MG sets, ig-arc converters and other conventional controllers used in earlier installations of traction systems by thyristor power ontrollers is a logical process of evolution. Solid-state hyristorised drives have numerous outstanding advantages, uch as, minimal maintainance, less bulk and weight, higher fficiency, faster time response and so on.

The phase-angle-control is commonly used in the olid-state control of dc drives fed from an ac supply. his is a simple control scheme, but the supply power factor eteriorates considerably with larger phase-angle delays. sides, harmonics in the ac supply line and ripple in the tput voltage is generated.Forced commutation is used to prove supply power factor [7,8] . In fact, this techni- e was successfully used in West Germany railway traction stem and many other parts of the world to minimise reactive wer drawn by single-phase ac-fed traction motor drives [5] .

This method is also used to minimise supply harmonics and reduce any particular undesirable harmonic and its multiples [9] . Inspite of the complexity of forced commutation which involves more power semiconductor switches and additional commutating elements, this principle is used and in fact operationally tested in traction systems to improve power factor [5] . The ripple voltage at the dc terminals can be minimised by increasing the number of phases of the ac supply which is the normal practice in the industrial field. However, in traction systems this is not possible since the traction motor drives are supplied from single-phase ac supply system. As a result, the railway power systems are weaker having low short-circuit capacity than industrial supply systems. Therefore, the problem of reactive power has always been given more attention in the field of traction than with stationary controlled drives in industrial field [5] .

The reactive power drawn from ac supply system can be minimised by external compensation. External compensation involves installation of power factor correction devices which take leading reactive current to compensate for the lagging current drawn by the thyristor-controlled dc traction drives. A bank of capacitors connected across the input terminals of a thyristor converter can serve as a power factor correction device to some extent. Because of a large

current and low frequency, large-sized capacitors are required. The external compensation is therefore not desirable from the standpoints of space and weight in traction locomotives. Furthermore, it is not economical to instal power factor correcting apparatus at the substation since a large number of substations feed traction power supplies. However, the power factor correction devices find widespread application in industrial power systems.

In traction systems, improvement in supply power factor can only be achieved by disconnecting the supply line from the load circuit and providing an alternate path for the load current to freewheel for some part of the period of the supply frequency. In forced commutated circuits, this can be arranged at any instant in the cycle. In line-commutated full bridge converter circuit, it is not possible to provide an alternate path for the load current with conventional triggering pulses as used in phase-angle control . With a free-wheeling diode connected across the full-bridge circuit, alternate path for the load current can be provided after the supply voltage reverses. Half-controlled bridge circuits provide inherent free-wheeling path for the load current when the ac supply voltage is disconnected from the load circuit by phase-angle control. There is a significant reduction in reactive power consumption in half-controlled thyristor bridge circuits when compared to that in full-

bridge circuit. However, the half-controlled bridge circuit provides only unidirectional output voltage and hence cannot sustain a negative voltage which is essential for regeneration. This is a serious limitation, especially in traction applications where regeneration of load energy to the supply line might result in substantial improvement in energy consumption. W. Farrer and D.F. Andrew [6] developed a novel control strategy for the full-bridge thyristor converter circuit which has given characteristics identical in form to those of a half-controlled thyristor bridge without sacrificing regenerative capability. The principles of this control technique are discussed in detail in the reference [6] .

In this chapter of the Thesis, the detailed study of input and output characteristics of full-bridge converter circuit with novel control strategy developed by W. Farrer and D.F. Andrew has been carried out. The performance characteristics such as power factor, fundamental power factor, harmonic factor and ripple voltage have been obtained assuming constant load current for (i) conventional fully controlled converter, (ii) fully controlled converter with facility for free-wheeling control as developed by W. Farrer and D.F. Andrew; (iii) forced commutated converter with single symmetrical pulse-width modulation control. The

performances are compared among the three control schemes and the merits and demerits of each of the schemes are outlined. A simple open-loop control circuit has been built to verify waveforms of fully-controlled converter with free-wheeling control. To corroborate the theoretical results, experimental results for thyristor converter with optional free-wheel are obtained with a large inductance in the load circuit.

2.2. PRINCIPLES OF OPERATION

2.2.1. Fully controlled converter circuit configuration

Fig. 2.1 shows single-phase fully controlled converter circuit. In traction systems, the load usually consists of dc motors. Inductors are also inserted in the load circuit to reduce ripple in the armature current. With a fairly large inductance in the load circuit, the load current may be assumed to be continuous and constant. The operation of the converter circuit is well documented in literature [1 , 3]. However for the sake of completeness, a brief explanation of the circuit operation is described. Thyristors T_1 , T_2 and T_3 , T_4 are turned-on at some delay angle, α in the positive and negative half cycles of the supply frequency respectively. When T_1 and T_2 are turned-on together in positive half cycle, current flows from source through T_1 to load and back to source

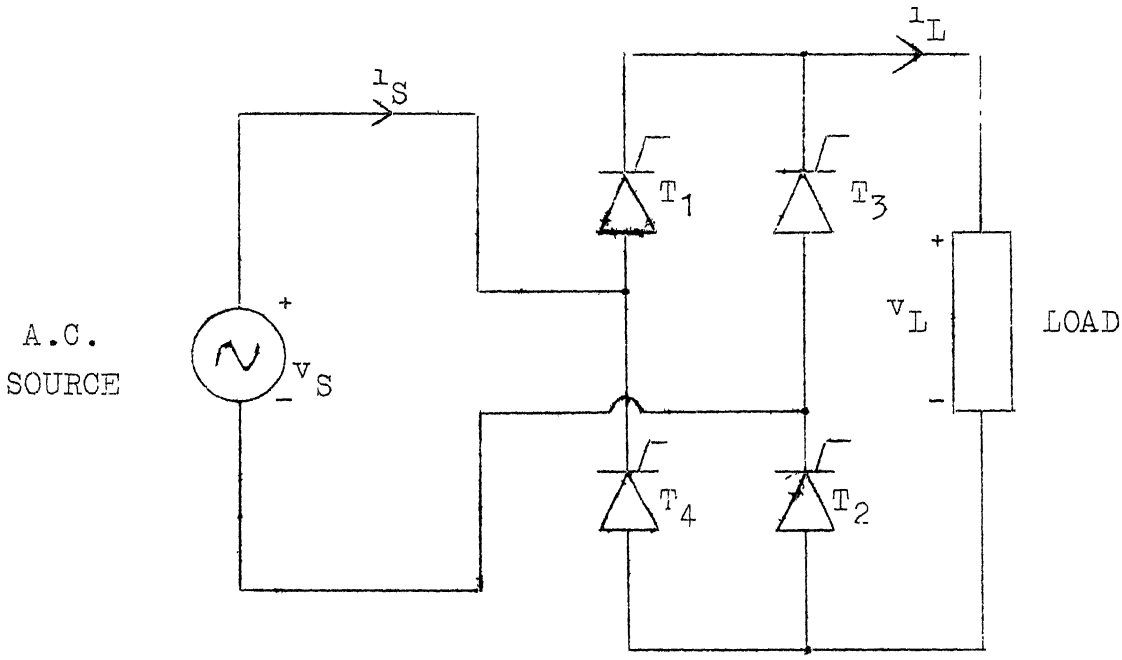

Fig. 2.1 Basic single phase fully controlled converter for DC drives.

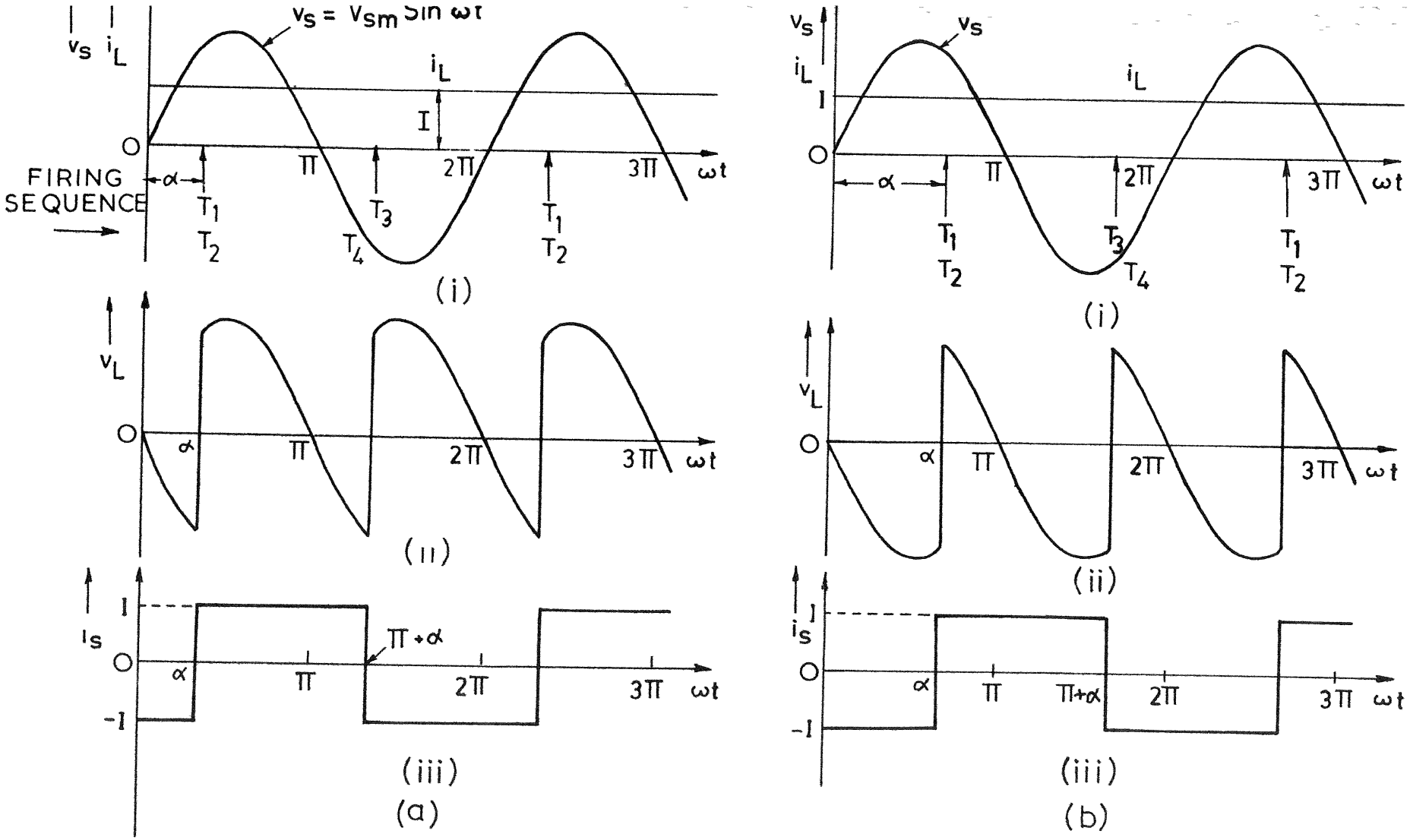

FIG 2·2 VOLTAGE AND CURRENT WAVEFORMS FOR CONVENTIONAL FULL CONTROL
(a) RECTIFICATION MODE (b) INVERSION MODE

(i) SOURCE VOLTAGE AND LOAD CURRENT (ii) LOAD VOLTAGE (iii) SQURCE CURRENT

through T_2 . By turning T_3 and T_4 on after one half period in the negative half cycle, a negative voltage appears across T_1 and T_2 , reverse biases them and turns them off by line commutation. The current now flows from source through T_3 to load and back to source via T_4 and thus gets reversed in the ac supply. Depending upon the value of α , the mean output voltage may be positive or negative. With positive mean output voltage, the converter operates as a rectifier with power flow from ac source to the load. On the other hand, the converter operates as a line commutated inverter with power flow from load to ac source when the mean output voltage is negative. The voltage and current waveforms of Fig. 2.1 are shown in Fig. 2.2 for rectification and inversion modes. The changeover from rectification to inversion takes place at $\alpha = 90°$ theoretically. It is clear from the waveforms that the load is always connected to the source.

2.2.2. Fully controlled converter with optional freewheeling

In the fully controlled converter circuit, source current whether positive or negative always flows unidirectionally in the load. Obviously, this results in low power factor especially at large delay angles. If T_1 and T_3 or T_3 and T_4 are replaced by power semiconductor

diodes or if a power semiconductor diode is connected across the output terminals, the source can be disconnected from the load circuit and an alternate free-wheeling path can be provided for the load current for some part of the period of the supply frequency. The converter circuit would then become the familiar half-controlled circuit [3] . Since no mean negative voltage can be developed across the output terminals of a half-controlled converter circuit , it is not possible to operate the converter circuit in the inversion mode. However, in traction locomotives, there may be significant energy saving if load energy is regenerated to the ac source. With a slight modification in the conventional triggering of the fully controlled converter circuit, it is possible to incorporate free-wheeling and inversion modes. In this triggering scheme, one phase shifter controls the triggering angle or angle of connection, α of the main thyristor pairs T_1 , T_2 and T_3 , T_4 as described in section 2.2.1 in the conventional manner. Also it involves another phase shifter which controls the free-wheeling interval. This additional phase shifter controls the triggering angle or angle of disconnection, ϕ of the series-aiding thyristor pairs T_1 , T_4 and T_2 , T_3 . Thyristors T_1 and T_2 are fired at some delay angle , α in the positive half cycle of the supply voltage and

current flows from source through T_1 to load and back to source via T_2 . T_1 and T_2 continue to conduct upto the instant $\emptyset$ in the next half cycle when T_3 is fired and gate pulse to T_2 is maintained. T_1 gets commutated by line commutation and the current is transferred to T_3 . Thus, the source is disconnected from the load and the load current free-wheels through T_2 and T_3. The free-wheeling of the load current continues upto α in the negative half cycle when T_4 is fired and the gate pulse to T_3 is maintained. As T_4 turns-on, T_2 gets commutated by the negative line voltage appearing across it and the source again gets connected to the load. The current now flows from the source through T_3 , load, T_4 and back to the source. Thus, the source current gets reversed when compared to the earlier half cycle. The current continues to flow upto $\emptyset$ in the next positive half cycle when T_1 is fired and the gate pulse to T_4 is maintained. T_3 gets commutated the moment T_1 turns on. The load current free-wheels through T_1 and T_4 . Again at α in the positive half, T_2 is fired and the gate pulse to T_1 is maintained. The source is now connected to load and the above mentioned events repeat. The firing sequence along with voltage and current waveforms are shown in Fig. 2.3.(a). In order to realize the benefit of maximum power factor in the

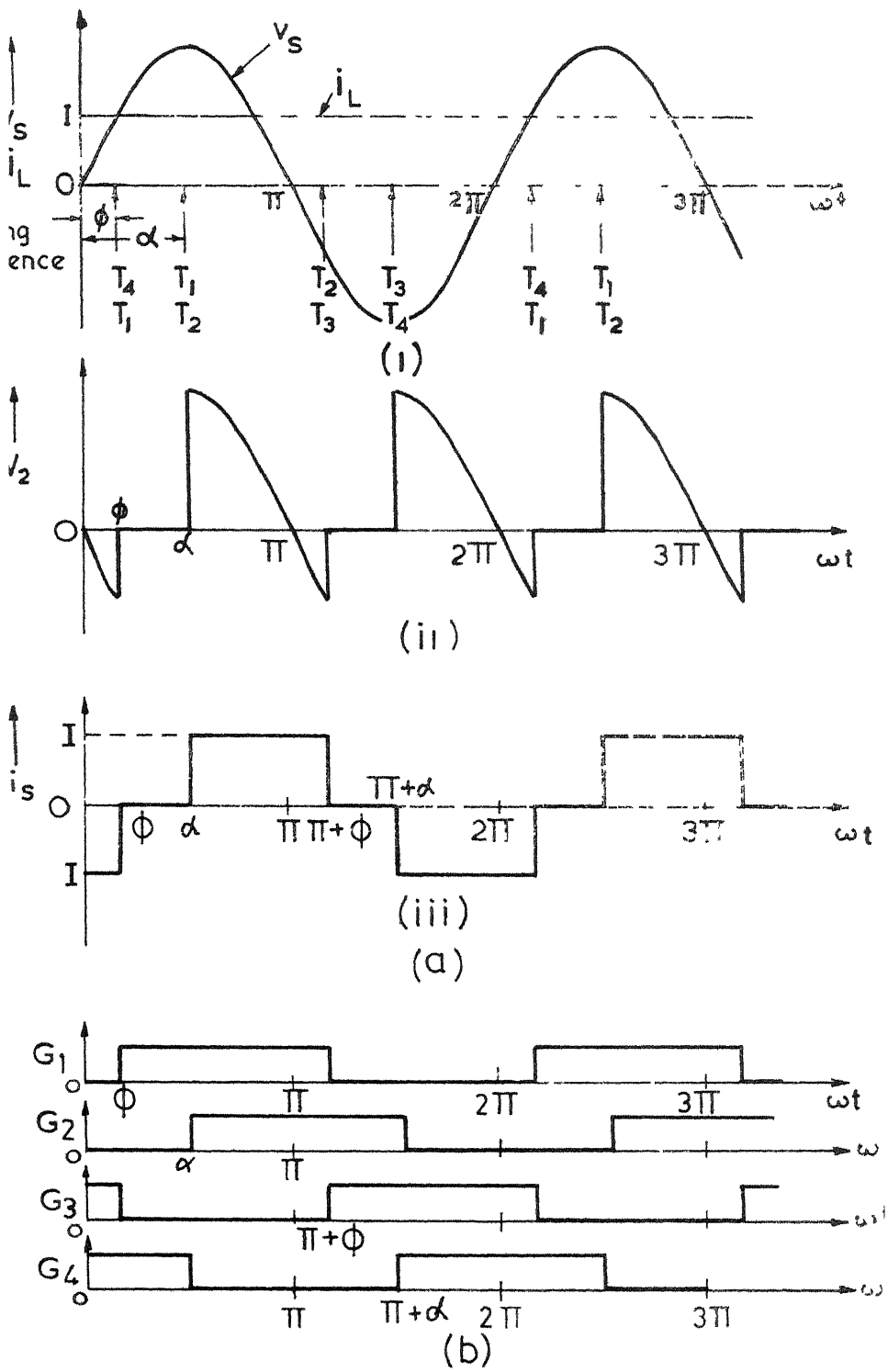

a) CURRENT AND VOLTAGE WAVEFORMS FOR OPTIONAL FREE WHEEL CONTROL WITH VARIABLE α & ϕ

b) FIRING PULSES

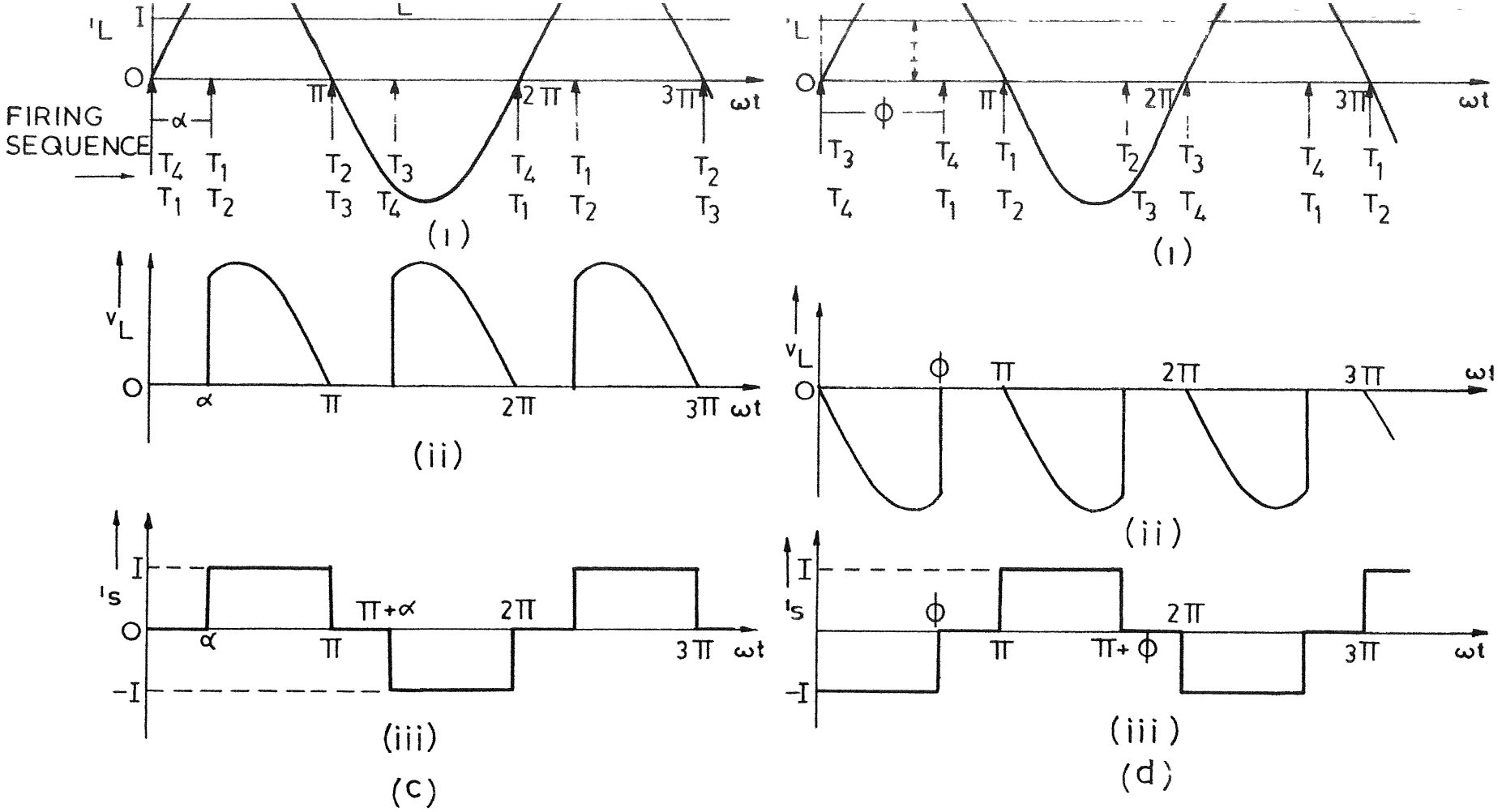

FIG 2.3 WAVEFORMS FOR OPTIONAL FREE WHEEL CONTROL (c) FOR RECTIFICATION MODE WITH $\phi = 0°$ (d) FOR INVERSION MODE WITH $\alpha = \pi$

rectification mode, the triggering angle, $\emptyset$ is held constant at zero and the triggering angle, α is varied from zero to π to vary the mean output voltage from positive maximum to minimum. The firing sequence along with current and voltage waveforms for a particular firing angle, α is shown in Fig. 2.3.(c). Similarly, in the inversion mode negative mean output voltage is varied from minimum to maximum by fixing α at π and varying $\emptyset$ from zero to π for maximum power factor. The voltage and current waveforms alongwith the firing sequence for a particular triggering angle, $\emptyset$ is shown in Fig. 2.3.(d). Although this triggering strategy results in maximum power factor, there are other performances such as output voltage ripple and input harmonic content which may not be minimum. Therefore, the fully controlled converter circuit with optional freewheeling is analysed for different combinations of triggering angles α and $\emptyset$.

2.2.3. Forced commutated converter circuit

Fig. 2.4. shows single-phase forced commutated converter circuit. The dotted box essentially consists of a thyristor with its commutation circuitry. In the positive half cycle, when terminal A is positive with respect to terminal B, thyristors T_1 and T_2 are turned on at α connecting the source to the load. If the source is to be disconnected from the load, T_1 is turned

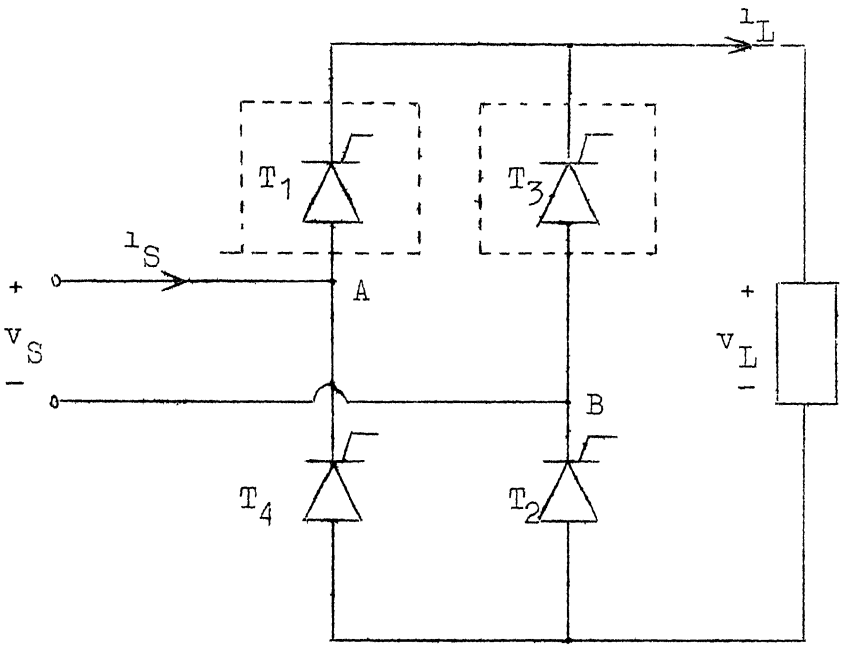

Fig. 2.4 Single phase forced-commutated converter circuit.

off at $(\pi - \alpha)$ by forced commutation and T_2 is gated on simultaneously so as to provide free-wheeling path for the load current. It is therefore not necessary to wait for the reversal of supply voltage for free-wheeling action. In the negative half cycle, T_3 and T_4 are turned on at $(\pi + \alpha)$ for connecting the source to the load. The free-wheeling action is provided by turning T_1 and T_4 on at $(2\pi - \alpha)$. This single symmetrical pulse-width modulation [8] provides maximum power factor in the forced commutation scheme. The waveforms of voltage and current along with firing sequence for the symmetrical single pulse width modulation for both rectification and inversion modes are shown in Fig. 2.5. Maximum to minimum positive mean dc output can be controlled by varying α from zero to $\pi/2$.

2.3. INPUT AND OUTPUT PERFORMANCES OF CONVERTER CIRCUITS CONNECTED TO TRACTION POWER SUPPLIES

Assuming constant load current, the main operating characteristics of interest are (i) fundamental power factor, (ii) total power factor of the input current from the ac source, (iii) input harmonic factor, and (iv) ripple voltage at the dc terminals.

(i) The fundamental power factor is defined as the power factor of the fundamental component in the source current.

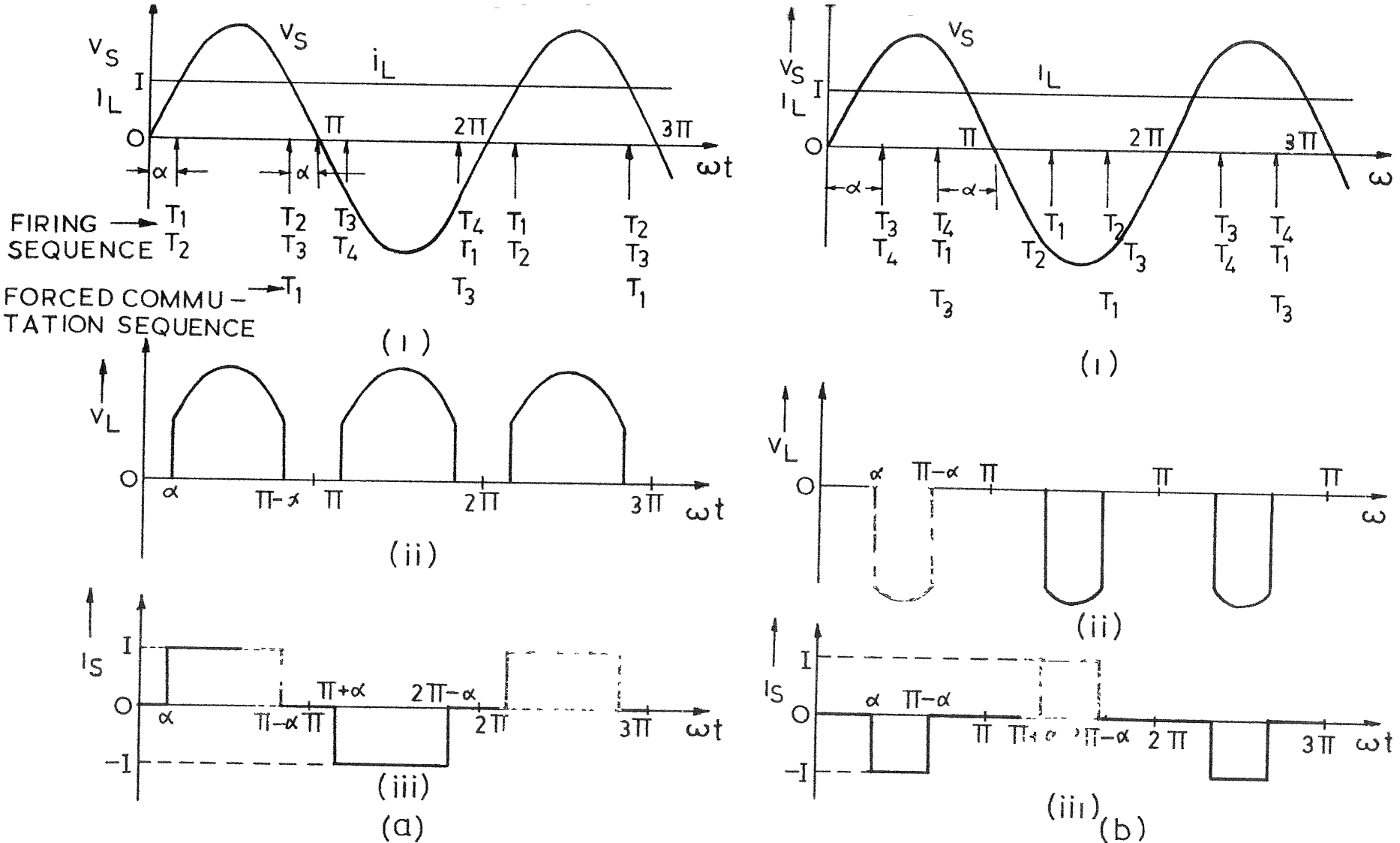

FIG 2.5 VOLTAGE AND CURRENT WAVEFORMS FOR SYMMETRICAL SINGLE PULSE WIDTH
(a) RECTIFICATION MODE (b) INVERSION MODE

(ii) The total power factor is defined as the ratio of active power input to the apparent volt-ampere input. Assuming sinusoidal ac source ,

Total Power Factor = $(I_{1RMS} / I_{SRMS}).\cos \psi_1$

where I_{1RMS} = RMS value of the fundamental component in the source current

I_{SRMS} = RMS value of the source current

$\cos \psi_1$ = Fundamental power factor

The ratio I_{1RMS} / I_{SRMS} is termed as the distortion factor and $\cos \psi_1$ as the displacement factor (DSP) [3] .

(iii) The input harmonic factor is a measure of harmonic distortion in the ac supply.

$$\text{Input Harmonic Factor} = \frac{\text{Input Harmonic content}}{\text{RMS value of fundamental component of the source current}}$$

$$= (I^2_{SRMS} - I^2_{1RMS})^{\frac{1}{2}} / I_{1RMS}$$

(iv) The ripple voltage at the dc terminals is expressed in terms of peak-to-peak (p-p) voltage ripple factor which is the per-unit value of the p-p output voltage ripple with base chosen as the maximum possible p-p output voltage ripple which is obtained in case of conventional scheme with $\alpha = 90°$. The maximum possible p-p output voltage ripple is obviously $2V_{Sm}$ where

V_{Sm} is the peak value of the source voltage. Thus,

P-p Voltage Ripple Factor = p-p output voltage ripple/$2V_{Sm}$

In what follows, the expressions for the average value of the output voltage (V_{LAV}), RMS value of the source current (I_{SRMS}), the RMS value of the fundamental component of the source current (I_{1RMS}) and displacement factor (cos ψ_1 or DSP) are derived for the different converter circuit configurations mentioned in section 2.2. in order to compute the input and output performances.

2.3.1. Conventional fully controlled bridge

Referring to Fig. 2.2., the following expressions can be easily obtained.

$V_{LAV} = (2V_{Sm}/\pi).\cos\alpha$

where V_{Sm} is the peak of supply voltage.

$I_{SRMS} = I$

$I_{1RMS} = 2\sqrt{2}\, I / \pi$

$\psi_1 = \alpha$

Fundamental power factor (DSP) = $\cos\psi_1 = \cos\alpha$

Total power factor = $(2\sqrt{2}/\pi).\cos\alpha$

$$\text{Input harmonic factor} = \frac{(I_{SRMS}^2 - I_{1RMS}^2)^{1/2}}{I_{1RMS}} = (\pi^2/8 - 1)^{1/2}$$

P - p voltage ripple factor = $0.5\ (1 + \sin\alpha)$

2.3.2. Fully controlled bridge with optional free-wheel control

The expressions for this case are easily obtained referring to Fig. 2.3.(a). They are given below.

$$V_{LAV} = (V_{Sm} / \pi)(\cos\phi + \cos\alpha)$$

$$I_{SRMS} = I \left[\frac{\pi + \phi - \alpha}{\pi}\right]^{1/2}$$

$$I_{1RMS} = (2I/\pi)\left[1 + \cos(\alpha - \phi)\right]^{1/2}$$

$$\psi_1 = (\alpha + \phi)/2$$

$$\text{Total power factor} = 2\cos\left(\frac{\alpha + \phi}{2}\right)\left[\frac{1 + \cos(\alpha - \phi)}{\pi(\pi + \phi - \alpha)}\right]^{1/2}$$

$$\text{Input harmonic factor} = (I_{SRMS}^2 - I_{1RMS}^2)^{1/2} / I_{1RMS}$$

$$= \left[\frac{1}{2}\left\{\frac{\pi(\pi + \phi - \alpha)}{1 + \cos(\alpha - \phi)}\right\}^{1/2} - 1\right]^{1/2}$$

The p-p (peak-to-peak) output voltage ripple will have different expressions depending on the values of α and ϕ. Thus, we obtain ,

P - p voltage ripple factor = $0.5\ (1 + \sin\phi)$,

for $0 \leq \phi \leq \pi/2$

and $0 \leq \alpha \leq \pi/2$

$= 0.5\ (\sin\alpha + \sin\phi)$,

for $0 \leq \phi \leq \pi/2$

and $\pi/2 < \alpha \leq \pi$

$= 0.5\ (\sin\alpha + 1)$,

for $\pi/2 < \phi \leq \pi$

and $\pi/2 < \alpha \leq \pi$

If rectification mode only is desired, the triggering angle ϕ is fixed at zero and α is varied from zero to π to control mean output voltage from maximum to zero. The expressions for this particular case are obtained by substituting $\phi = 0$ in the above general expressions for optional fly-wheel. Thus, we get,

$$V_{LAV} = (V_{Sm} / \pi)\ (1 + \cos\alpha)$$

$$I_{SRMS} = I \left[\frac{\pi - \alpha}{\pi}\right]^{1/2}$$

$$I_{1RMS} = (2I/\pi)\ (1 + \cos\alpha)^{1/2}$$

Fundamental power factor = $\cos\ (\alpha/2)$

$$\text{Total power factor} = 2\cos\ (\alpha/2) \left[\frac{1 + \cos\alpha}{\pi(\pi - \alpha)}\right]^{1/2}$$

$$\text{Input harmonic factor} = \left[\frac{1}{2}\left\{\frac{\pi(\pi-\alpha)}{1+\cos\alpha}\right\}^{1/2} - 1\right]^{1/2}$$

$$\text{P - p voltage ripple factor} = 0.5 \quad , \text{ for } 0 \leq \alpha \leq \pi/2$$

$$= 0.5 \sin\alpha \quad , \text{ for } \pi/2 < \alpha \leq \pi .$$

Similarly, if inversion mode is desired, the triggering angle, α is fixed at π and ϕ is controlled from zero to π for variable output voltage. The expressions for this case are obtained by substituting $\alpha = \pi$ in the general expressions for optional freewheel. Thus, we get

$$V_{LAV} = (V_{Sm}/\pi)(\cos\phi - 1)$$

$$I_{SRMS} = I(\phi/\pi)^{1/2}$$

$$I_{1RMS} = (2I/\pi)(1 - \cos\phi)^{1/2}$$

$$\text{Fundamental power factor} = -\sin(\phi/2)$$

$$\text{Total power factor} = -2\sin(\phi/2)\left[\frac{1-\cos\phi}{\pi\cdot\phi}\right]^{1/2}$$

$$\text{Input harmonic factor} = \left[\frac{1}{2}\left(\frac{\pi\cdot\phi}{1-\cos\phi}\right)^{1/2} - 1\right]^{1/2}$$

$$\text{P - p voltage ripple factor} = 0.5\sin\phi \quad , \text{ for } 0 \leq \phi \leq \pi/2$$

$$= 0.5 \quad , \text{ for } \pi/2 < \phi \leq \pi .$$

2.3.3. Symmetrical single pulse-width modulation control scheme

Referring to Fig. 2.5.(a) , for rectification operation, the different expressions are obtained as follows:

$$V_{LAV} = (2V_{Sm} / \pi) \cos \alpha$$

$$I_{SRMS} = I \left(\frac{\pi - 2\alpha}{\pi} \right)^{1/2}$$

$$I_{1RMS} = (2\sqrt{2}\, I / \pi) \cos \alpha$$

$$\psi_1 = 0$$

Fundamental power factor = $\cos \psi_1 = 1$

Total power factor = $2\sqrt{2} \cos \alpha / \left[\pi (\pi - 2\alpha) \right]^{1/2}$

$$\text{Input harmonic factor} = \left[\frac{\pi (\pi - 2\alpha)}{8 \cos^2 \alpha} - 1 \right]^{1/2}$$

P - p voltage ripple factor = 0,5

Similarly, the expressions for inversion mode are obtained referring to Fig. 2.5.(b) . For this mode, the expressions are the same as those obtained for rectification mode. However, because of power flow from the output to ac source, the expressions for average load voltage, fundamental power factor and total power factor

become negative.

2.4 CONTROL CIRCUIT FOR THYRISTOR CONVERTER WITH OPTIONAL FREE-WHEEL

The main block diagram of the firing circuit is shown in Fig. 2.6 which produces triggering pulses to thyristors in the sequence shown in Fig. 2.3 (b) . The supply sinusoid is fed as the input to the synchronised ramp generator at the output of which a ramp is produced in each half cycle of the supply sine wave. At the α-control comparator the ramp is compared with $V_{ref(\alpha)}$ to get rectangular pulses in each half cycle. The position of the rising edge of the rectangular pulse that fixes triggering angle, α can be controlled from zero to π by the variation of $V_{ref(\alpha)}$. Similarly $\emptyset$ can be varied from zero to π by controlling $V_{ref(\emptyset)}$ at the other comparator. These rectangular pulses are then stretched to 180° by pulse stretchers. The pulse-stretcher output in the $\emptyset$ control channel is the gate pulse for T_1 and its complement is the gate pulse for T_3 as seen from Fig. 2.3 (a) that G_3 and G_1 are complementary. Similarly, the pulse stretcher output in the α-control channel and its complement are the gate pulses for G_2 and G_4 respectively. Of course, these gate pulses go through high frequency modulation, pulse amplification and pulse transformer stages before being finally applied to the gate of the thyristors.

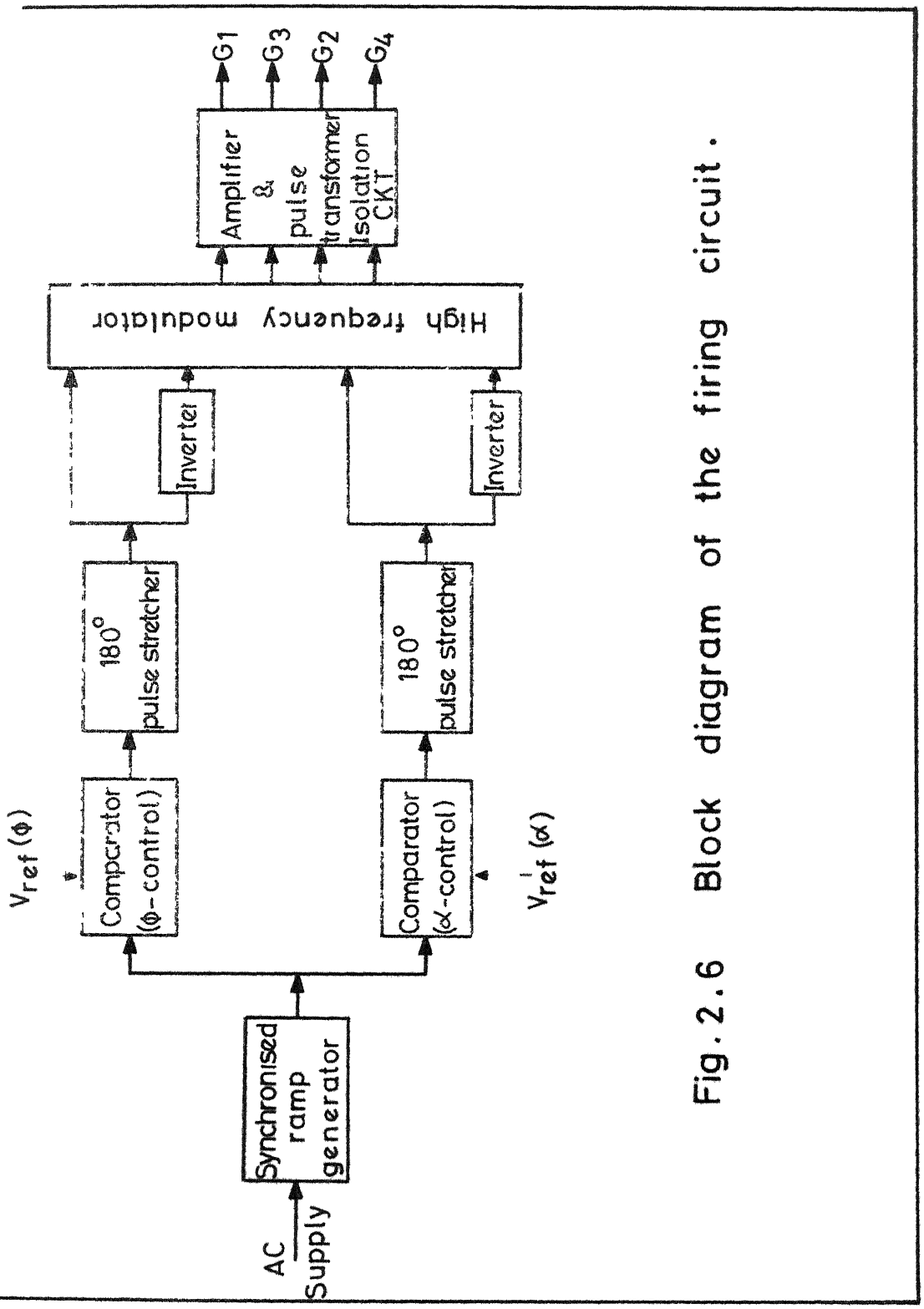

Fig. 2.6 Block diagram of the firing circuit.

The pulse transformers provide isolation between power circuit and the firing circuit. The associated circuits for different blocks are described illustrating pertinent waveforms.

Synchronised ramp generator: The circuit is shown in Fig. 2.7.(a) . The 230V supply is first stepped down to 9V and fed to the non-inverting input of an opamp operating in the open-loop mode to get a square wave output synchronised to the supply sine wave. The 5.1V zener diode connected across the output makes it TTL compatible. The waveform at the point marked (A) is shown in Fig. 2.8 . This is fed to a dual monostable. One of the monostables is triggered by the rising edge and the other by the falling edge of the square wave. The external components R and C are so chosen that the monostable output pulse-width is just enough to completely discharge the 0.2μF charging capacitor in the ramp generator. R and C have been chosen as 47k and 0.01μF respectively. The outputs of the dual monostable are ANDed using NAND gates and fed to the input of the ramp generator. The ramp generator is realized using discrete components. It gives fairly linear ramp output because of the charging of the capacitor by constant current source. The amplitude of the ramp is adjusted to +5V by the 4.7k potentiometer. Further linearization of the ramp is achieved using an opamp as shown in Fig. 2.7.(a).

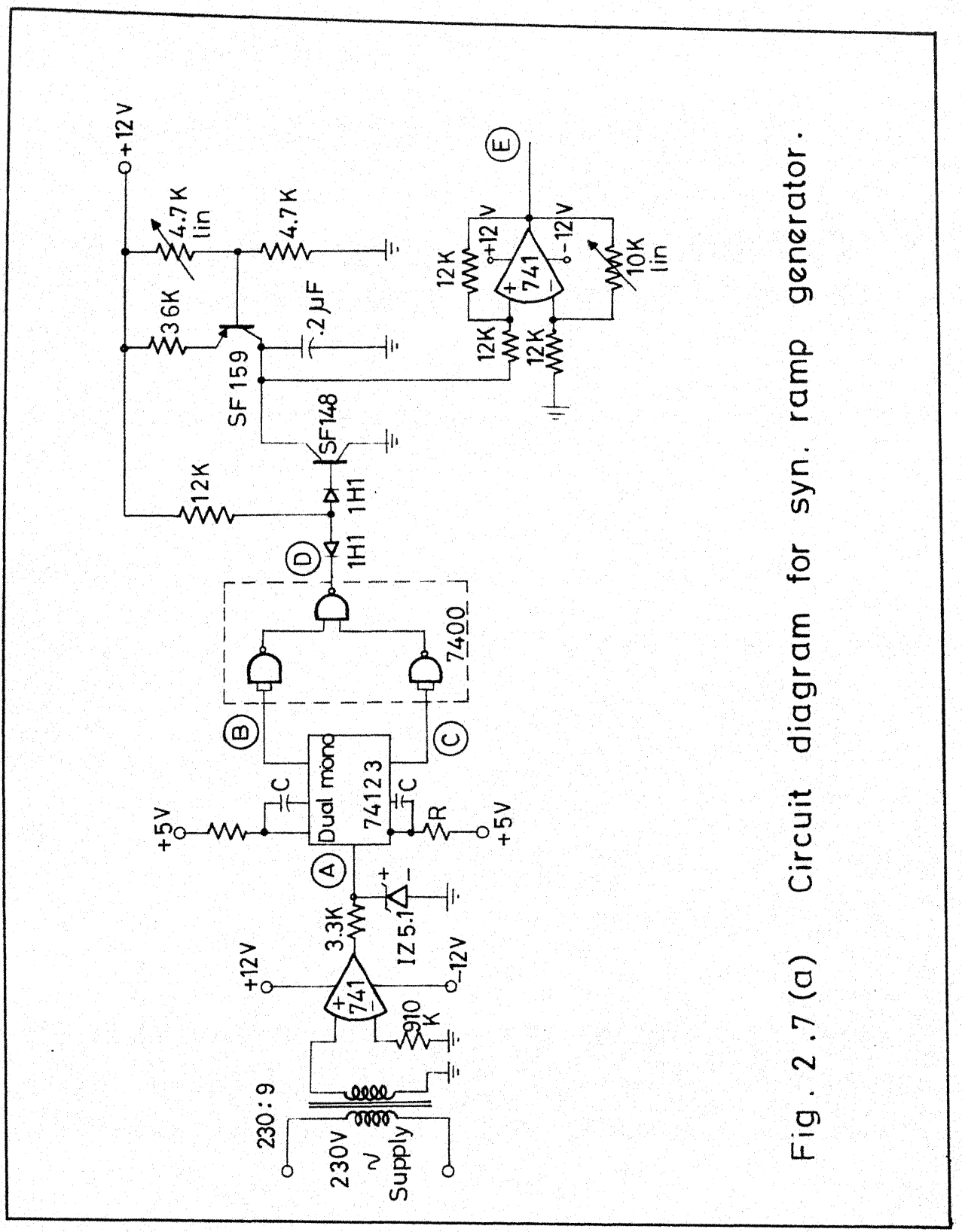

Fig. 2.7 (a) Circuit diagram for syn. ramp generator.

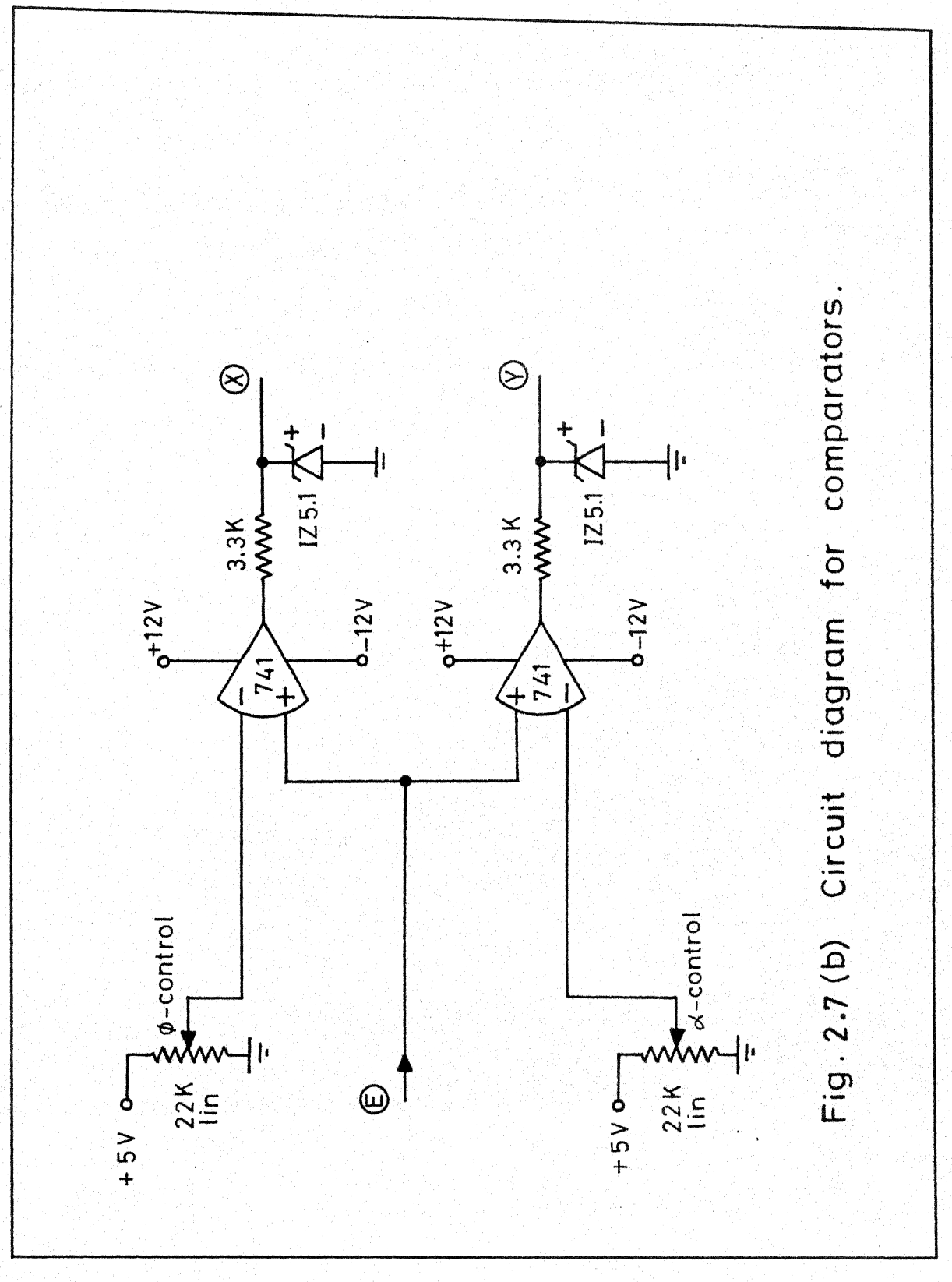

Fig. 2.7 (b) Circuit diagram for comparators.

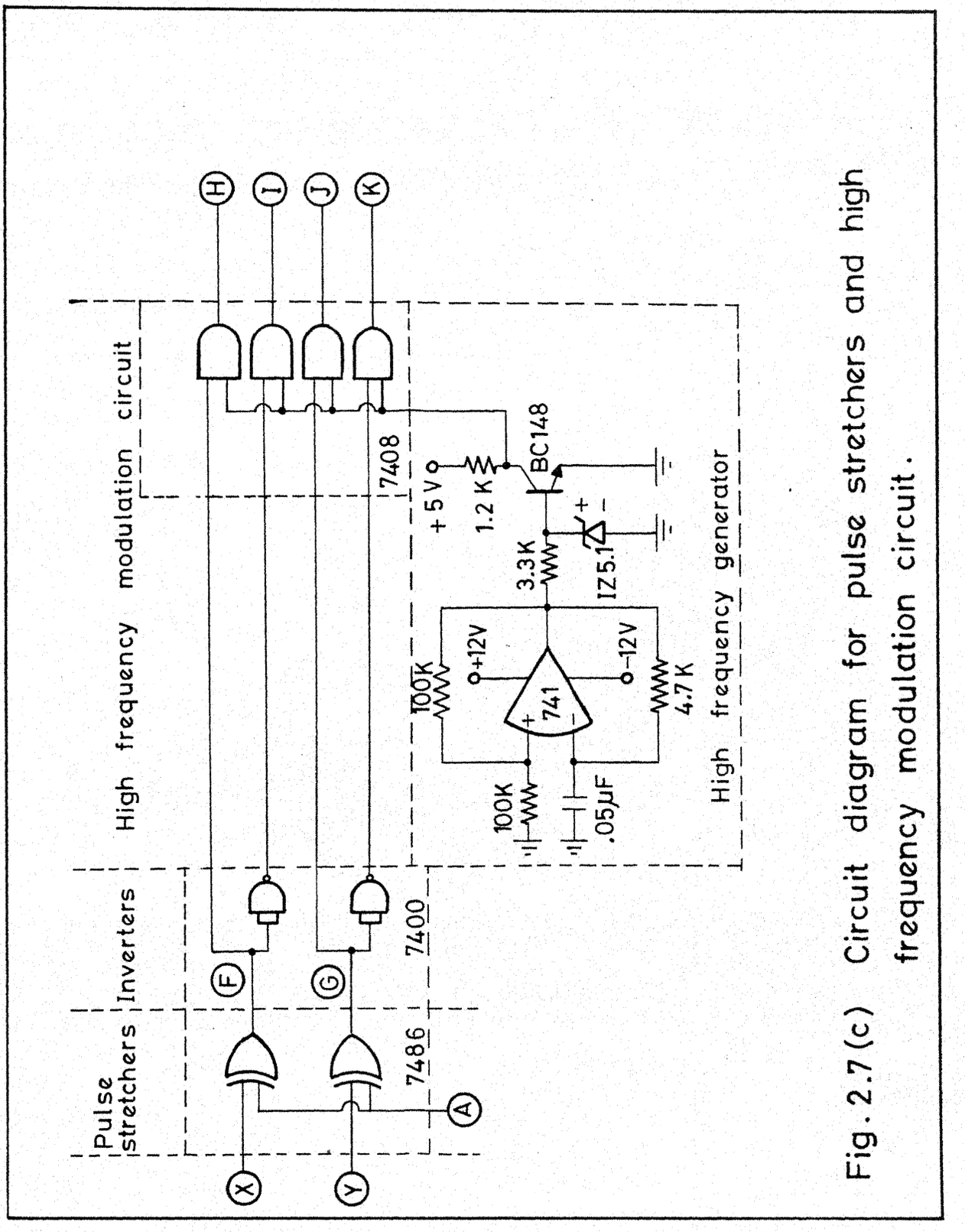

Fig. 2.7 (c) Circuit diagram for pulse stretchers and high frequency modulation circuit.

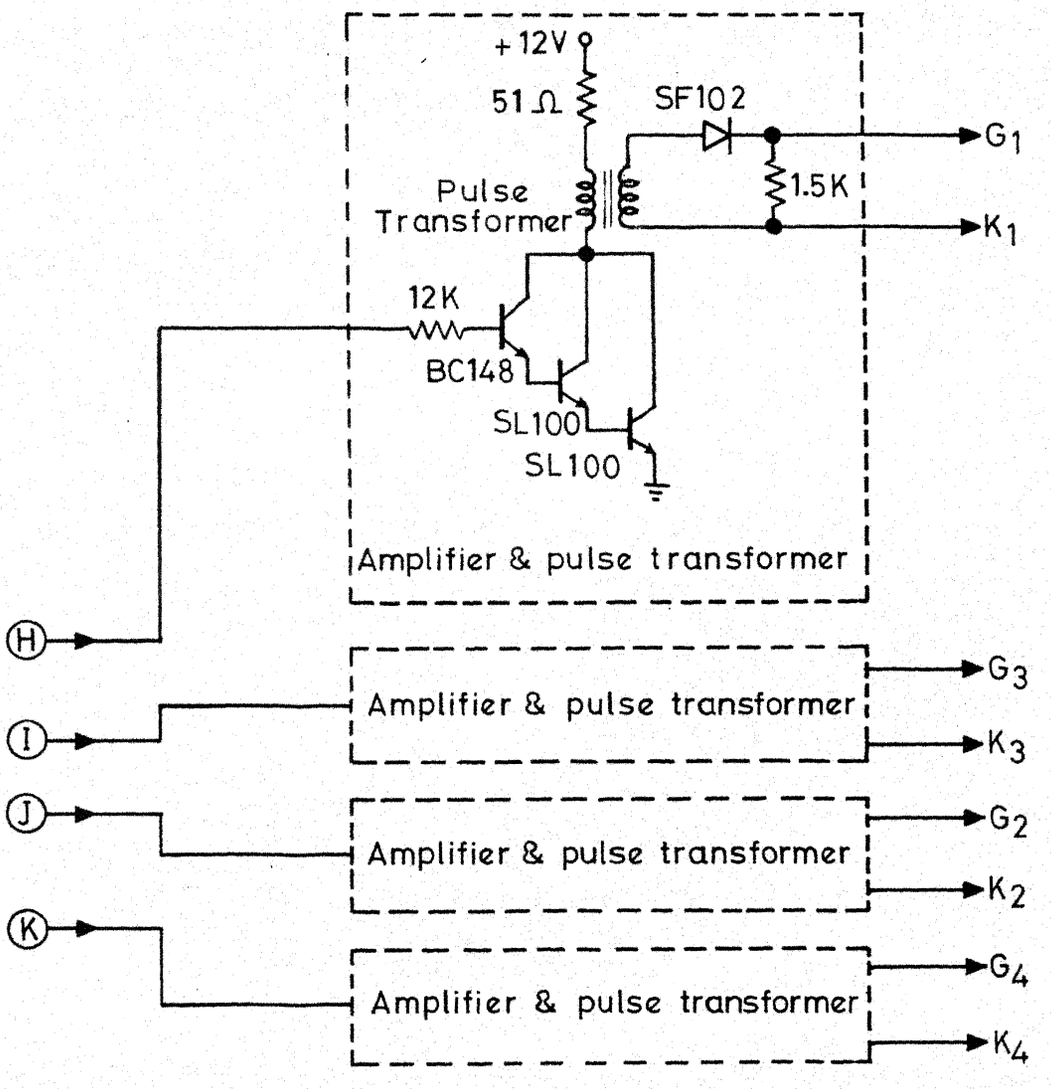

Fig. 2.7(d) Circuit diagram for amplifier and pulse transformer isolation circuit.

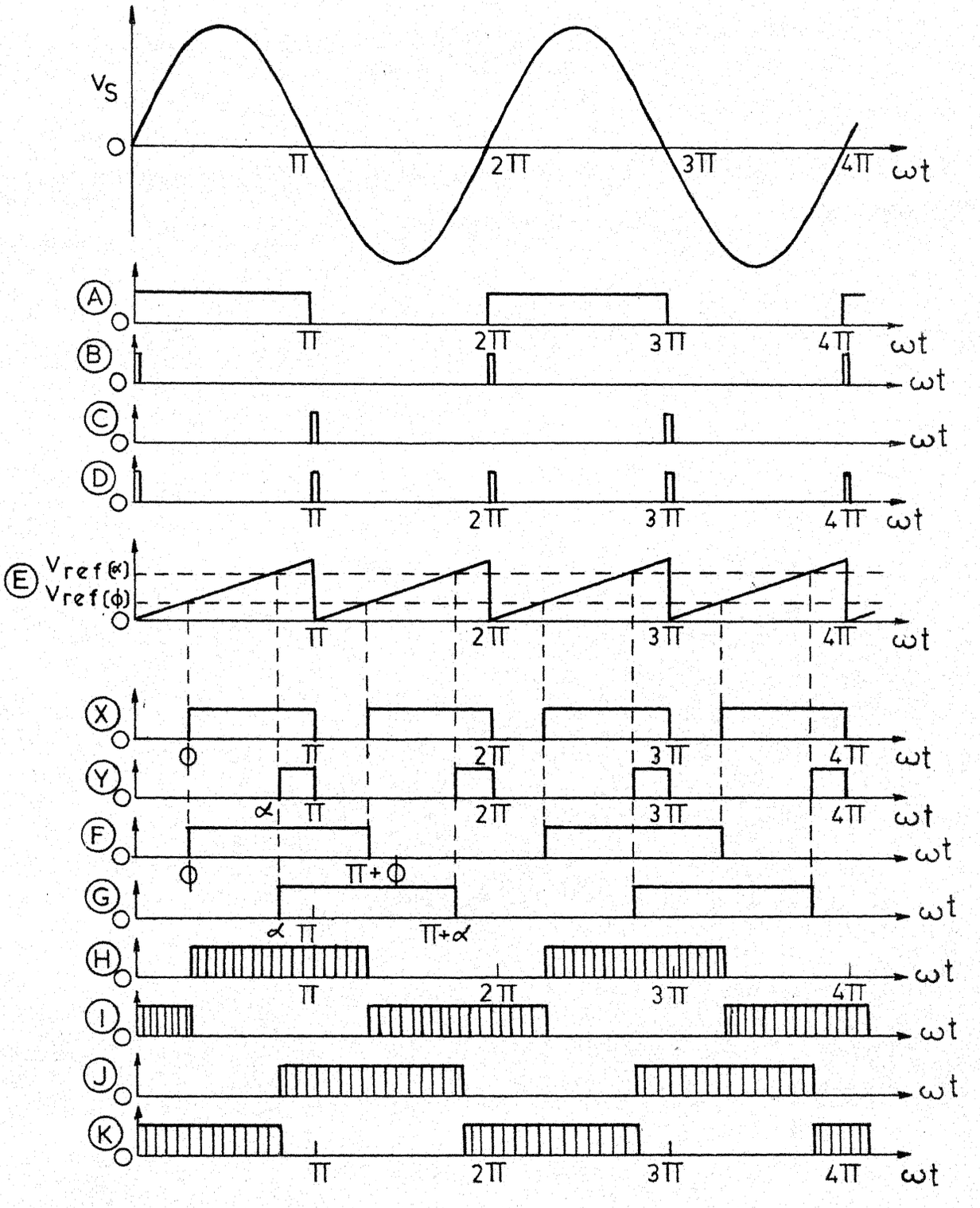

G. 2·8 WAVEFORMS AT DIFFERENT POINTS OF THE CONTROL CIRCUIT

The waveforms at different points of the circuit marked by capital alphabets are shown in Fig. 2.8.

Comparators : The comparator circuits used are shown in Fig. 2.7.(b) . An opamp in open-loop mode is used as the comparator. The ramp is fed to the non-inverting input and the dc reference voltage is given to the inverting input. The position of the leading edge of the output rectangular pulses at (X) and (Y) as shown in Fig. 2.7.(b) can be controlled from zero to π in each half cycle of the supply voltage by varying the reference voltage input with the help of potentiometers.

Pulse stretchers : The 180° pulse stretchers are easily realized using EXCLUSIVE-OR gates. The circuit details are given in Fig. 2.7.(c) . With the pulses at (X) and (A) as inputs to an EXCLUSIVE-OR gate, it gives an output square wave which has a width equal to one half cycle of the sine wave, the leading edge of which coincides with that of the rectangular pulse at (X) . Similarly, 180° stretching of the rectangular pulse at (Y) is also obtained. The stretched pulses at (F) and (G) are also shown in Fig. 2.8.

Inverters : The inversion of the square waves at (F) and (G) are necessary to obtain the gate pulses at ($\pi + \emptyset$) and at ($\pi + \alpha$) for the thyristors T_2 and T_4 respectively. This

is achieved using NAND gates as shown in Fig. 2.7.(c).

High frequency modulation circuit : In order to include the pulse transformers for isolation of the gate circuit from the power circuit, high frequency modulation of the gate pulses is necessary. The opamp astable circuit shown in Fig. 2.7.(c) is designed for approximately 10kHz output. The high frequency signal is shaped and made TTL compatible. The pulses are then modulated with the high frequency signal. The resulting modulated gate pulses at (H) , (I) , (J) and (K) are shown in Fig. 2.8.

Amplifier and pulse transformer isolation circuit : In order to trigger SCR's reliably, the gates have to be driven hard and the pulse magnitude should be large but within the maximum limits. Each pulse train at points (H) , (I) , (J) and (K) is amplified and isolated using individual Darlington's amplifier configuration and pulse transformer and fed to the gate of respective thyristor. The pulse transformer provides isolation for gate pulses. The circuit details of this block is shown in Fig. 2.7.(d).

2.5. EXPERIMENTAL RESULTS AND COMPARATIVE STUDY OF PERFORMANCES

The control circuit developed in section 2.4 is employed to study the performances experimentally for the converter circuit configuration with optional free-wheel control. Large inductance is inserted in the load circuit to make the load current constant as far as possible.

Table 2.1 gives the details of experimental set-up.

Table 2.1

Quantity	Value
Load resistance	13.5 Ω
Load inductance	3.72H
V_{Sm}	99V
Load EMF for inversion mode	0-30V dc
1 pu output voltage	63.02V

By measuring input voltage, input current and input power from ac source, the total power factor is computed. A distortion analyser is used to measure the harmonic factor. Fig. 2.9.(a) shows oscillograms of input and output waveforms of voltage and current in the rectification mode while Fig. 2.9.(b) gives the same waveforms

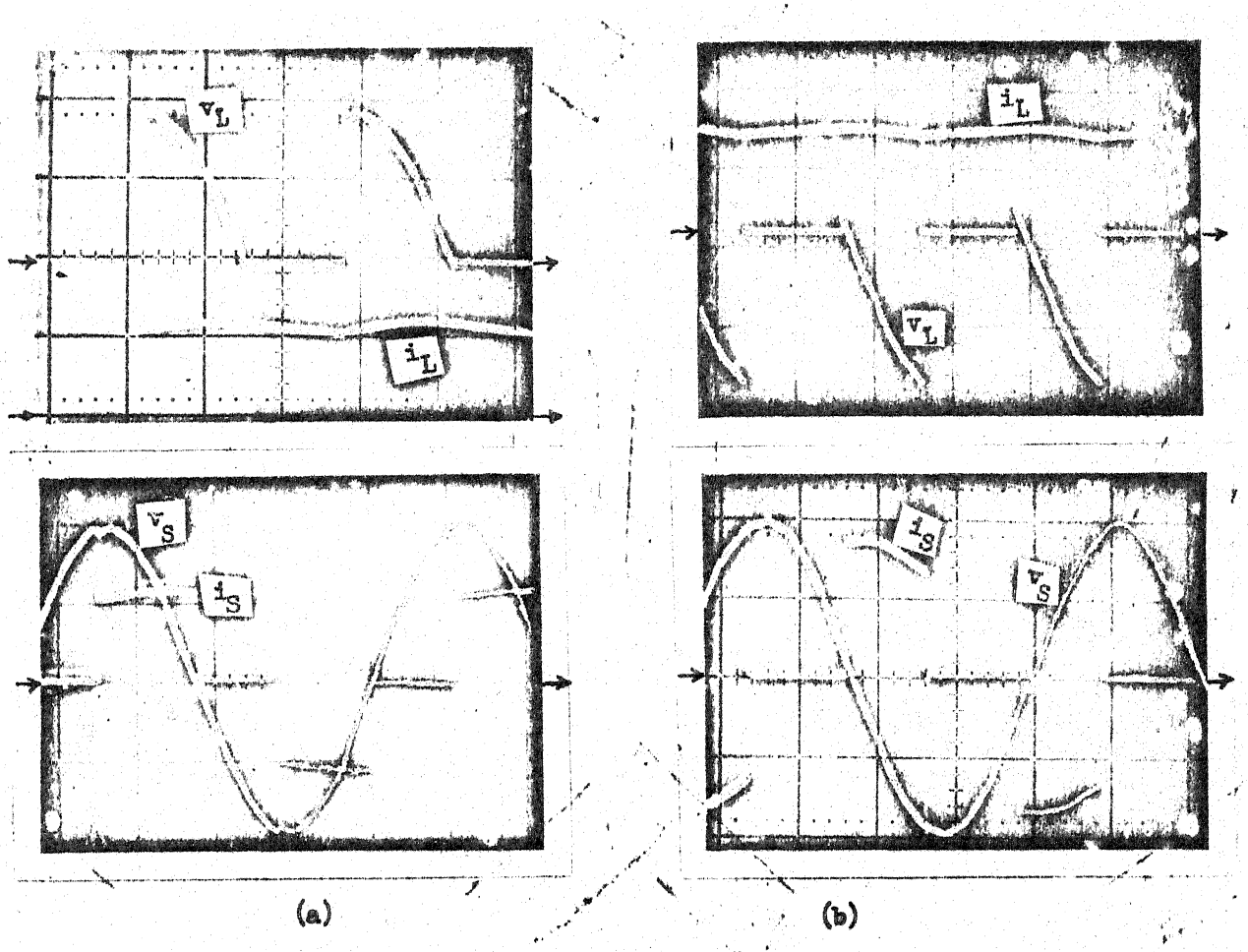

v_L : Load voltage
v_S : Supply voltage
} 50 volts/division .

i_L : Load current
i_S : Supply current
} 2 amps/division .

Fig. 2.9 Oscillograms of input and output voltage and current waveforms for fully controlled converter with optional freewheel control .

(a) Rectification operation with $\phi \approx 0^\circ$.

(b) Inversion operation with $\alpha \approx 180^\circ$.

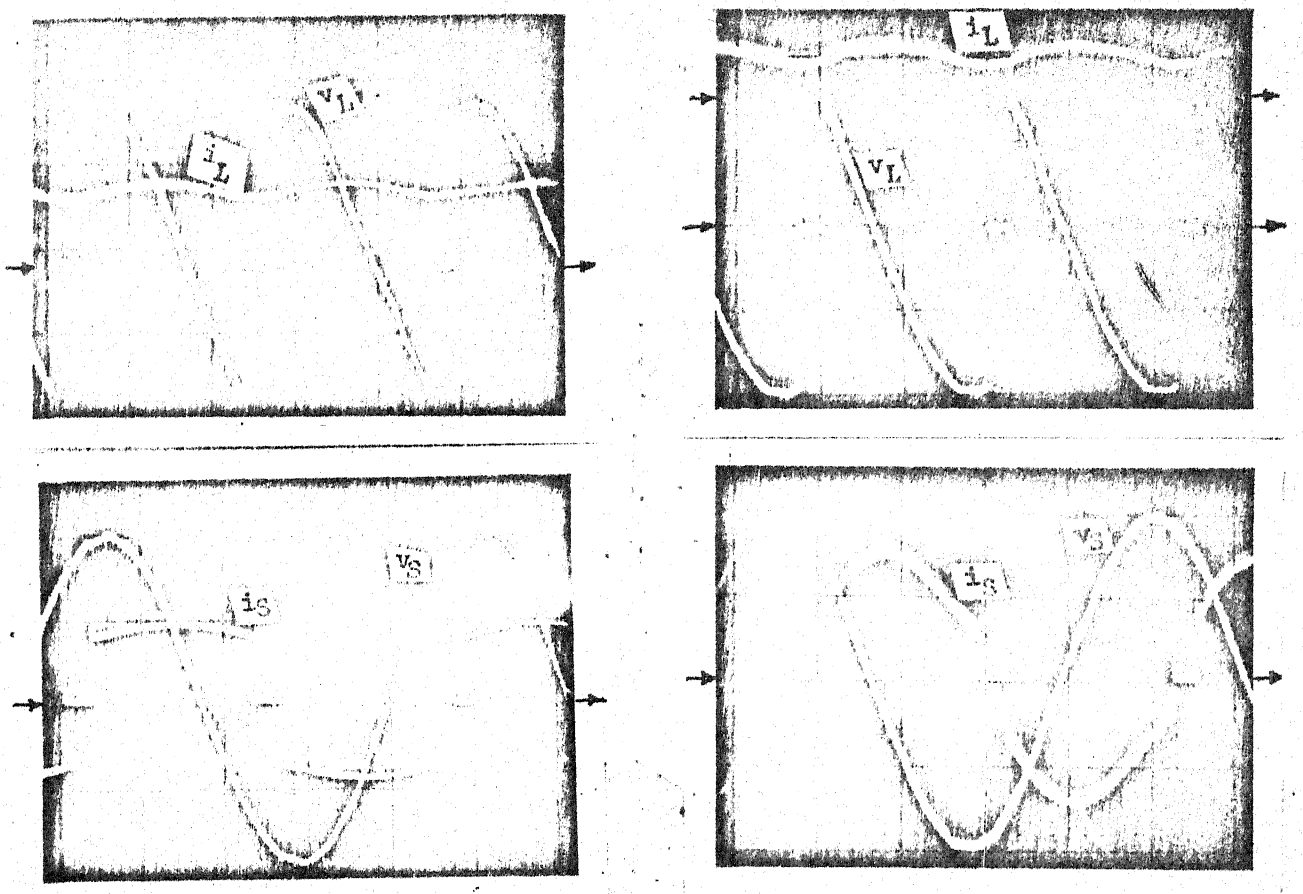

(c) (d)

v_L : Load voltage
v_S : Supply voltage
} 50 volts/division .

i_L : Load current — 2 amps/division .

i_S : Supply current — { 2 amps/division in (c) . 1 amp/division in (d) .

Fig. 2.9 Oscillograms of input and output voltage and current waveforms for fully controlled converter with optional freewheel control .

(c) Rectification operation with $\alpha = 60^\circ$ and $\phi = 45^\circ$.

(d) Inversion operation with $\alpha = 150^\circ$ and $\phi = 105^\circ$.

in the inversion mode. These waveforms correspond to maximum possible free-wheeling interval in rectification and inversion modes. The waveforms corresponding to optional free-wheel with particular values of α and $\emptyset$ in rectification and inversion modes are shown in Fig. 2.9.(c) and (d) respectively.

The expressions derived in section 2.3 are used to obtain different performances for fully controlled converter, fully controlled with optional free-wheel and forced commutated converter at various output voltages. A comparative study of the fundamental power factor, total input power factor, input harmonic factor and p - p voltage ripple factor for the same average voltage under different converter circuit configurations is presented.

The fundamental power factor (DSP) gives an idea of the active power requirement from the supply. This is shown in Fig. 2.10. for rectification and inversion modes. The symmetrical pulse-width control scheme offers maximum power factor of unity over entire output voltage range in both modes of converter circuit. As expected, it is minimum in the case of conventional full-controlled converter. Especially at light load conditions, that is corresponding to low output voltages, the fundamental power factor is very poor in this case. The performance of the

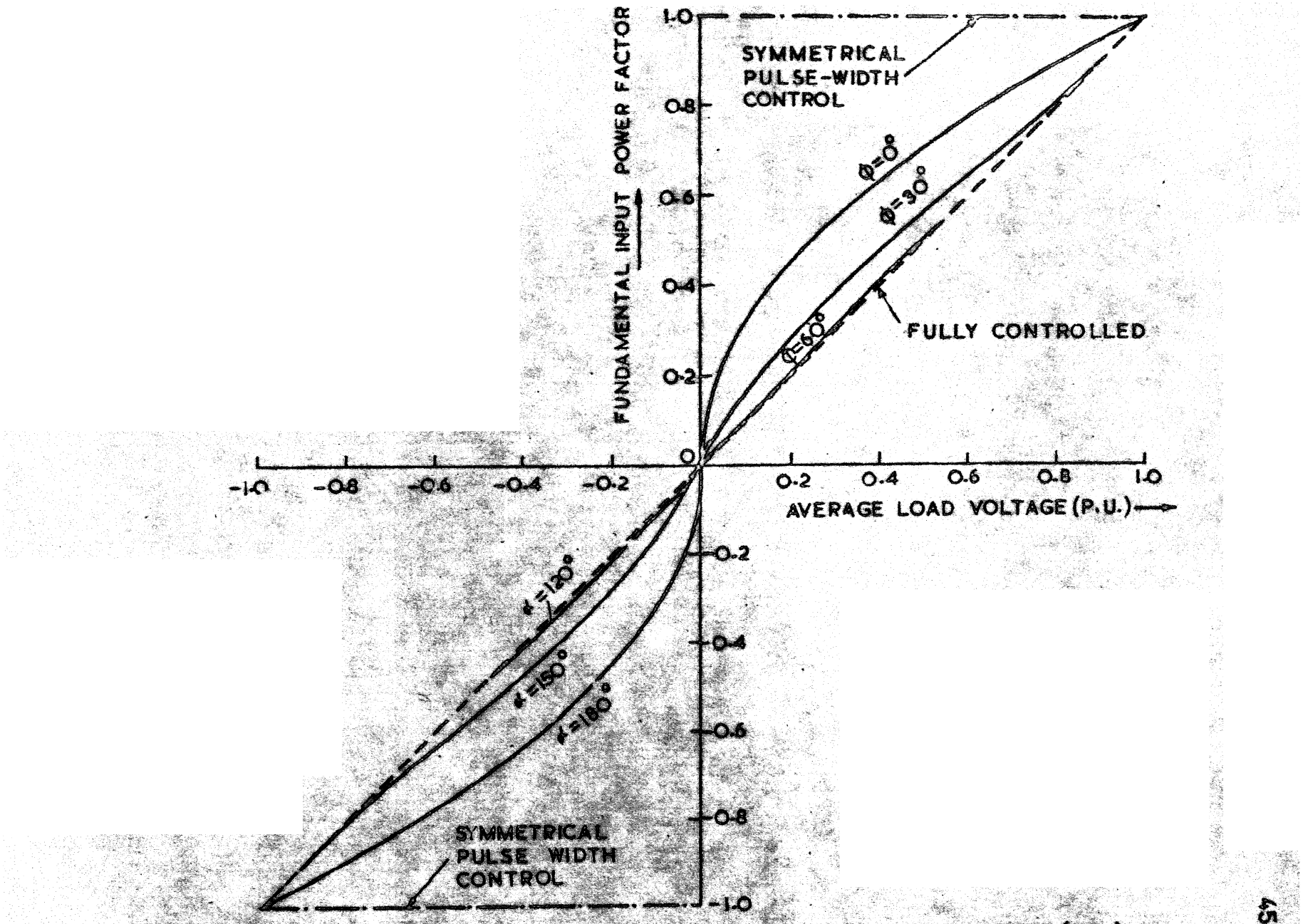

FIG. 2.10 FUNDAMENTAL POWER FACTOR VARIATION WITH LOAD VOLTAGE (P.U.)

converter with optional free-wheel control with $\emptyset$ equal to zero for positive voltages and α equal to π for negative voltages shows significant improvement over that of the conventional converter. As free-wheel interval decreases with increasing values of $\emptyset$ and α in rectification and inversion modes respectively, there is less improvement in DSF compared to that in fully controlled converter.

The total input power factor is an important performance as it decides the volt-ampere requirement of input power apparatus. This is shown for the three converter circuit configurations in Fig. 2.11. The characteristics in the first quadrant correspond to rectification mode while those in the fourth quadrant correspond to regenerative mode. The symmetrical pulse width control compared to other schemes offers maximum power factor in the ac supply system. In this case also, the optional free-wheel with $\emptyset$ fixed at zero for positive output voltages or α fixed at π for negative output voltages provides better power factor compared to fully controlled circuit. The improvement in power factor decreases as the free-wheel interval decreases in the converter with optional free-wheel.

The harmonic factor is defined as the ratio of

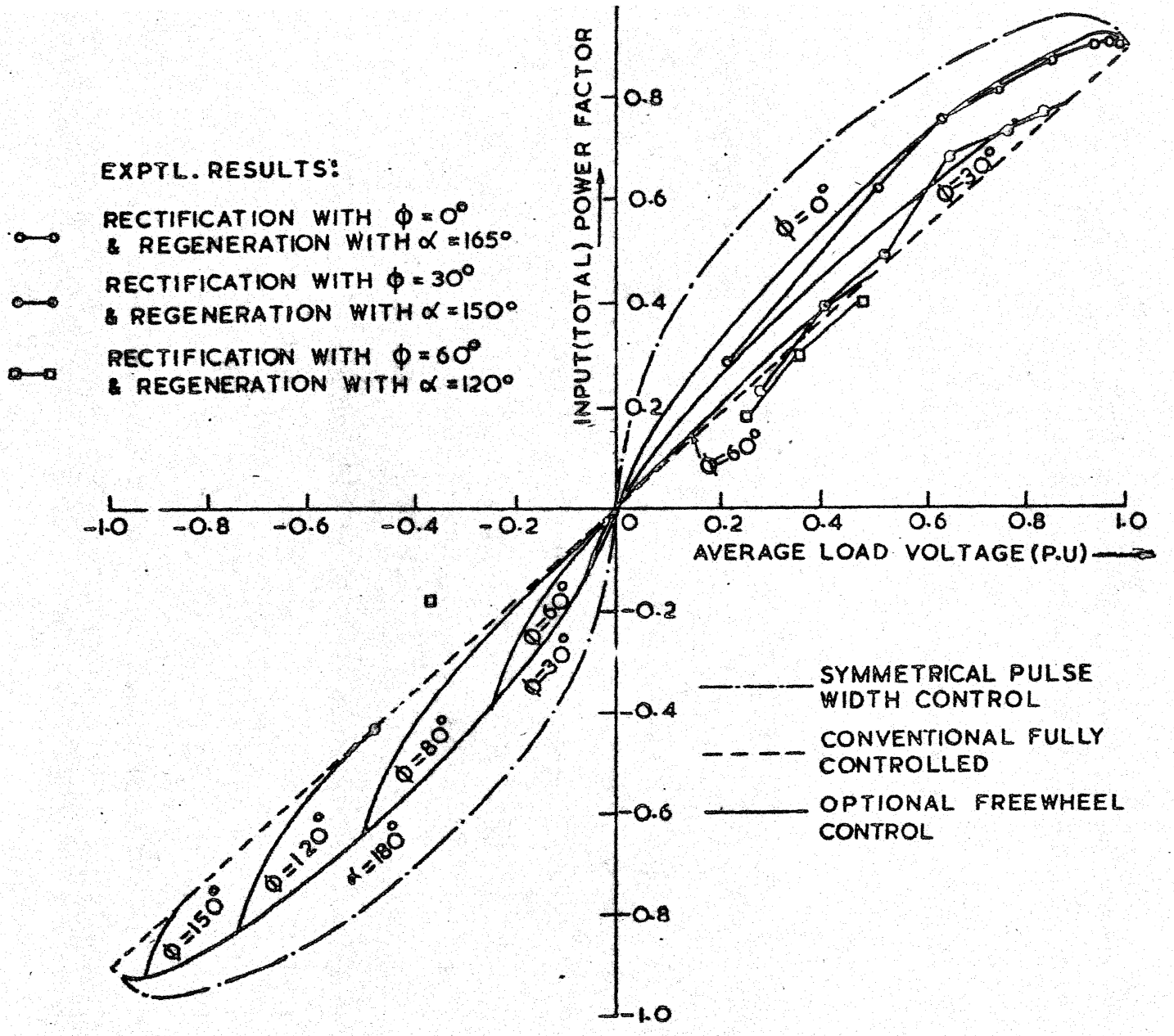

FIG. 2.11 TOTAL POWER FACTOR VARIATION WITH LOAD VOLTAGE (P.U.)

harmonic content to the rms fundamental component in the ac supply current. This is illustrated in Fig.2.12 . It remains constant over the entire range of the output voltage in case of the conventional fully controlled scheme. The harmonic factor increases astronomically as the output voltage approaches zero in case of symmetrical pulse-width control. It, of course, decreases with the increase in the mean output voltage in rectification and inversion modes. It is less than that of the conventional fully-controlled bridge for higher output voltages. The harmonic factor in case of fully-controlled bridge with half-controlled characteristics, that is, $\emptyset$ equal to zero for positive mean output voltages and α equal to π for negative mean output voltages, is lesser than that of the symmetrical pulse-width control scheme for a wide range of the output voltage. At very large output voltages does the difference between them become insignificant. However, it is more than that of the conventional fully-controlled scheme at lower output voltages. For higher output voltages it is lesser than that of the conventional full-controlled scheme. As free-wheeling interval decreases with increasing values of $\emptyset$ in the rectification mode and decreasing values of α in the inversion mode, the harmonic factor decreases. For triggering angle $\emptyset$ less than about 60° and for α greater than about 120° , the

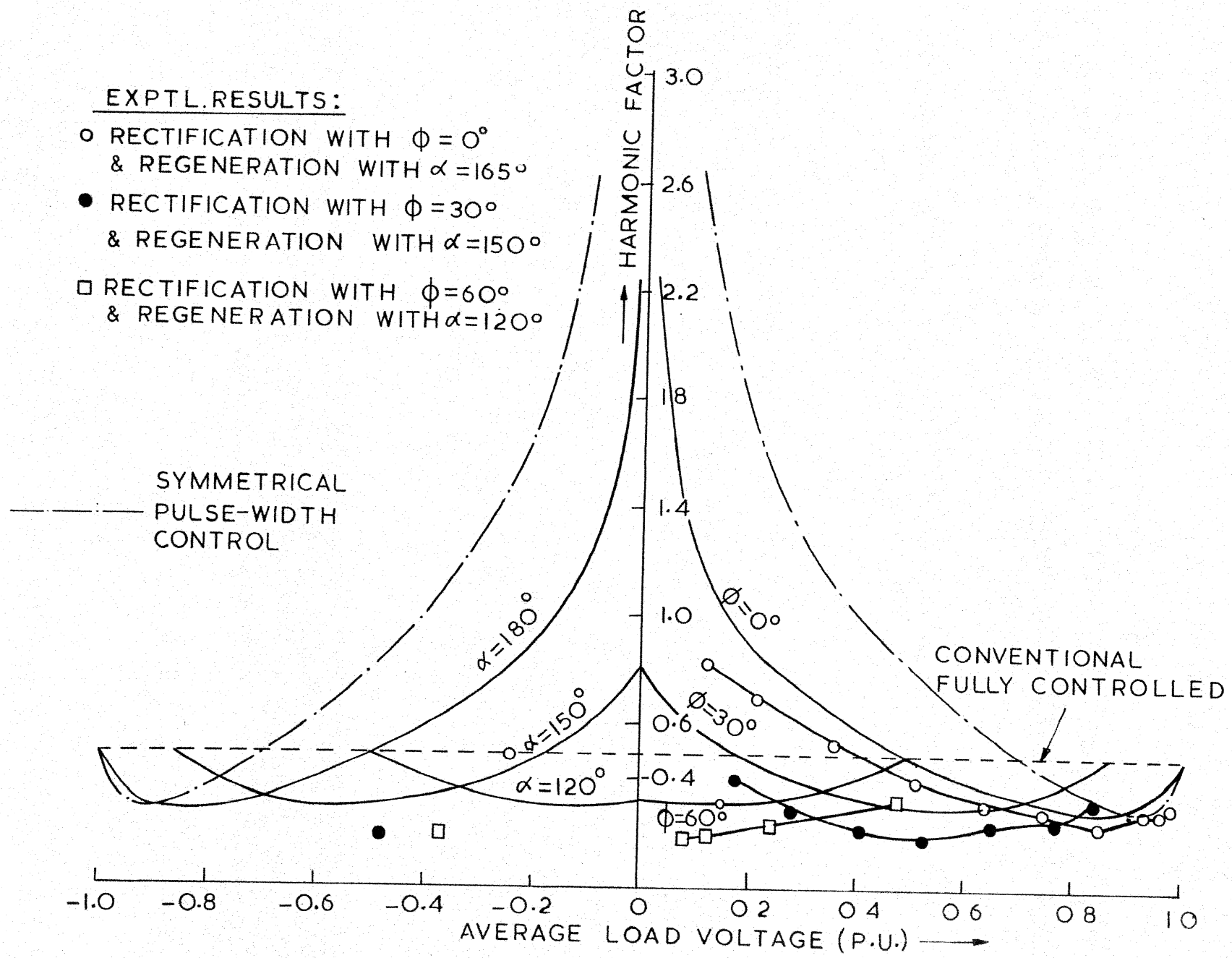

FIG. 2·12 INPUT HARMONIC FACTOR VERSUS AVERAGE LOAD VOLTAGE (P.U.)

harmonic factor decreases with increasing output voltages in both rectification and inversion modes. However, for higher values of ϕ or lower values of α, it appears to be constant for low output voltages but increases slightly with further increase in the output voltage for a particular value of ϕ or α.

Experimental results are also shown for optional free-wheel. A good number of observations are recorded for the rectification mode. However, because of non-availability of variable dc supply with wider range, only a few readings are noted in the regenerative mode. The theoretical results appear to be somewhat conservative due to the assumption of constant current. In the actual experimental set-up, the load current does consist of some ripple, however small it may be. The discrepancy between experimental and theoretical results may be attributed to the finite ripple present in the load current. Notice from Figs. 2.11. and 2.12. that there is good agreement between experimental and theoretical results at higher output voltages when the ripple in the load current is negligibly small.

The peak-to-peak voltage ripple factor is shown in Fig. 2.13 . The fully controlled converter with half-controlled characteristics, that is, ϕ equal to zero

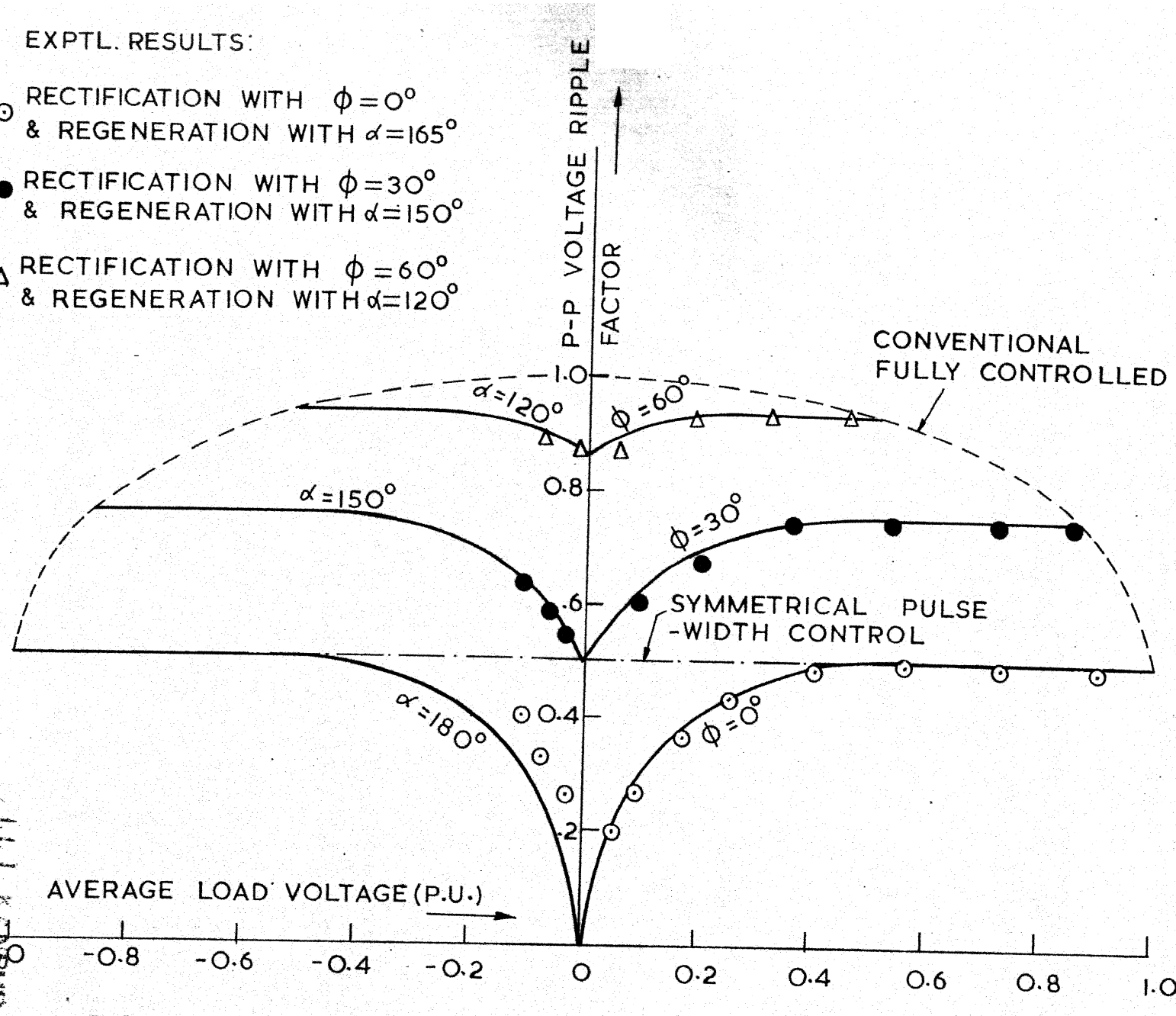

FIG. 2.13 P-P VOLTAGE RIPPLE FACTOR VS. AVERAGE LOAD VOLTAGE (P.U.)

for positive output voltages and α equal to π for negative output voltages, shows the least p - p voltage ripple factor. It is constant over half of the higher output voltage range and decreases rapidly as the output voltage decreases. For operation with other combinations of α's and ϕ's the voltage ripple is always less than that of the conventional fully controlled converter. The ripple is constant over the entire voltage range in symmetrical pulse-width control. For higher output voltages, the ripple is the same in case of symmetrical pulse-width control and fully-controlled converter with half-controlled characteristics.

2.6. CONCLUSIONS

The comparative study of different circuit configurations in traction power supply has revealed that the symmetrical pulse-width modulation technique offers maximum power factor. But it generates maximum distortion in the source current especially at low output voltages. Besides, it requires additional commutating elements and complex control circuitry since it works on the principle of forced commutation. On the other hand, the thyristor converter configuration with optional free-wheel works on line commutation requiring no additional commutating elements. For maximum power factor at low output voltages in the rectification mode, the triggering angle ϕ is

held at zero and the triggering angle α is varied for variable output voltages. Alternatively, the triggering angle α is held constant at π and the triggering angle ϕ is varied for variable output voltage in order to realize maximum power factor in the inversion mode. This triggering strategy also offers least ripple in the output dc voltage. However, if harmonic distortion is to be minimised without affecting power factor much, it appears that both ϕ and α have to be controlled simultaneously. Further improvement in performances may be obtained by a series connection of several thyristor converter configurations [3, 6]. The single-phase fully-controlled thyristor converter configuration with optional free-wheel control provides better performance characteristics in traction power supplies compared to fully controlled thyristor converter and, therefore, can be regarded as an obvious choice in traction locomotives employing line commutated converter circuit configurations.

CHAPTER III

CONSTRUCTION OF OPERATING DIAGRAM AND ESTIMATION OF MINIMUM INDUCTANCE IN FULLY CONTROLLED CONVERTER WITH OPTIONAL FREEWHEELING

3.1 INTRODUCTION

In the preceding chapter the operating characteristics of fully controlled converter with provision for optional freewheel control have been obtained assuming the load current to be continuous and constant. This assumption can be made when the converter feeds a traction motor with a large inductance in the armature circuit in addition to the motor armature inductance. Furthermore, the possibility of discontinuous armature current conduction is low with dc series motors since the motor EMF is a function of the load current. However, these converters are also widely used in industry for the control of dc shunt motors which have comparatively low armature inductance. Moreover, the motor EMF is independent of load current. Hence, the load current can be either continuous or discontinuous depending upon the triggering angles and actual load circuit parameters, namely, load phase angle and also load EMF. In case of continuous current operation the load voltage waveform is made up of portions of the ac supply voltage waveform and,

hence, determination of operating characteristics is trivial. In case of discontinuous current operation, however, different types of load voltage waveforms are encountered. These are recognised here as "modes". The expressions for voltage and current necessary to determine the operating characteristics are different for the different modes. Hence, a prior knowledge of the exact mode is desirable to determine the performance characteristics from the appropriate set of equations. In this chapter, the different modes that are possible for the fully controlled converter with optional freewheel control in both rectification and inversion operations are identified. In the preceding chapter, it has been concluded that rectification operation is achieved with $\emptyset$ set to zero and variable α while inversion operation is achieved with α held constant at π and variable $\emptyset$ in order to realize maximum supply power factor. Hence, mode identification is carried out for these cases with the help of related operating diagrams [1].

In case of converter-fed motor drives, discontinuous current operation introduces adverse effects [14] like speed fluctuations, excessive instantaneous commutator bar-to-bar voltage and poor dynamic response. Also it requires a great deal of consideration for the control technique. These adverse effects can be overcome by

introducing additional inductance just sufficient to make the current continuous. In this chapter, a graphical procedure making use of the operating diagrams along the lines given in reference [13] is presented for the determination of minimum inductance for the fully controlled converter with optional freewheel for both rectification and inversion operations.

3.2 OPERATING DIAGRAMS

The operating diagram of a converter defines the possible and permissible conditions of operation of the converter. In this diagram, the transition lines for different load impedance angles separating the discontinuous current region from that of the continuous current are shown with the triggering angle and the normalised load EMF as the variables [1] . In order to distinguish the control variables α and ϕ of the converter circuit, the operating diagrams are drawn separately for rectifier and inverter operations. The thyristors in converter circuits are generally provided with maintained trigger pulses so that the devices turn on reliably with inductive and back EMF loads. The gate pulses to the thyristors are, therefore, assumed to be 180°-stretched while deriving the operating diagrams for the converter circuit. The source impedance is neglected in the present analysis.

3.2.1 Computation

The operating diagrams are drawn on the basis of computational results. For different load impedance angles, θ , the load current is computed for various combinations of firing angles and normalised load EMFs to determine whether it is continuous or discontinuous. To obtain these results, it is necessary to compute the load current for only the first cycle of the supply voltage input to the converter circuit. In this section the expressions for the load current for different periods during the first cycle of the supply frequency are derived. These expressions are then used on a digital computer to obtain the operating diagrams of the converter circuit. In the following paragraphs the ac supply voltage is denoted by $V_{Sm} \sin \omega t$ while the load comprises of a resistance, R, inductance, L, and EMF, E.

(i) Rectifier Operation:

In the first half cycle, the main thyristor pair T_1 and T_2 (Fig. 2.1) turn on at $\omega t = \alpha_{act}$ (α_{act} denotes the actual turning on instant being equal to α or γ as the case may be). The operating circuit is as shown in Fig. 3.1 (a). The load current during the period $\alpha_{act} \leq \omega t \leq \pi$ is given by [1]

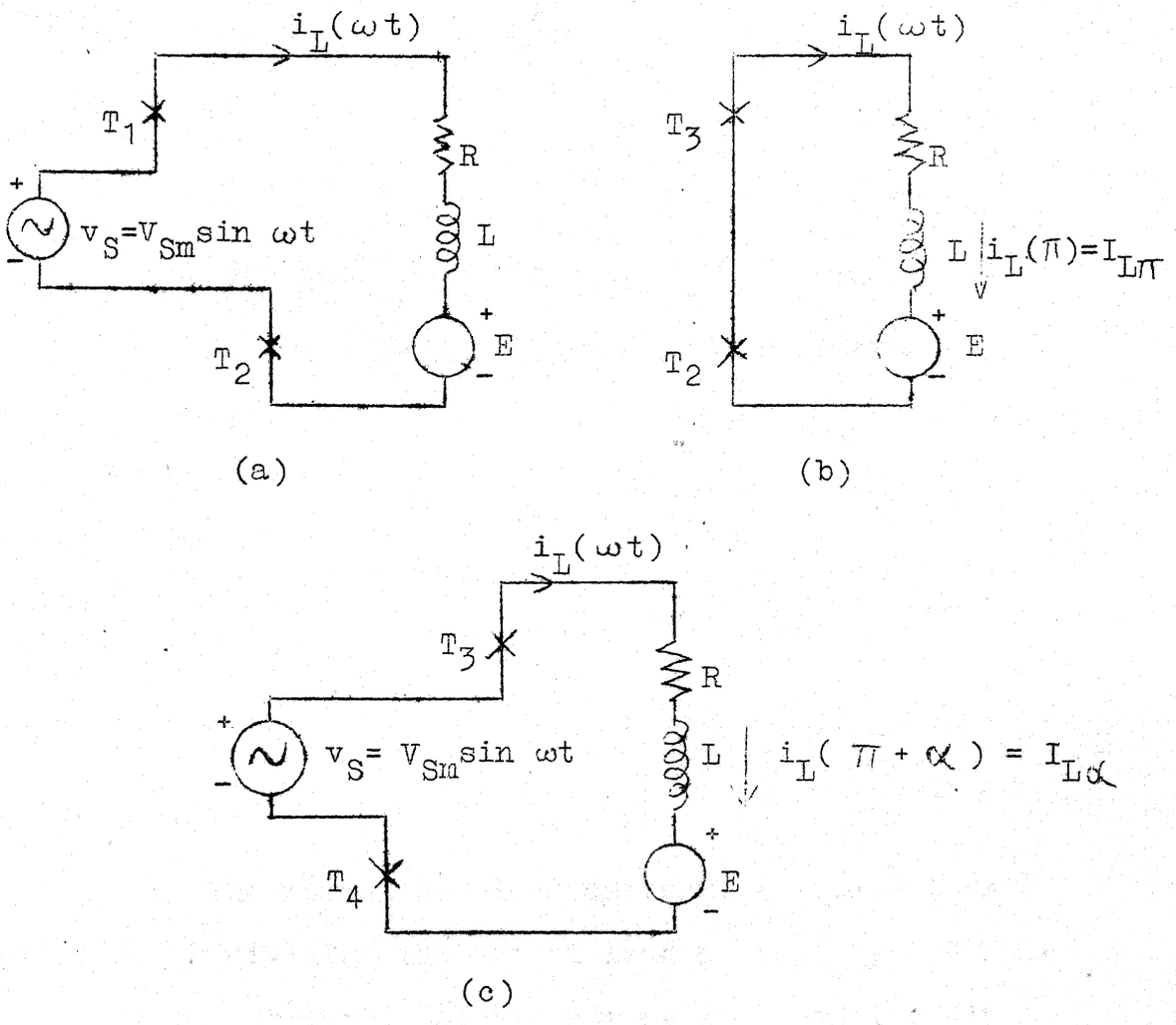

Fig. 3.1 Different operating circuits for rectifier operation

(a) Power interval ($\alpha_{act} \leq \omega t \leq \pi$)

(b) Freewheeling interval ($\pi \leq \omega t \leq \pi + \alpha$)

(c) Power interval ($\pi + \alpha \leq \omega t \leq 2\pi$)

$$i_L(\omega t) = (V_{Sm}/Z) \sin(\omega t - \theta) - (E/R) + A.\exp(-Rt/L)$$

where

$$Z = \left[R^2 + (\omega L)^2\right]^{1/2}$$

$$\theta = \tan^{-1}(\omega L/R)$$

A is a constant and can be evaluated from the initial condition $i_L(\omega t) = 0$ at $\omega t = \alpha_{act}$. Substituting this initial condition in the above equation, we obtain,

$$i_L(\omega t) = (V_{Sm}/Z) \sin(\omega t - \theta) - (E/R) + \left[(E/R) - (V_{Sm}/Z) \sin(\alpha_{act} - \theta)\right].\exp\left[-R(\omega t - \alpha_{act})/\omega L\right] \quad (3.1)$$

The normalised load current, $i_{LN}(\omega t)$, is obtained by dividing the actual load current by a factor V_{Sm}/Z (1 pu current). Also denoting the quantity E/V_{Sm} by the normalised load EMF, m, eqn.(3.1) reduces to

$$i_{LN}(\omega t) = \sin(\omega t - \theta) - (m/\cos\theta) + \left[(m/\cos\theta) - \sin(\alpha_{act} - \theta)\right].\exp\left[-(\omega t - \alpha_{act})/\tan\theta\right] \quad (3.2)$$

Freewheeling starts when the series-aiding thyristors are turned on at $\omega t = \pi$. Referring to the operating circuit of Fig. 3.1 (b) for this period

$\pi \leq \omega t \leq \pi + \alpha$, the load current is given by

$$i_L(\omega t) = - (E/R) + B \cdot \exp(-Rt/L)$$

where B is a constant.

Solving the above eqn. with the initial condition $i_L(\omega t) = I_{L\pi}$ at $\omega t = \pi$. we get,

$$i_L(\omega t) = - (E/R) + \left[I_{L\pi} + (E/R)\right] \times \exp\left[- R (\omega t - \pi)/\omega L\right] \qquad (3.3)$$

Rewriting eqn. (3.3) in the normalised form, we have,

$$i_{LN}(\omega t) = - (m/\cos\theta) + \left[I_{L\pi N} + (m/\cos\theta)\right] \times \exp\left[- (\omega t - \pi)/\tan\theta\right] \qquad (3.4)$$

The thyristors T_3 and T_4 are triggered at $\omega t = \pi + \alpha$. The operating circuit for this period, $\pi + \alpha \leq \omega t \leq 2\pi$, is shown in Fig. 3.1 (c). The load current during this interval is given by,

$$i_L(\omega t) = - (V_{Sm}/Z) \sin(\omega t - \theta) - (E/R) + D \times \exp(-Rt/L)$$

where D is a constant and is obtained by putting the initial condition $i_L(\omega t) = I_{L\alpha}$ at $\omega t = \pi + \alpha$ in the above equation. We obtain,

$$i_L(\omega t) = -(V_{Sm}/Z)\sin(\omega t - \theta) - (E/R) + \left[(E/R) + I_{L\alpha} - (V_{Sm}/Z)\sin(\alpha - \theta)\right] \times \exp\left[-R(\omega t - \pi - \alpha)/\omega L\right] \quad (3.5)$$

The normalised load current is given by

$$i_{LN}(\omega t) = -\sin(\omega t - \theta) - (m/\cos\theta) + \left[(m/\cos\theta) + I_{L\alpha N} - \sin(\alpha - \theta)\right] \times \exp\left[-(\omega t - \pi - \alpha)/\tan\theta\right] \quad (3.6)$$

It should be noted that the above eqns. for the load current do not hold good for load impedance angle, $\theta = 90°$ as the term $m/\cos\theta$ becomes infinite for this case. Hence, the expressions for load current for this special case are derived by putting $R = 0$ in the basic differential equations [1]. Thus, for $\theta = 90°$, the expressions for the load current corresponding to eqns. (3.2), (3.4) and (3.6) respectively are easily obtained as

$$i_{LN}(\omega t) = \cos\alpha_{act} - \cos\omega t - m(\omega t - \alpha_{act}) \qquad \alpha_{act} \leq \omega t \leq \pi \quad (3.7)$$

$$i_{LN}(\omega t) = I_{L\pi N} + m(\pi - \omega t), \quad \pi \leq \omega t \leq \pi + \alpha \quad (3.8)$$

and $$i_{LN}(\omega t) = \cos\alpha + \cos\omega t - m(\omega t - \pi - \alpha) + I_{L\alpha N} \qquad \pi + \alpha \leq \omega t \leq 2\pi \quad (3.9)$$

(ii) Inverter Operation : At the instant $\omega t = 0$ in the

first half cycle when the main thyristor pair T_3 and T_4 (Fig. 2.1) is triggered, the source gets connected to the load and the operating circuit is as shown in Fig. 3.2 (a). The load current during this period, $0 \leqslant \omega t \leqslant \emptyset$, is obtained as

$$i_L(\omega t) = (E/R) - (V_{Sm}/Z) \sin (\omega t - \theta) + A.\exp(-Rt/L)$$

where A is a constant and can be evaluated from the initial condition $i_L(\omega t) = 0$ at $\omega t = 0$. We obtain,

$$i_L(\omega t) = (E/R) - (V_{Sm}/Z) \sin (\omega t - \theta) - [(E/R) + (V_{Sm}/Z) \sin \theta] . \exp (-R\omega t/\omega L) \qquad (3.10)$$

By normalising the load current, eqn. (3.10) reduces to

$$i_{LN}(\omega t) = (m/\cos \theta) - \sin (\omega t - \theta) - [(m/\cos \theta) + \sin \theta]. \exp (-\omega t/\tan \theta) \qquad (3.11)$$

Freewheeling starts when the series-aiding thyristor pair T_1 and T_4 is triggered at $\omega t = \emptyset$. The operating circuit for the free-wheeling interval $\emptyset \leqslant \omega t \leqslant \pi$, is shown in Fig. 3.2 (b) . Also, freewheeling takes place through T_2 and T_3 during the interval, $(\pi + \emptyset) \leqslant \omega t \leqslant 2\pi$. The eqn. for load current during this period is given by

$$i_L(\omega t) = (E/R) + B . \exp (-Rt/L)$$

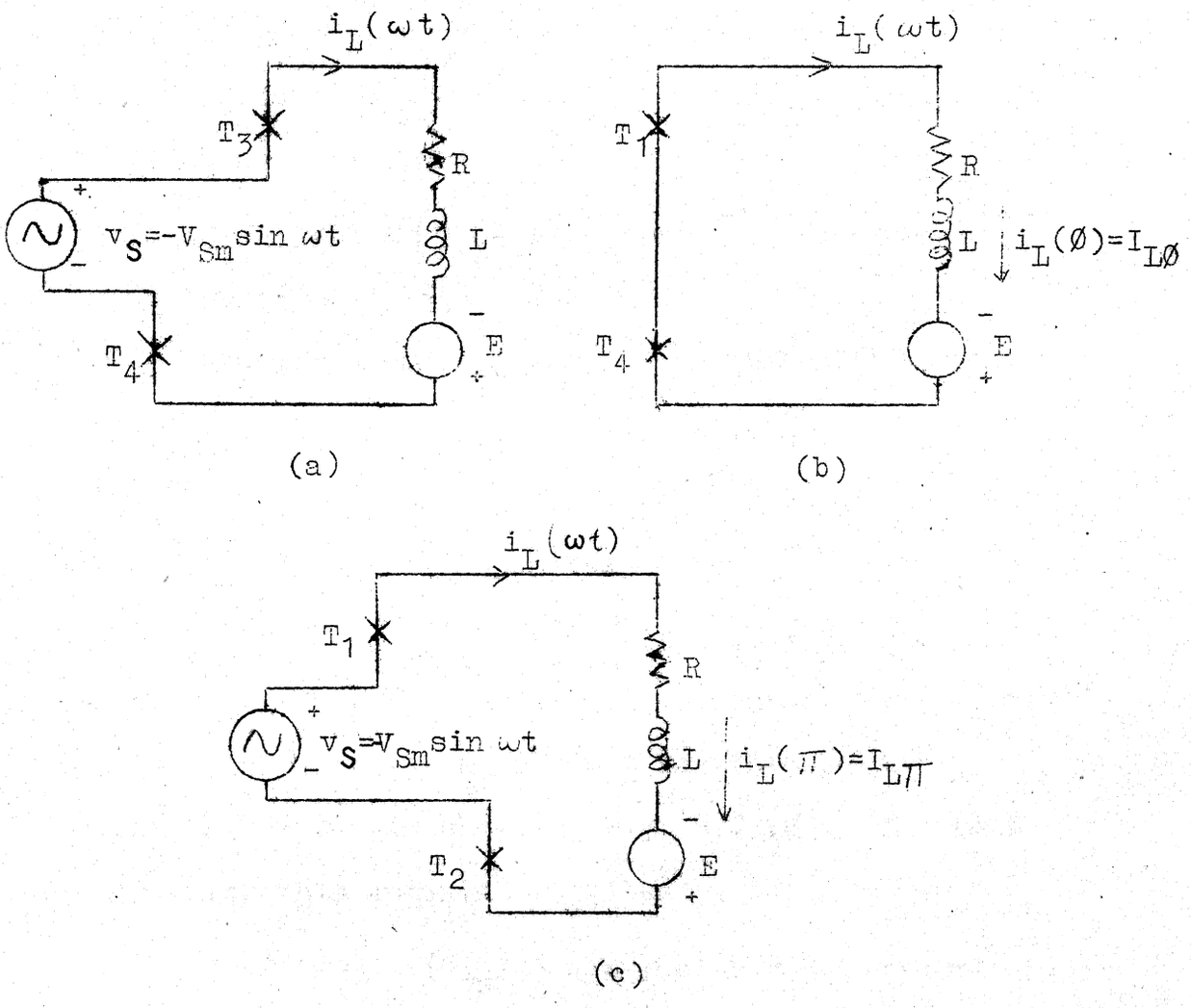

Fig. 3.2 Different operating circuits for inverter operation

(a) Power interval $(0 \leq \omega t \leq \emptyset)$

(b) Freewheeling interval $(\emptyset \leq \omega t \leq \pi)$

(c) Power interval $(\pi \leq \omega t \leq \pi + \emptyset)$

where B is a constant and can be evaluated from the initial condition $i_L(\omega t) = I_{L\emptyset}$ at $\omega t = \emptyset$. Thus the above equation reduces to

$$i_L(\omega t) = (E/R) + [I_{L\emptyset} - (E/R)].\exp[-R(\omega t - \emptyset)/\omega L] \quad (3.12)$$

Rewriting eqn. (3.12) in the normalised form, we have,

$$i_{LN}(\omega t) = (m/\cos\theta) + [I_{L\emptyset N} - (m/\cos\theta)] \times \exp[-(\omega t - \emptyset)/\tan\theta] \quad (3.13)$$

Freewheeling continues till $\omega t = \pi$ when the thyristors T_1 and T_2 are triggered to connect the source to the load. The operating circuit for this period $\pi \leq \omega t \leq \pi + \emptyset$, is shown in Fig. 3.2 (c). The load current during this interval is given by

$$i_L(\omega t) = (E/R) + (V_{sm}/Z)\sin(\omega t - \theta) + D.\exp(-Rt/L)$$

where D is a constant which can be evaluated from the initial condition $i_L(\omega t) = I_{L\pi}$ at $\omega t = \pi$ as follows.

$$i_L(\omega t) = (E/R) + (V_{Sm}/Z)\sin(\omega t - \theta) + [I_{L\pi} - (E/R) - (V_{Sm}/Z)\sin\theta].\exp[-R(\omega t - \pi)/\omega L] \quad (3.14)$$

The normalised load current is obtained from eqn. (3.14) as

$$i_{LN}(\omega t) = (m/\cos\theta) + \sin(\omega t - \theta) + [I_{L\pi N} - (m/\cos\theta) - \sin\theta].\exp[-(\omega t - \pi)/\tan\theta] \quad (3.15)$$

As pointed out in the case of rectification, eqns. (3.11), (3.13) and (3.15) will not hold good when $\theta = 90°$. They are to be drived from the first principles. It can be easily shown that the equations for the load current when $\theta = 90°$ are as given below.

$$i_{LN}(\omega t) = m.\omega t - 1 + \cos\omega t, \quad 0 \leq \omega t \leq \emptyset \quad (3.16)$$

$$i_{LN}(\omega t) = I_{L\emptyset N} + m(\omega t - \emptyset), \quad \emptyset \leq \omega t \leq \pi \quad (3.17)$$

$$i_{LN}(\omega t) = I_{L\pi N} + m(\omega t - \pi) - 1 - \cos\omega t \quad \pi \leq \omega t \leq \pi + \emptyset \quad (3.18)$$

The normalised equations are used to find the load current at different instants in the first cycle of the supply frequency. The flow-charts of the computer programs used to obtain data for constructing the operating diagrams are shown in Fig. 3.3 and 3.4 for rectifier and inverter operations respectively. In addition to the operating diagrams of the converter circuit, the different possible modes of current conduction are obtained using these flow-charts. The classification and identification of different modes is explained in the next section.

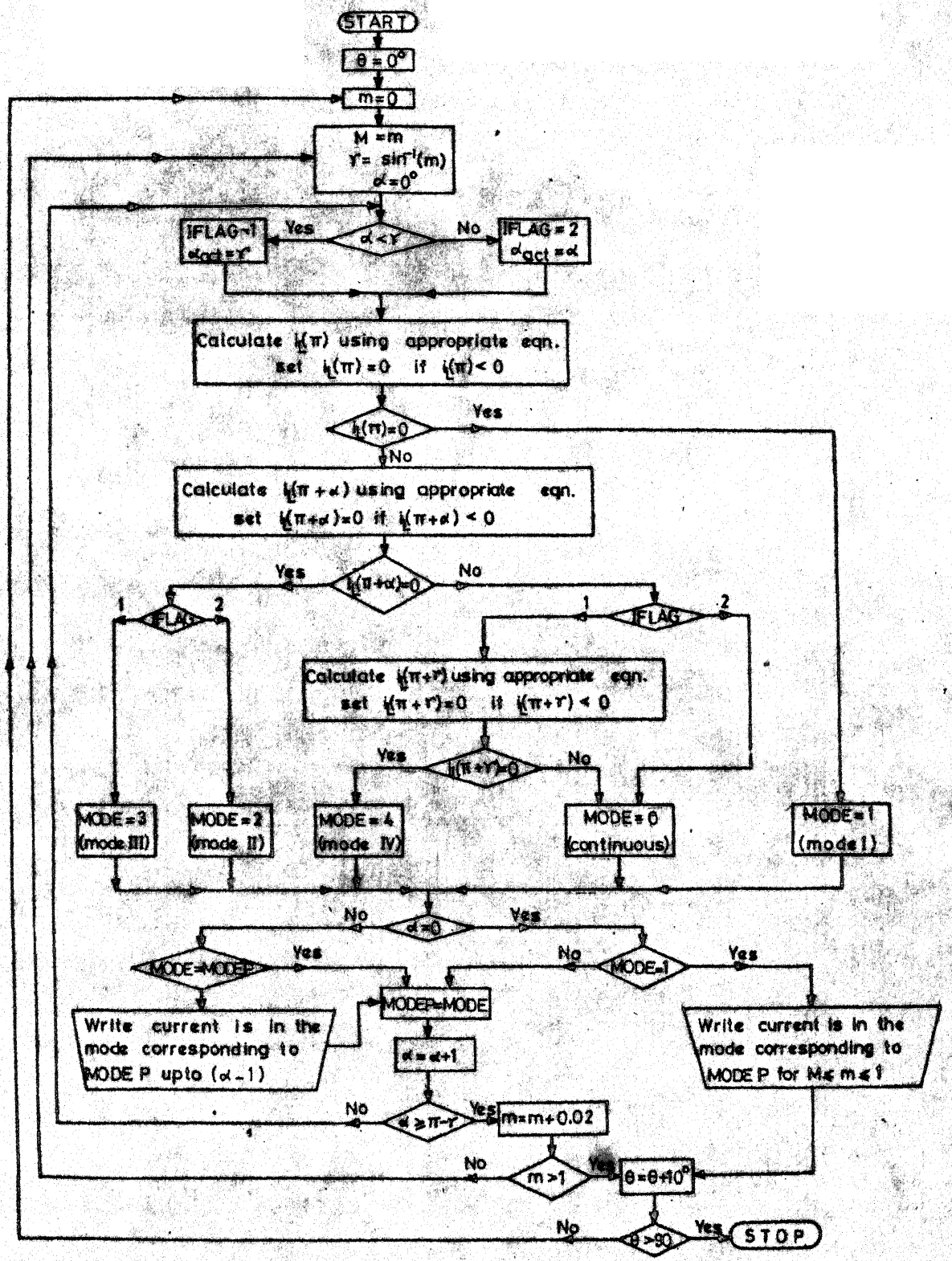

Fig. 3.3 Flow-chart of the computer program to obtain operating diagram and for identification of modes for rectifier operation.

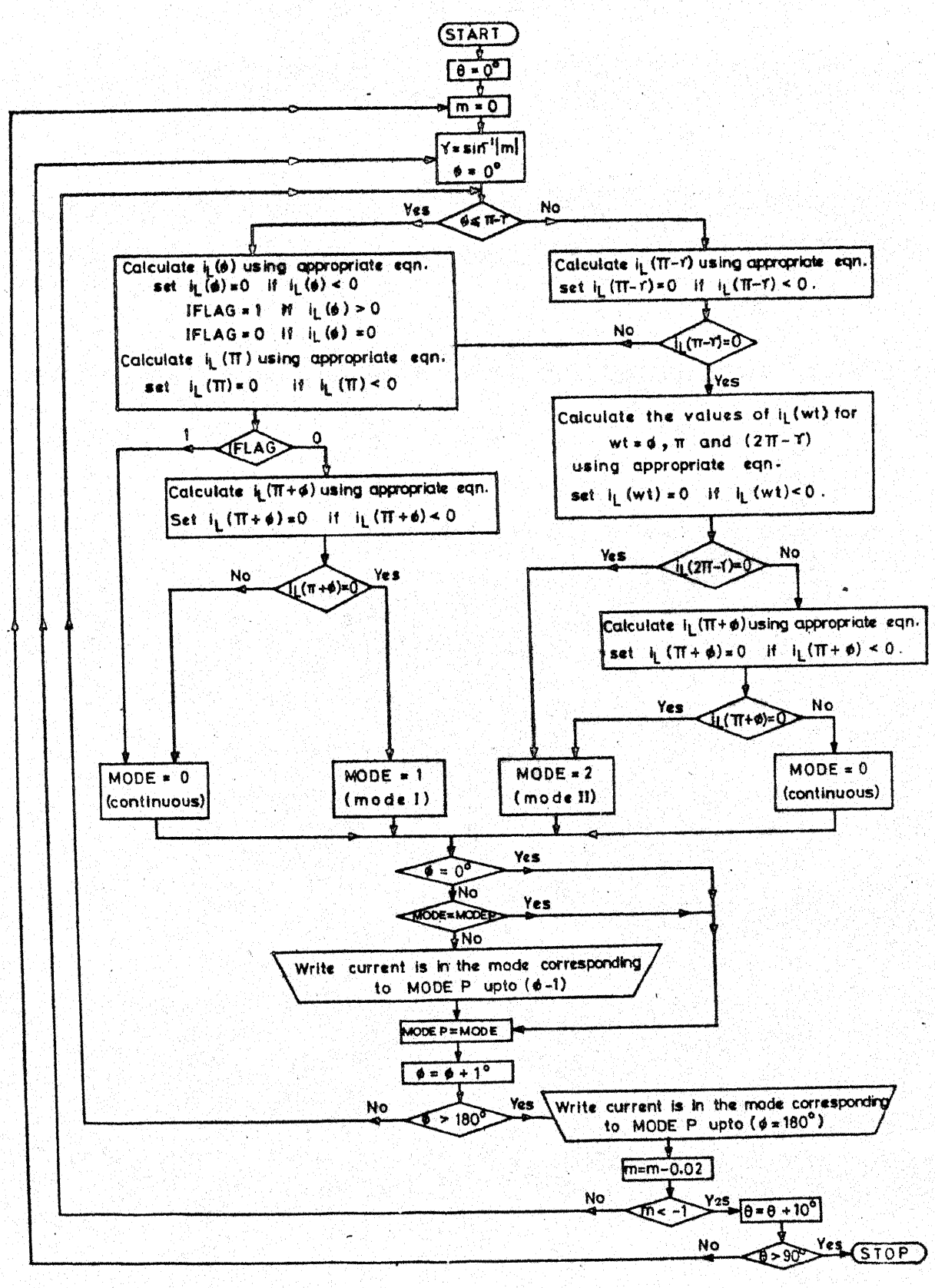

Fig. 3.4 Flow-chart of the computer program to obtain operating diagram and for identification of modes for inverter operation.

3.3 CLASSIFICATION OF MODES AND THEIR IDENTIFICATION ON THE OPERATING DIAGRAMS

3.3.1 Rectifier Operation

Apart from the continuous current mode, there are different modes of operation when the load current becomes discontinuous. The normalised equations for the load current derived in section 3.2.1 are used to construct the operating diagram. Fig. 3.5 shows operating diagram of the fully controlled converter with half-controlled characteristics in the rectifier operation. Operation of the converter is possible for any point below the boundary PQE . For any given values of θ and m, the solid curves in the diagram represent the transition from continuous current operation to discontinuous current operation as α is increased. For any given θ, any point lying below the corresponding curve represents continuous current operation, and any point above represents discontinuous current operation.

As an example, let us consider the load impedance angle $\theta = 60°$ in our discussion. SRE is the transition curve. Any point in the region SRETS represents operation with continuous current. The region SRTS corresponds to $\alpha \leqslant \gamma$ while the region TERT corresponds to $\alpha > \gamma$. In the continuous region the thyristors turn on the instant they

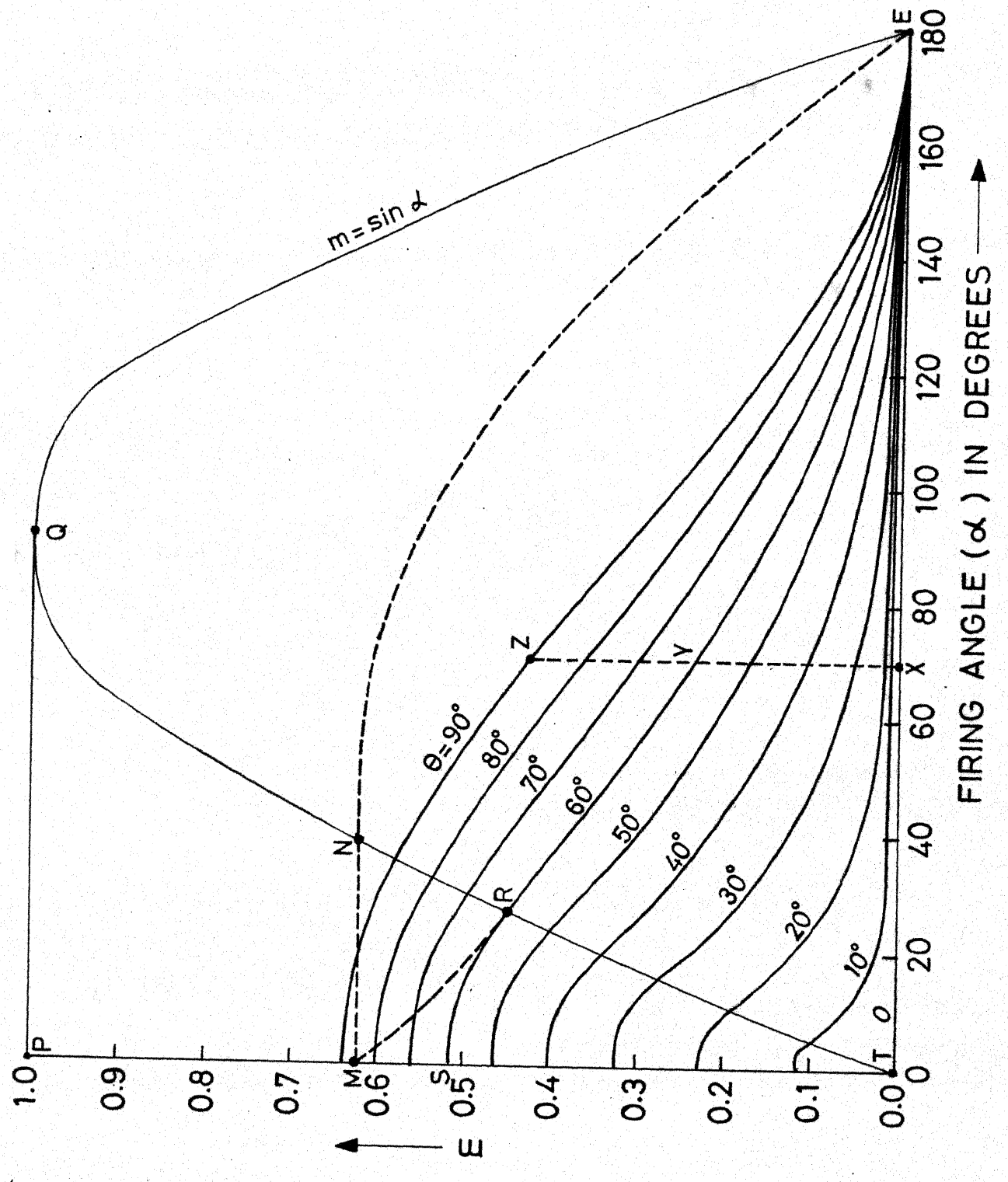

Fig. 3.5 Operating diagram for rectifier operation

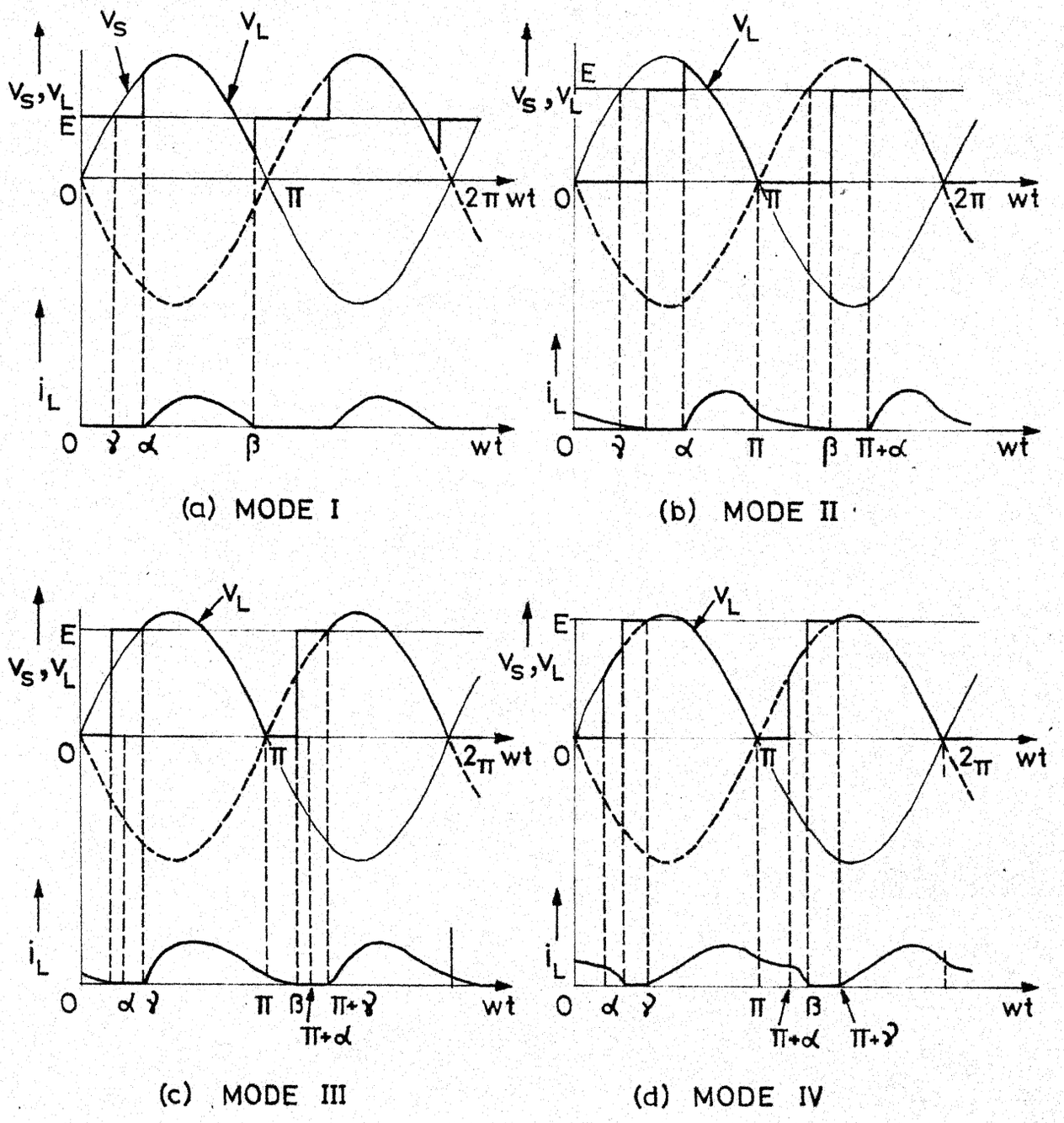

Fig. 3.6 Steady-state voltage and current waveforms for different modes of discontinuous current for rectifier operation.

are triggered whether the triggering is done before or after $\omega t = \gamma$. A point in the region PQERSP represents a condition of discontinuous current operation. There are four distinct possible modes of operation in the discontinuous region.

Mode I : The load voltage and load current waveforms alongwith the supply voltage for this mode are shown in Fig. 3.6 (a). The main thyristor pairs turn-on at α or γ depending on whether $\alpha \geq \gamma$ or $\alpha < \gamma$. Here, γ represents the instant when instantaneous value of the supply voltage equals the load circuit EMF as shown in Fig. 3.6 . This mode is characterised by the load current falling to zero before the next half cycle of the supply voltage starts. This means there is no freewheeling of load current at all and $\beta \leq \pi$. Here, β represents the extinction angle of the load current. This mode is identified by the region PQENMP in the operating diagram (Fig. 3.5) .

Mode II : This mode exists when $\alpha \geq \gamma$. The main thyristor pair turn on when triggered at $\omega t = \alpha$ and freewheeling commences at $\omega t = \pi$ by triggering the respective series-aiding thyristors. The load current falls to zero before the other main thyristor pair is turned on at $\omega t = \pi + \alpha$ in the next half cycle, i.e., $\beta \leq \pi + \alpha$ for this mode. The associated waveforms are shown in

Fig. 3.6 (b) and the region NERN represents this mode in the operating diagram of Fig. 3.5 .

Mode III : This mode may occur for $\alpha < \gamma$. Though triggered earlier the main thyristor pair turn on only at $\omega t = \gamma$. However, the load current falls to zero before the other main thyristor pair is triggered at $\omega t = \pi + \alpha$ in the next half cycle as depicted in Fig. 3.6 (c) , This mode is identified by the region MNRM in the operating diagram as shown in Fig. 3.5 .

Mode IV : The different waveforms for this mode are shown in Fig. 3.6 (d) . The sequence of operations are same as those in mode III except that load current is present when the main thyristor pairs are triggered at α in each half cycle. Hence, these thyristors turn on and the source gets connected to the load at that instant. However, the load current falls to zero before the ac supply voltage reaches the load circuit EMF level. Thus, $(\pi + \alpha) < \beta < (\pi + \gamma)$ for this mode. In the operating diagram (Fig. 3.5), this mode is represented by the region MRSM.

3.3.2 Inverter Operation

Fig. 3.7 shows the operating diagram for inverter operation of the fully controlled converter with half-

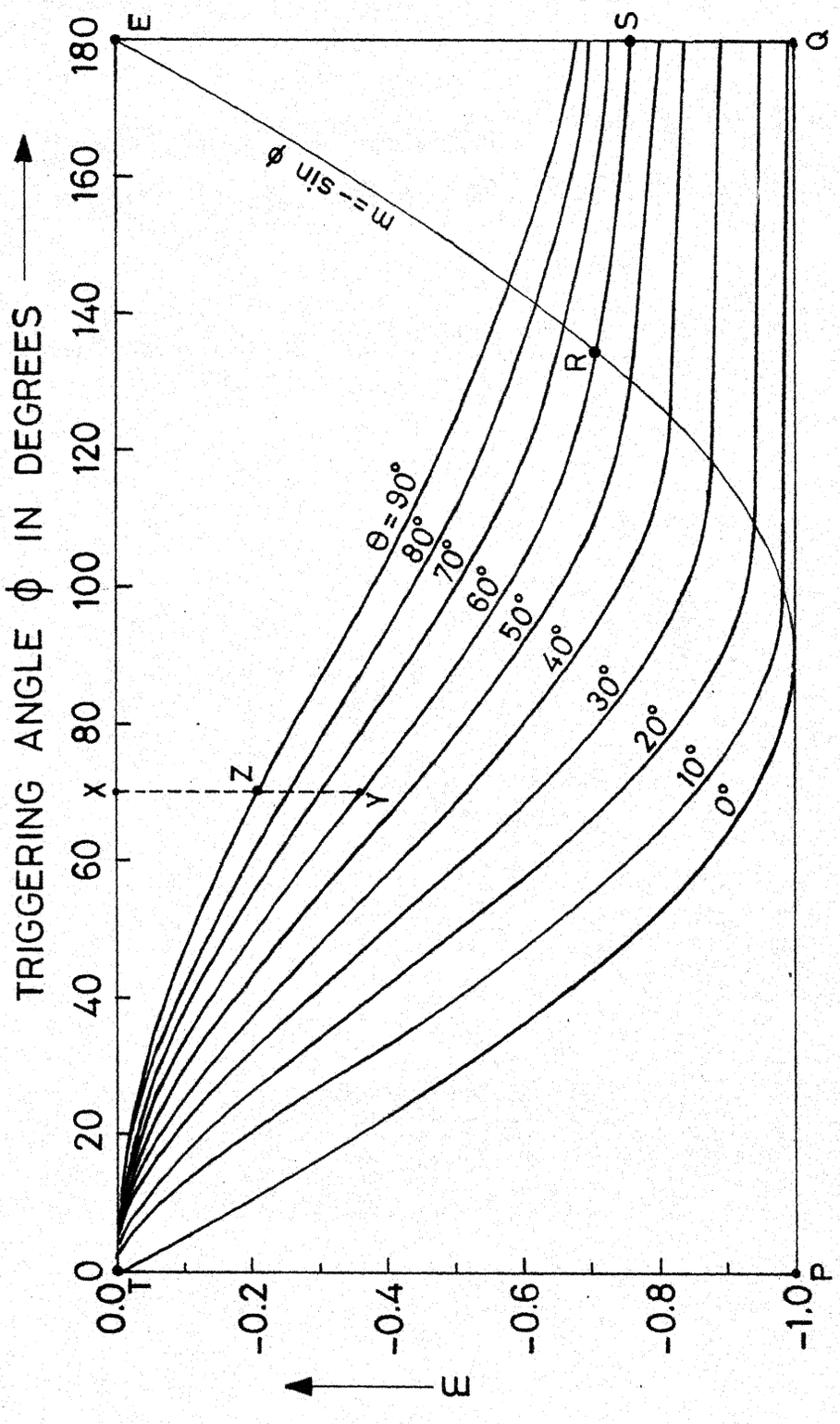

Fig. 3.7 Operating diagram for inverter operation

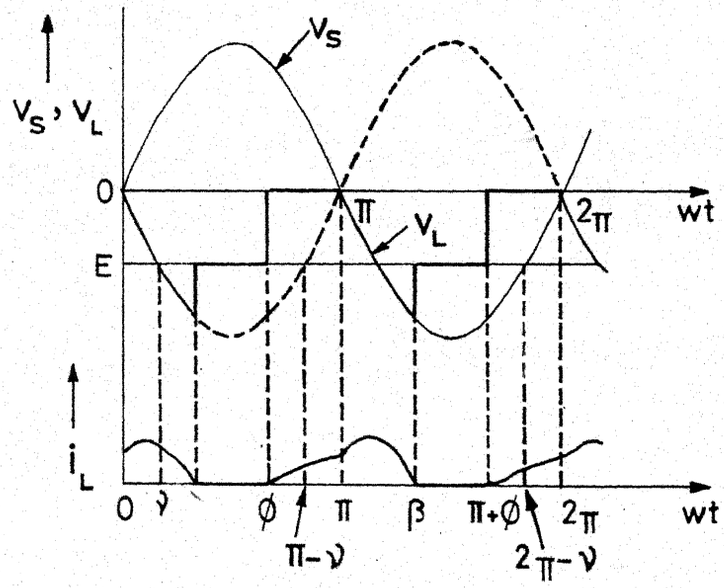

(a) MODE I

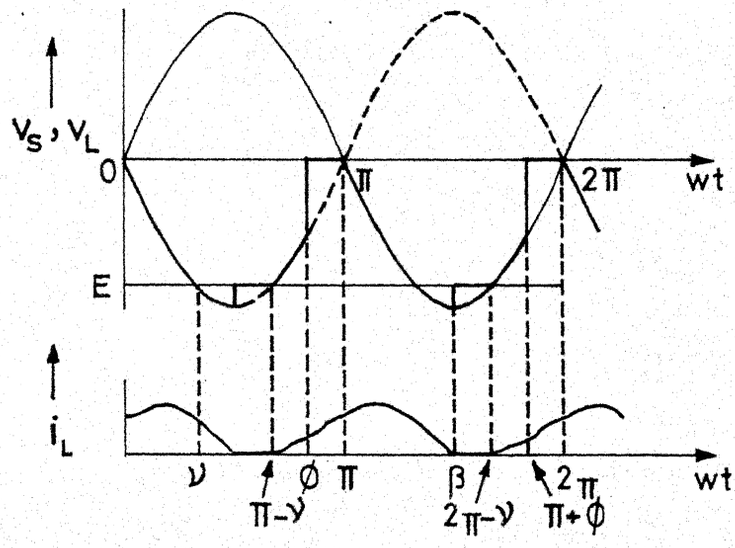

(b) MODE II

Fig. 3.8 Steady state voltage and current waveforms for different modes of discontinuous current for inverter operation.

controlled characteristics. Inverter operation is possible at any point inside the region TEQP. As in the case of rectifier operation for a given θ, any point lying below the corresponding curve represents continuous current operation, and any point above represents discontinuous current operation. As an example, let us again consider $\theta = 60°$ in our discussion. TRS is the separating curve.

Any point in the region TRSQPT represents a condition of continuous current operation while that in the region TESRT represents a condition of discontinuous current operation. In the discontinuous current region, there are two distinct possible modes.

Mode I : The associated waveforms for this mode are shown in Fig. 3.8 (a). The load gets connected to the source at $\omega t = 0$ when the main thyristor pair (T_3 and T_4) is triggered. However, the load current falls to zero before $\omega t = \emptyset$ when the freewheeling is initiated by triggering the corresponding series-aiding thyristor pair. Freewheeling continues till $\omega t = \pi$ when the other main thyristor pair (T_1 and T_2) is triggered to connect the load to the source and the process is repeated. This mode is identified by the sub-region TERT in the operating diagram as shown in Fig. 3.7 .

Mode II : This mode is possible for larger values

of ϕ when $\phi > (\pi - \gamma)$. The main thyristor pair (T_3 and T_4) is turned on at $\omega t = 0$ and current flows to the load from the source. The load current falls to zero before $\omega t = \pi - \gamma$. However, these thyristors are forward biased at $(\pi - \gamma)$. Since the thyristors are triggered by 180°-stretched pulses, they turn on once again in the same half cycle at $\omega t = (\pi - \gamma)$ thereby connecting the source to the load. Thus, some load current is present at $\omega t = \phi$ when the respective series-aiding thyristor pair is triggered so as to provide freewheeling path for the load current. The extinction angle $\beta < (2\pi - \gamma)$. This mode is demonstrated in Fig. 3.8 (b) while in the operating diagram of Fig. 3.7 the region ERSE represents this mode.

3.4 MINIMUM INDUCTANCE ESTIMATION

It may be desirable to insert additional inductance in the load circuit to avoid discontinuous current operation. An analytical method [14] describes calculation of minimum inductance necessary to achieve continuous current operation in conventional fully controlled converter system when the load resistance is negligible. The same method may be applied for minimum inductance estimation in case of fully controlled converter with half-controlled characteristics. The load resistance, however, cannot be neglected in some applications where the

converter is used for the control of a small dc machine. A graphical method for estimating the minimum inductance necessary to achieve continuous current operation is presented for the fully controlled converter with half-controlled characteristics taking the load resistance also into account. This graphical procedure is along the lines given in the reference [13] .

For example, consider the operating diagram for rectifier operation of the converter as shown in Fig. 3.5 . For certain triggering angle, α indicated by the point X in the diagram, the ordinate XY gives the normalised value of the load circuit EMF, E/V_{Sm} at the limit of continuous current operation with $\theta = 90°$. The ordinate XZ gives the normalised value of the average output voltage, V_{LAV}/V_{Sm}, at the limit of continuous current operation since the average voltage across a pure inductor ($\theta = 90°$) is zero. Therefore, for the triggering angle, X, the ordinate YZ equals the normalised value of the average voltage drop, $I_L R/V_{Sm}$, across the load circuit resistance. This is represented by point A in the plane whose co-ordinates are α and $I_L R/V_{Sm}$ as shown in Fig. 3.9 . Similarly, the normalised average voltage drop across the resistance at the limit of continuous current operation for other values of triggering angle

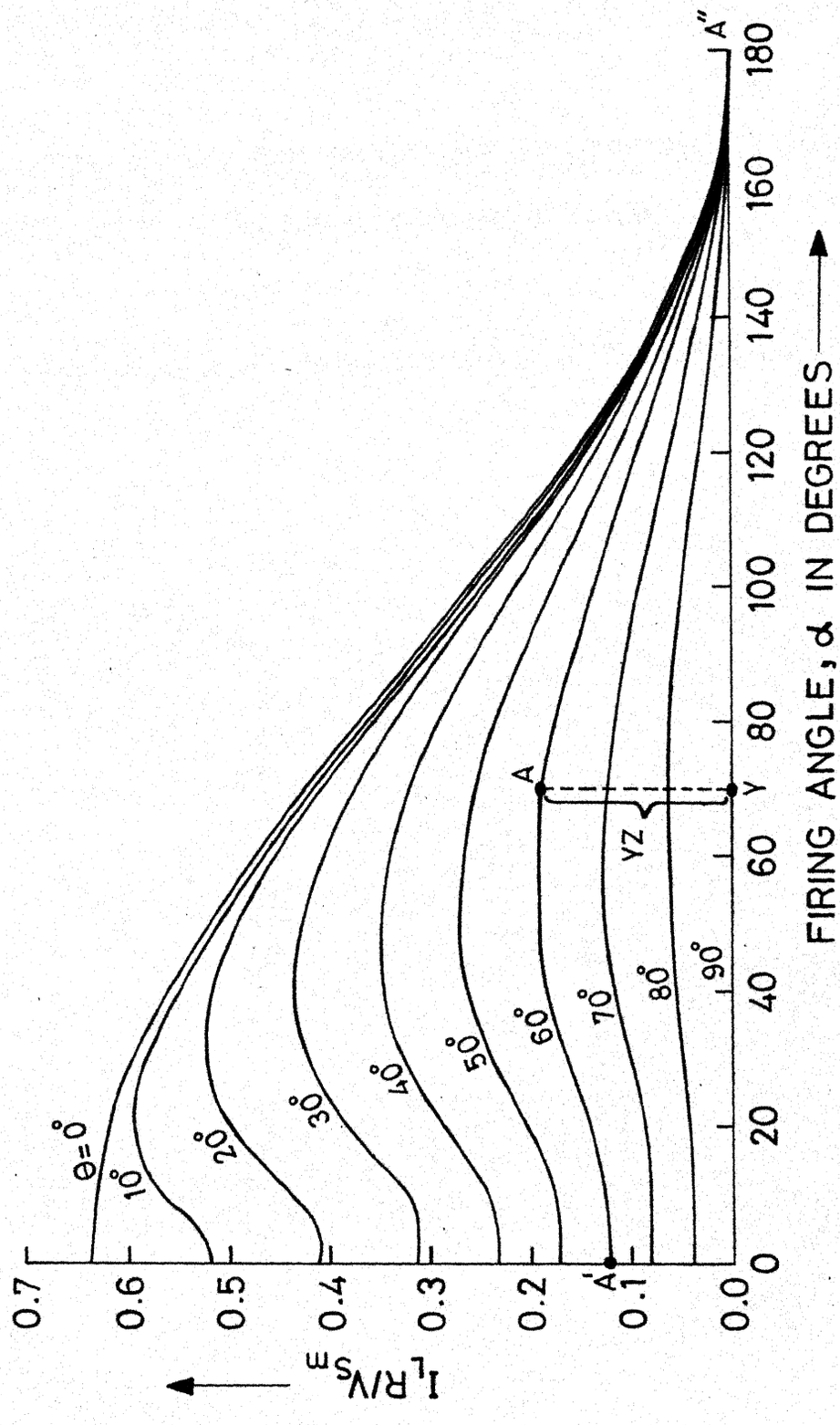

Fig.3.9 Minimum load impedance angle for continuous current in rectifier operation.

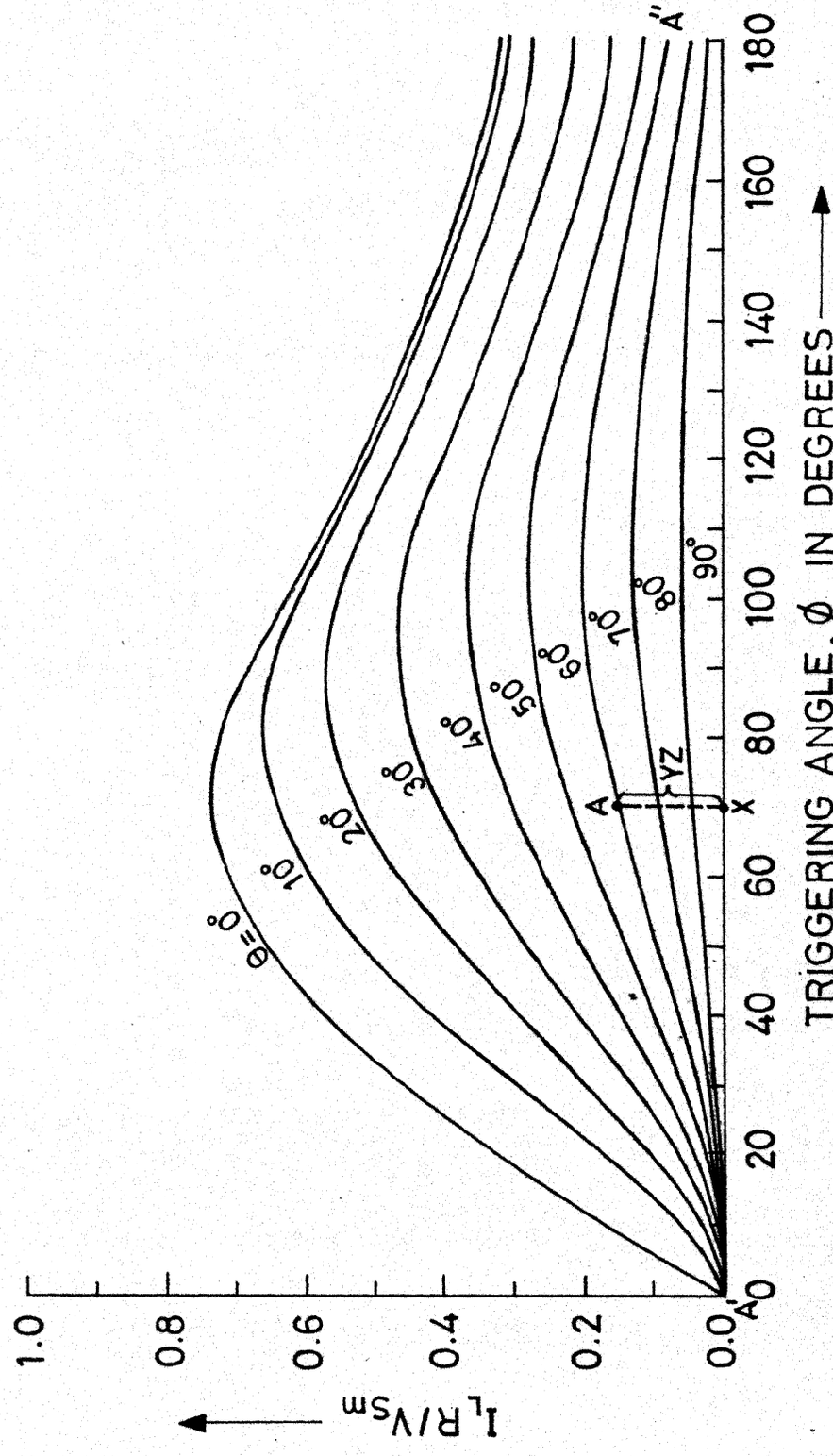

Fig. 3.10 Minimum load impedence angle for continuous current in inverter operation.

result in the curve $A' A A''$ in Fig. 3.9 . Using a similar procedure the curves in Fig. 3.9 for other values of load impedance angle, θ, are obtained. The same method when used with the operating diagram shown in Fig. 3.7 for inverter operation result in the curves shown in Fig. 3.10 . The curves in Fig. 3.9 and 3.10 provide information regarding minimum inductance estimation for continuous current operation. As an example, let us consider the rectifier operation of the converter on a dc motor whose armature resistance, R_m , and armature inductance, L_m , and hence armature circuit load angle, θ_m , are known. For a particular firing angle, α , and back EMF , E ,in the operating region of the motor, the load current may become discontinuous which is known from the operating diagram of Fig. 3.5 . In that case, the average load current is calculated and the normalised average resistive drop $I_L R/V_m$ is found out. Let the corresponding operating point when located on the diagram of Fig. 3.9 fall on the curve $A' A A''$. Since this curve represents the normalised value of average resistive drop at the limit of discontinuous current operation for $\theta = 60°$, it means the minimum value of θ for continuous current operation amounts to 60°. If $\theta_m < 60°$, then the additional inductance, L_{add}, to be connected in series with the motor armature to make the load current just continuous amounts to

$$L_{add} = (\tan 60^\circ - \tan \theta_m) \cdot R_m/\omega \quad .$$

This gives the value of the additional inductance for a particular operating point. If the region of operation of converter-fed motor is known apriori for both rectification and inversion, the additional inductance can be calculated for different operating points in the entire region following the above procedure. Choosing the maximum value of these additional inductances would then assure converter operation in the continuous current mode.

3.5 CONCLUSIONS

The single-phase fully controlled converter with half-controlled characteristics is potentially suitable for the control of not only traction drives but also industrial drives owing to improved performance characteristics. The industrial drives may also consist of separately excited dc motors. The load current is likely to become discontinuous more with these motors. Operating diagrams are established for the fully controlled converter with half-controlled characteristics for both rectifier and inverter operations. Different possible modes of discontinuous current operation of this converter are recognised and identified on the operating diagrams. The single-phase converters are generally used to control

industrial drives of lower ratings upto about 7.5 kw where the motor resistance may not be negligible. A graphical procedure making use of the operating diagrams is described in this chapter to calculate the minimum inductance necessary to achieve continuous current operation.

CHAPTER IV

REACTIVE POWER COMPENSATION IN INDUSTRIAL POWER SYSTEMS

4.1 INTRODUCTION

The industrial load accounts for the maximum power consumption in the power system. Unlike household consumers, the industrial load comprising of mostly induction motors draws large amount of lagging reactive power from the power supply system. Transformers used in power transmission and distribution network also consume reactive power owing to magnetizing current drawn by them. The induction furnaces which are widely used in industries also draw large amount of lagging kVAR. The household consumers also require lagging kVAR, however small it may be compared to that of the bulk consumers, due to the extensive use of fluorescent lights, fans and various other appliances using fractional horse power ac motors. Thus, the reactive power requirement on the power system adds up to a large amount. This wattless power causes the system to operate at low power factor. There are many disadvantages as pointed out in Chapter I if the supply power factor is low.

These disadvantages can be overcome to a large

extent if the power factor is improved externally. In fact, it is a practice since the inception of ac power transmission to install reactive power compensators for power factor improvement. The reactive power compensators are external devices which supply and compensate the lagging reactive power consumed by the load thereby relieving the burden on the ac supply. These compensators are also known as power factor correcting devices. Obviously, these reactive power compensators are connected across the load terminals to relieve the transmission lines also from the excess current. Hence, they are called Shunt compensators.

With the passage of time, the shunt compensators have gone through several modifications with the rapid developments in the power system as regards the increase in the operating voltage level and complex interconnections of large networks. In what follows, a review of such reactive shunt compensators has been presented.

4.2 SHUNT REACTIVE POWER COMPENSATORS

4.2.1 Fixed Capacitor Banks

Shunt capacitors were first employed for power factor correction in the year 1914 [4]. The leading current drawn by the shunt capacitors compensates the lagging current drawn by the load. They are located at the service entrance of large industries or at the sub-

station supplying an industrial area. Initially, the use of capacitors was limited due to high cost per kVAR, large size and weight. However, over the years , capacitor usage has increased phenomenally due to reduction in selling price, improved design and manufacturing methods resulting in small size and weight and above all, better understanding of the system benefits that result from their use.

The selection of shunt capacitors is dependent on many factors the most important of which is the amount of lagging kVAR taken by the load. In the earlier days, this posed no problem since the reactive power requirements at a load bus could be very accurately determined as there were no complex interconnections of networks. Thus, the improvement in Power factor could be successfully achieved with the use of fixed shunt capacitors. However, with this interconnection of large power systems, the power flow at a particular substation also depends on loads at other buses of the system and the variation of kVAR occurs over a wide range. Thus, a fixed capacitor bank may lead to either over-compensation or under-compensation resulting in lower power factor in the ac power supply system.

4.2.2 Switched Capacitors

The wide range of variation in lagging kVAR on

the system has caused the necessity for dynamic VAR compensation, that is, controlled compensation of the reactive power to achieve desired power factor at all load conditions. This is achieved using switched capacitors. Depending on the total kVAR requirement, a number of capacitors are used which can be switched into or switched out of the system individually. The control is accomplished by continuously sensing the load kVAR. If more compensation is required, then the required number of capacitors are switched into the circuit so as to take the extra leading kVAR and, conversely, the required number of capacitors are switched out if the load kVAR falls. The smoothness of control is solely dependent on the number of capacitor switching units used. A very fine control over the power factor can be achieved at the expense of economy by using a large number of small such units. The switching is conventionally accomplished using relays and circuit breakers. One such method uses a master control relay in addition to a time-delay relay for each unit [4] . For one-step automatic control the master relay energizes the closing element of the time-delay relay, and if the master-relay contacts stay closed for the time required for the time-delay relay contacts to make, then the operating circuit is energized and the capacitor breaker closes. A similar process in reverse trips the capacitor breaker. For more accuracy and

reliability, multi-step control [4] is preferred. However, these methods using mechanical switches and relays invariably suffer from the drawbacks of being sluggish, unreliable, introducing switching transients and requiring frequent maintainance. With the advent of high power solid state devices, thyristors have replaced the mechanical switches. Sophisticated electronic circuits have made the system highly reliable. Thyristors switching of static capacitors has made it possible to achieve virtually continuous control of reactive power generation on a large scale [15] . Each small unit of capacitors is switched on and off individually using thyristors as switching elements as shown in Fig. 4.1 (a). The switching-on transients are avoided by selecting the switching-on instant at the time when the network voltage corresponds in magnitude and polarity to the capacitor voltage. Switching-off transients are not a problem since turning-off of the thyristors occurs at the next current zero after the removal of the gate trigger. The capacitor then remains charged to either positive or negative peak value of the network voltage and is prepared for a new switching-on which will be free from transients. The time required for switching-on or off is made up of the time to detect the magnitude of the desired change in reactive power (one-half cycle), plus a variable

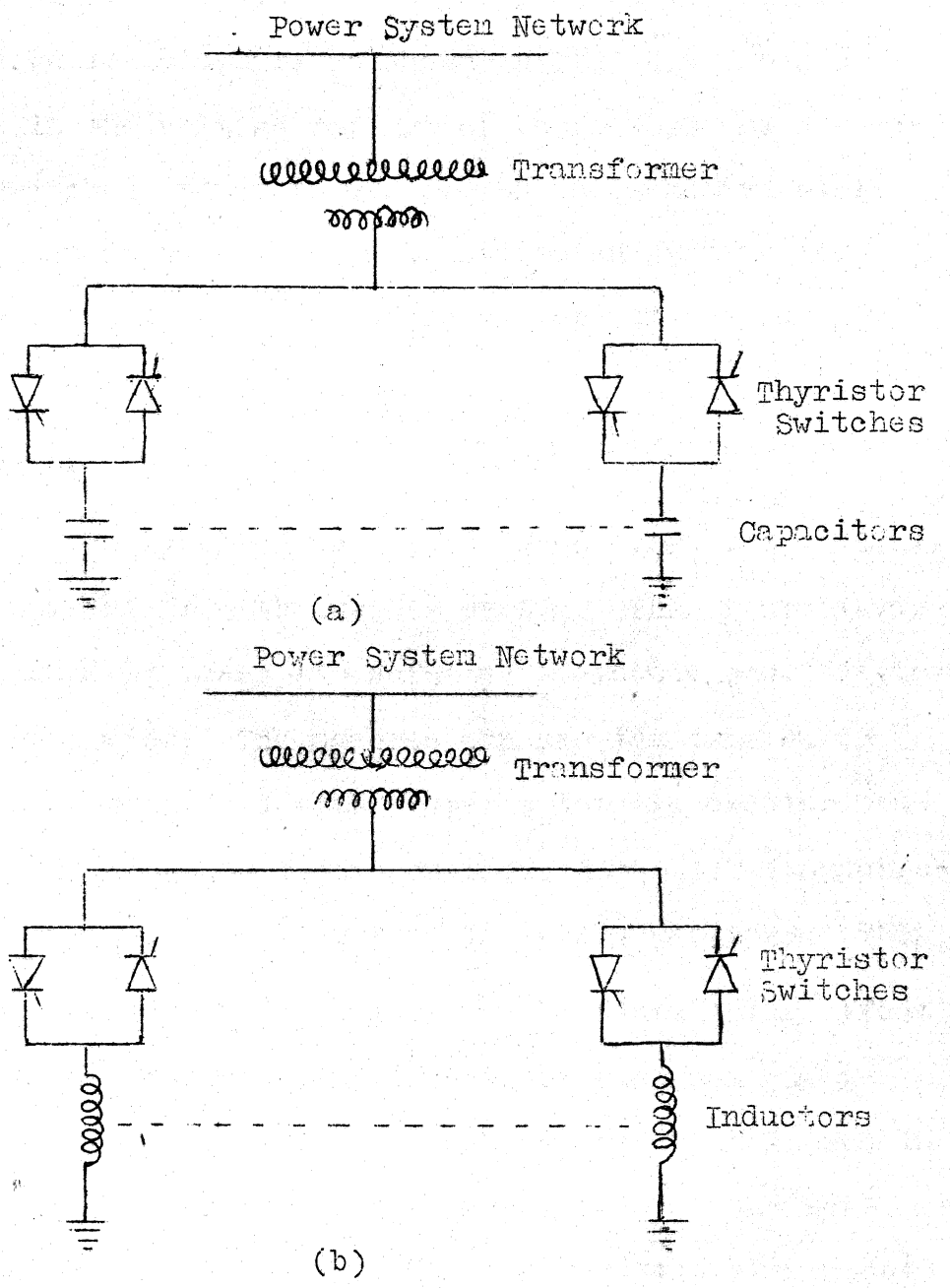

Fig. 4.1 (a) Thyristor-Switched Capacitors.

(b) Thyristor-Switched Inductors.

time (maximum of one-half cycle) waiting for suitable switching conditions. Switching-on or off is, therefore, achieved within one cycle of power frequency. Usually, a step-down transformer, as shown in Fig. 4.1 is necessary to suit the voltage ratings of thyristors and capacitors. Switched inductors working on the same principle are also extensively used in transmission systems for direct compensation of the charging capacitance of a line [15] .

4.2.3 Synchronous Condenser

The synchronous machine when over-excited draws leading current from the supply system. This characteristic particularly makes it useful as a dynamic power factor correction device. The machine can provide continuous kVAR balance when used with proper automatic exciter control system. The short time overload capacity of synchronous compensator is larger than that of capacitors. The synchronous condenser has also greater stabilizing effect upon system voltages. However, it has also many drawbacks as compared to the shunt capacitors. The losses in the synchronous condensers are much greater. For synshronous condensers the full-load losses vary from about 1½ percent to 3 percent of the kVA rating whereas for capacitors the losses are about 1/3 percent of the kVA

rating [4] . The capacitors are more effective since they lend themselves to distribution at several locations closer to the load throughout the network. It will be very costly to distribute small synchronous condensers throughout the system. The kVAR rating of a capacitor installation can be easily changed with the variation in loads and system requirements day by day, which is impractical with synchronous condensers. The failure of a synchronous condenser compared to a single unit in a bank of capacitors is less likely to occur. However, any such failure in a sychronous condenser completely affects entire ability to produce kVAR. This is not so in capacitor banks since there are several other capacitors in a bank even if a particular unit fails. Synchronous condensers increase the short-circuit current of a system and thus higher rating breakers are required. The response of the synchronous condenser is slow due to the inherent mechanical inertia.

4.2.4 Static Reactor Compensator

The aim to achieve fine control over the entire kVAR range as in case of the synchronous condenser without sacrificing the advantages of static capacitors has been fulfilled by the development of static reactor compensator. This essentially consists of a controllable reactor in parallel to a shunt capacitor as shown in Fig. 4.2 . By

choosing proper values for the capacitor and the inductor, it is possible to achieve smooth and stepless control of kVAR from lagging to leading over a wide range to compensate for the wide variations in the load kVAR. This is accomplished by continuous control of the effective fundamental reactance of the inductor. Since there is greater requirement for leading kVAR, preferably a number of capacitors are switched in steps to provide a wide range of leading kVAR [16] . The controllable reactor can be realized using different methods some of which are listed below.

(a) Reactors with dc current-controlled saturation : The current in a reactor can be controlled by a direct current fed into a control winding mutually coupled to the main reactor winding. In power systems, a transformer is usually preferred to ordinary reactor. The alternating current in the primary is controlled by a direct current fed into secondary control winding coupled to normally delta-connected secondary. The arrangement is shown in Fig. 4.3 . By varying the control current, the primary alternating current can be controlled from practically zero when the cores are unsaturated to a maximum at fully saturated cores [15] . The primary is connected to the high voltage power system without an auxiliary transformer. The dc control current thus changes the effective reactance posed to the power

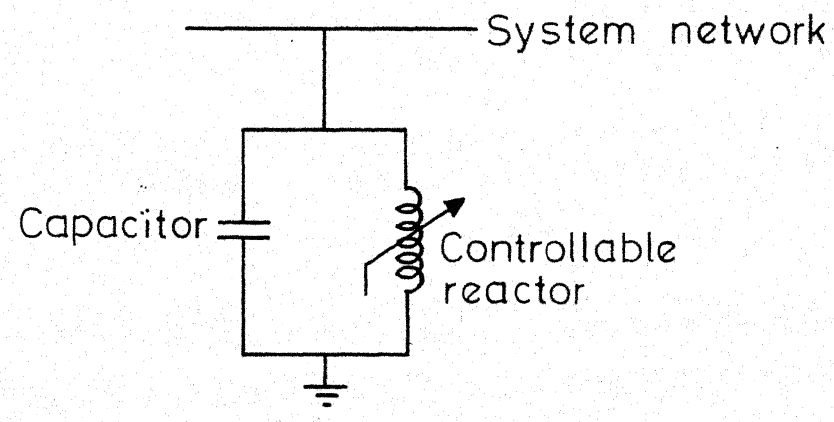

Fig. 4.2 Basic static reactor compensator

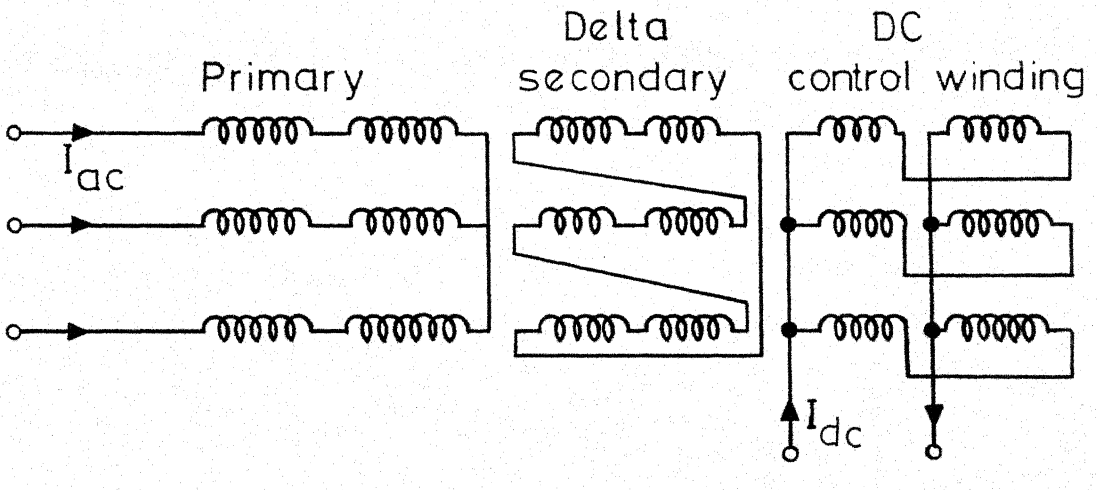

Fig. 4.3 Reactor using dc current-controlled saturation.

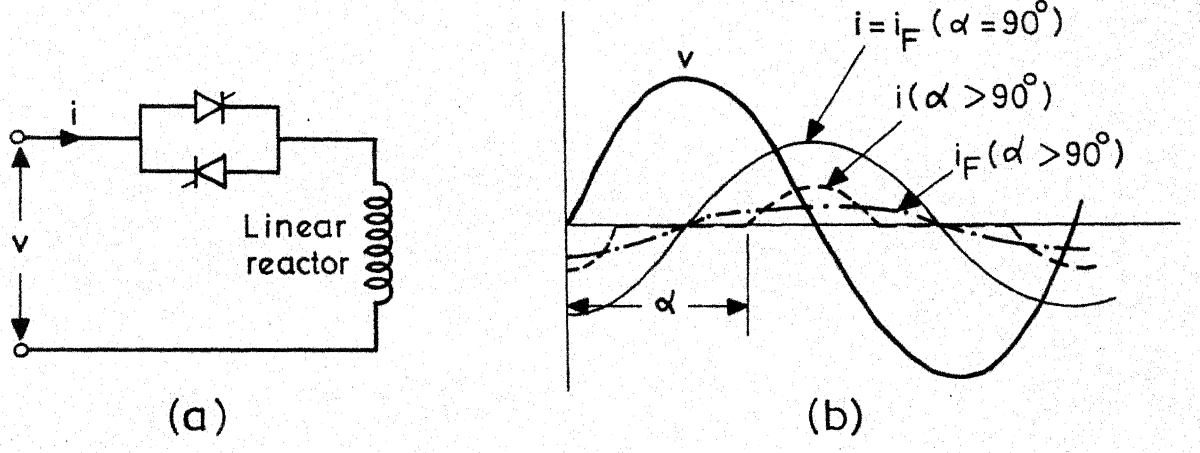

Fig. 4.4 Thyristor-controlled reactor
(a) Line diagram
(b) Voltage and current waveforms.

system [17] . Though the operating principle is very simple, the transient behaviour of the reactor with dc current-controlled saturation is very complicated and cannot be characterised by a simple time constant. However, with special techniques [15] the time for changing the primary currents by control actions can be minimized to a fraction of a second. In addition, a dc source, usually a thyristor rectifier of relatively low power rating, is necessary for its operation.

(b) Thyristor-controlled shunt reactors : With the increase in the size and complexity of power system, fast reactive power compensation has become necessary in order to maintain the stability of the system. The thyristor-controlled shunt reactors make it possible to reduce the response time to a few milliseconds. Thus, reactive power compensators utilizing the thyristor-controlled shunt reactors are becoming increasingly popular. The basic operating principle of a thyristor-controlled reactor is illustrated in Fig. 4.4 . A reactor operating in its linear region is connected to the ac system in series with back-to-back connected thyristors as shown in Fig. 4.4 (a). The inductive reactive current is continuously controlled by phase-control of the thyristors, one being fired in the positive half cycle of the supply frequency and the other in the

negative half cycle. Thyristors operating in this mode are known as ac controllers [1]. Fig. 4.4 (b) shows the supply voltage and current waveforms for two different firing angles. For firing angle, $\alpha = 90°$, maximum current is drawn from the supply. If the firing instants of the thyristors are delayed beyond 90° , current becomes discontinuous. This is illustrated by the dotted line in Fig. 4.4 (b). The conduction interval decreases as the firing angle, α increases and finally no current flows for $\alpha = 180°$. The fundamental component of the current which is shown by chain curve in Fig. 4.4 (b) , however, always lags the voltage by 90° and it is this component which accounts for the effective reactive power compensation. Due to the discontinuous conduction, the current has a certain finite harmonic content. A detailed treatment to static shunt reactor compensator utilizing thyristor-controlled reactor is presented in section 4.3.2 . Normally for linear operation over a wide range, gapped core type reactors are used [15] . Economics show that a step-down transformer is necessary to connect the reactors and the thyristors to the low voltage winding. The transient response time of thyristor-controlled reactors is within one cycle of power frequency [15] .

(c) Thyristor-controlled high-impedance transformer : Since a transformer is necessary for connection of thyristor-controlled reactors, it is economical to construct a transformer with high leakage reactance and to control the primary current by phase-control of thyristors connected to the secondary windings, thus eliminating separate reactors [15]. The transformer is designed for linear magnetic characteristic with 100% leakage reactance between primary and secondary windings [16]. The primary winding is star-connected with the star point grounded. The secondary winding connection and its voltage are determined such as to match to voltage and current ratings of the thyristors [16]. Controlling the secondary current by phase-control inherently introduces harmonics in the current of the compensator under partial loading conditions. Only at full load (corresponding to $\alpha = 90°$) and no load ($\alpha = 180°$) are the harmonics zero. The actual harmonic content, however, depends on the type of connection of both secondary windings and thyristors. Table 4.1 gives a brief summary of the properties of three different connections. They are

(1) The secondary winding as well as the thyristors are star-connected. The star points are inter-connected and grounded.

(2) Star connection of the secondary windings and thyristors, but there is no connection between star points.

(3) The secondary winding as well as the thyristors are delta-connected.

Table 4.1

Connection	Thyristor rating		Maxm. harmonic currents in %				
	Voltage X $\sqrt{2}/\sqrt{3}$	Current r.m.s	3	5	7	9	11
1	1.0	1.0	13.7	5.0	2.55	1.55	1.0
2	1.5	1.0	-	9.5	3.4	-	1.7
3	$\sqrt{3}$	$1/\sqrt{3}$	-	7.6	3.85	-	1.5

The triplen harmonics in connection (1) can be eliminated by providing an additional delta-connected tertiary winding closely coupled to the secondary. Thus, connection (1) is the most suitable one as regards harmonic generation and thyristor rating though with some extra cost. Where even the remaining higher order harmonic content cannot be tolerated, it can be further reduced by using additional filters connected to the delta tertiary winding [16].

4.3 APPLICATIONS OF STATIC THYRISTOR-CONTROLLED SHUNT COMPENSATORS FOR LOAD COMPENSATION

4.3.1 Fundamentals of load compensation

Due to their fast response and very smooth VAR control, there has been a rapid increase in the number of static thyristor-controlled shunt compensators in industrial and utility systems for load compensation, transmission line voltage regulation and other purposes [16, 18]. In industrial power systems load compensation means cancellation of the reactive power demand of large and fluctuating industrial loads such as electric arc furnaces, induction furnaces, rolling mill drives used in steel industries etc., and to balance the real power drawn from the three phases of the ac supply system. In simpler terms, load compensation involves two distinct acts; one being power factor correction and the other load balancing in the three phases. If both are carried out, they determine together the total reactive power needed for compensation.

Any 3-phase unbalanced linear steady state load can be compensated by three appropriate reactive impedances (capacitive and inductive) connected between the three phases [18]. The load on a power system varies with time which can be represented by a series of "steady state" impedances at discrete time instants close to one another.

The compensation, therefore, requires variable reactances that can be adjusted according to the load variation.

4.3.2 Practical Approach

Under steady-state conditions the compensating susceptances can be expressed in terms of the load impedance [18]. Since the load impedances are directly measurable, the compensating susceptances can always be determined by direct use of appropriate analytical expressions. However, the parameters of a transmission network in which changes both in loads and generations can take place frequently cannot be known accurately. Hence, for effective dynamic compensation of kVAR in power systems, the following are required:

(i) rapidly variable compensating susceptances

(ii) fast measurement of load parameters

(iii) rapid signal processing and fast-acting feedback control.

A static shunt compensator using thyristor-controlled reactor (TCR) is capable of meeting all the three desired requirements and, hence, has found extensive use.

Realization of variable reactances : The different schemes for realizing variable reactance (or susceptance)

have been outlined in section 4.2 . The basic scheme using a fixed capacitor in parallel with a TCR is illustrated in Fig. 4.5 .

Since the capacitor draws a fixed amount of current from the source, the resultant current drawn from the source is effectively controlled by controlling the conduction interval of thyristor switches using phase-control. The supply voltage and inductor current waveforms are shown in Fig. 4.6 for a particular value of firing angle, α . The range of variation of triggering angle, α , is from 90° to 180° .

The current, i_{TCR} through the inductor when thyristor T_1 is fired at delay angle, α is given by

$$L\, di_{TCR}(\omega t)/dt = \sqrt{2}\, V_{SRMS} \sin \omega t \qquad (4.1)$$

Solving the differential equation (4.1) with the initial condition $i_{TCR} = 0$ at $\omega t = \alpha$ and after simplification, the current through the TCR is obtained as

$$i_{TCR}(\omega t) = (\sqrt{2}\, V_{SRMS}/\, \omega L)(\cos\alpha - \cos\, \omega t)$$
$$\alpha \leq \omega t \leq \beta \ . \qquad (4.2)$$

The current i_{TCR} is again zero at the extinction angle, β as seen from Fig. 4.6 . Substituting this condition in eqn. (4.2) , we obtain

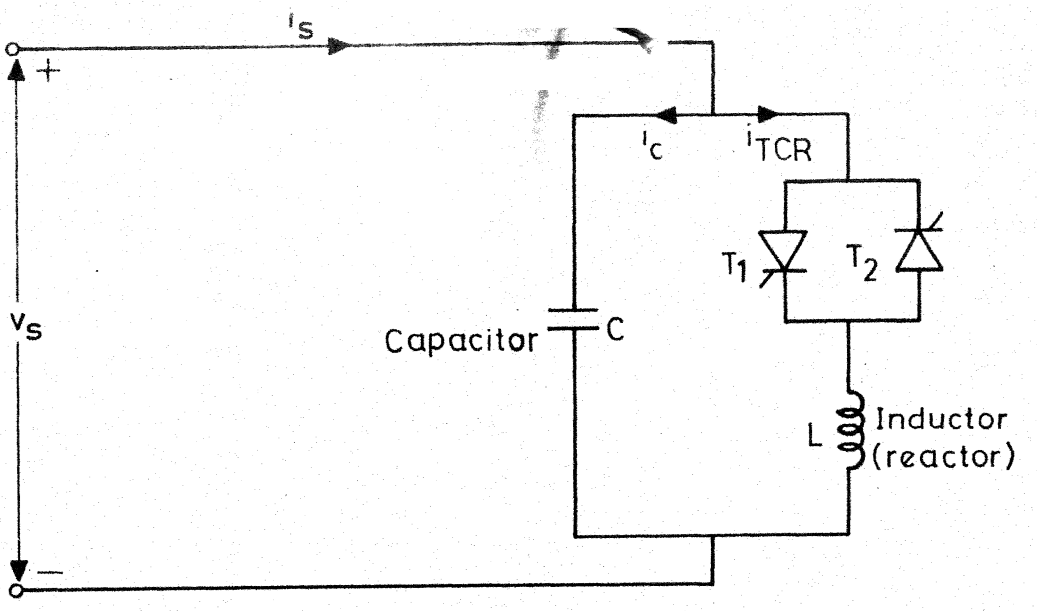

Fig. 4.5 Basic fixed capacitor, thyristor-controlled reactor type compensator.

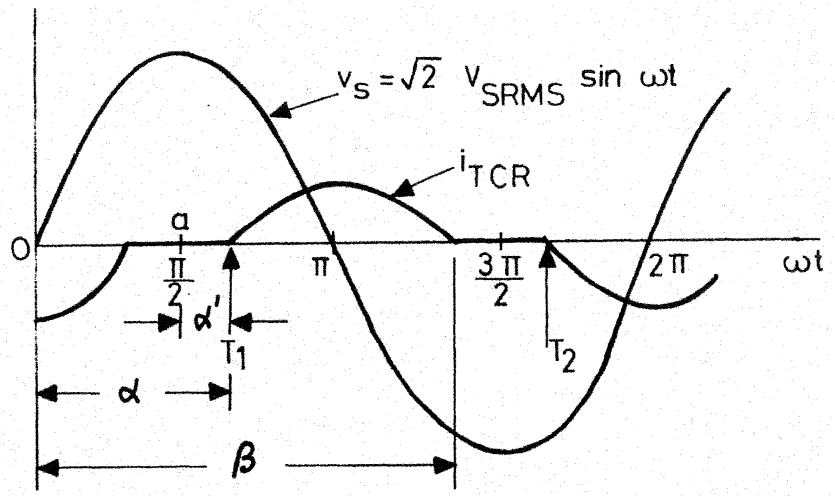

Fig. 4.6 Supply voltage and TCR current waveforms.

$$\cos \alpha = \cos \beta$$

Since the extinction angle is greater than the firing angle, but less than 2π radians, we obtain

$$\beta = 2\pi - \alpha \tag{4.3}$$

Similarly, considering the thyristor T_2 which is fired in the other half cycle of the supply frequency, we obtain

$$i_{TCR}(\omega t') = (\sqrt{2}\, V_{SRMS}/\omega L)(\cos \alpha - \cos \omega t') \qquad \alpha \leq \omega t' \leq \beta \tag{4.4}$$

where $\omega t' = \omega t + \pi$

The current is sinusoidal and lags the voltage by 90° when $\alpha = 90°$, neglecting commutation intervals of thyristors. The current becomes discontinuous for $\alpha > 90°$. And the discontinuous period increases with increase in firing angle, α. The TCR current can be expressed by the Fourier series ;

$$i_{TCR}(\omega t) = \frac{a_0}{2} + \sum_{n=1}^{\infty} (a_n \cos n\omega t + b_n \sin n\omega t)$$

The Fourier coefficients are obtained as follows:

$$a_0/2 = \frac{1}{2\pi} \int_0^{2\pi} i_{TCR}(\omega t)\ d(\omega t)$$

$$a_n = \frac{1}{\pi} \int_0^{2\pi} i_{TCR}(\omega t) \cos n\omega t \; d(\omega t)$$

$$b_n = \frac{1}{\pi} \int_0^{2\pi} i_{TCR}(\omega t) \sin n\omega t \; d(\omega t)$$

The fundamental and harmonic coefficients are given below.

$$a_1 = (\sqrt{2}\, V_{SRMS}/2\pi\omega L)\left[\sin 2\alpha - \sin 2\beta - (2\beta - 2\alpha) - 4\cos\alpha\{-\sin\beta + \sin\alpha\}\right] \quad (4.5)$$

$$b_1 = (\sqrt{2}\, V_{SRMS}/2\pi\omega L)\left[-\cos 2\alpha + \cos 2\beta - 4\cos\alpha(\cos\beta - \cos\alpha)\right] \quad (4.6)$$

$$a_n = (\sqrt{2}\, V_{SRMS}/2\pi\omega L)\left[\{2/(n+1)\}\{\sin(n+1)\alpha - \sin(n+1)\beta\} - \{2/(n-1)\}\{\sin(n-1)\alpha - \sin(n-1)\beta\} - (4\cos\alpha/n)\{-\sin n\beta + \sin n\alpha\}\right], \quad n > 1 \quad (4.7)$$

$$b_n = (\sqrt{2}\, V_{SRMS}/2\pi\omega L)\left[\{2/(n+1)\}\{-\cos(n+1)\alpha + \cos(n+1)\beta\} - \{2/(n-1)\}\{-\cos(n-1)\alpha + \cos(n-1)\beta\} - (4\cos\alpha/n)\{\cos n\beta - \cos n\alpha\}\right], \quad n > 1 \quad (4.8)$$

The rms value of the n-th order harmonic and its phase angle, ψ_n are then given by

$$I_{nRMS} = (a_n^2 + b_n^2)^{1/2} / \sqrt{2}$$

$$\psi_n = \tan^{-1} \left| a_n / b_n \right|$$

The per-unit values of the fundamental and different harmonics are computed for different α's and are shown in Fig. 4.7 .

Substituting the value of β from eqn. (4.3) in eqns. (4.5) and (4.6) , we obtain,

$$a_1 = (-\sqrt{2}\, V_{SRMS}/\pi\omega L)(2\pi - 2\alpha + \sin 2\alpha)$$

$$b_1 = 0$$

Hence, the fundamental component,

$$I_{1RMS} = I_{TCRF}(\alpha) = (a_1^2 + b_1^2)^{1/2} / \sqrt{2}$$

$$= (V_{SRMS}/\pi\omega L)(2\pi - 2\alpha + \sin 2\alpha)$$

$$\pi/2 \leq \alpha \leq \pi \qquad (4.9)$$

Phase angle, $\psi_1 = \tan^{-1} \left| a_1/b_1 \right| = 90°$ (lagging)

The TCR (thyristor-controlled reactor) current changes from its maximum value to zero when the firing angle, α is varied from 90° to 180° . It may be more convinient to fix the reference point or origin at 90° as indicated by point 'a' in Fig. 4.6 . Let us recognise a new firing angle notation , α' such that

$$\alpha' = \alpha - (\pi/2) \qquad (4.10)$$

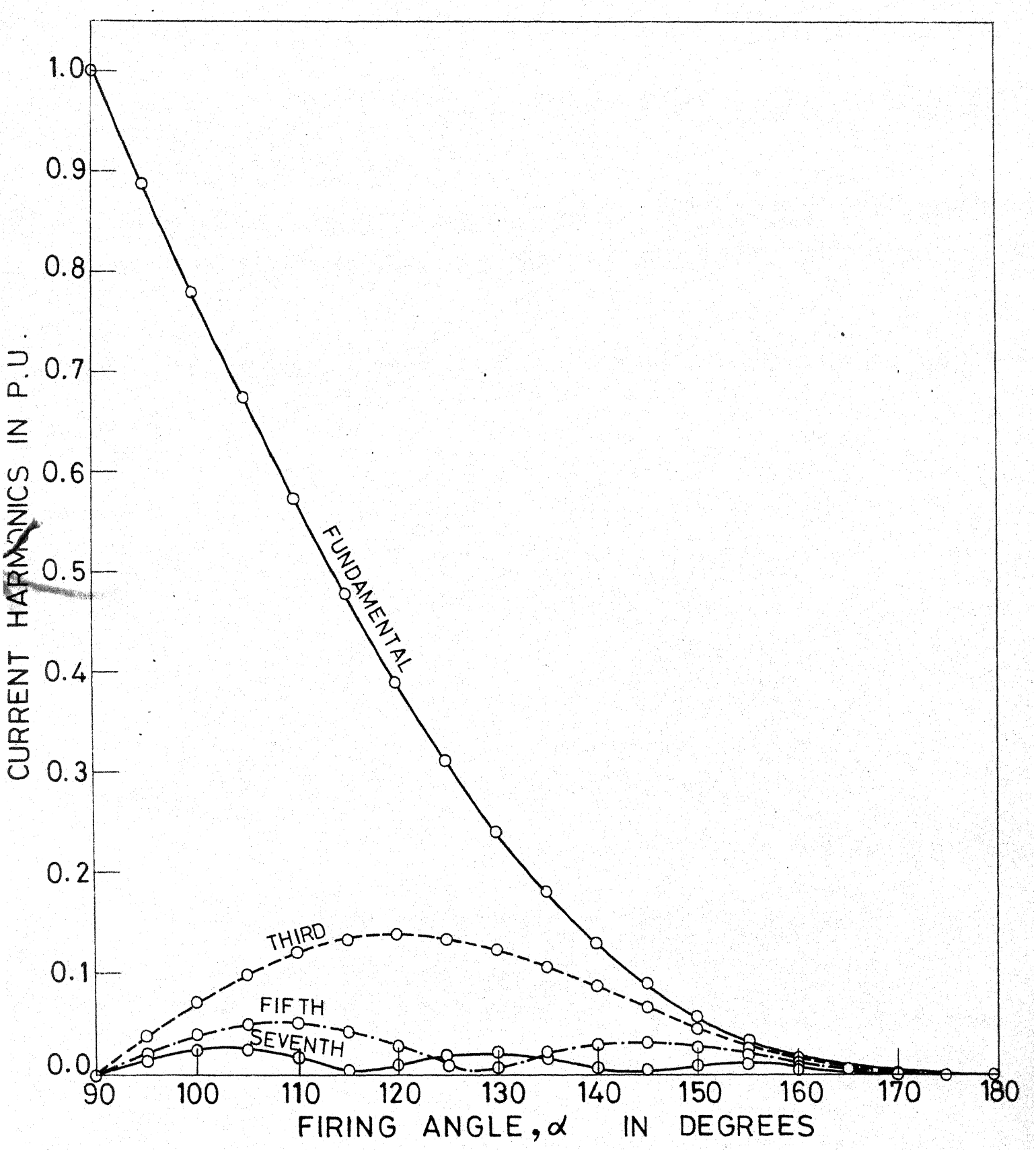

Fig. 4.7 Fundamental and harmonics values in TCR current.

Substituting the relation (4.10) in the expression (4.9) , the fundamental component of TCR current is obtained as :

$$I_{TCRF}(\alpha) = (V_{SRMS}/\omega L)\left[1 - (2/\pi)\alpha' - (1/\pi)\sin 2\alpha'\right] \qquad 0 \leq \alpha' \leq \pi/2 \qquad (4.11)$$

Thus, the magnitude of the total fundamental current drawn by the static compensator is

$$I_{SF}(\alpha) = I_C - I_{TCRF}(\alpha) \qquad (4.12)$$

$$= V_{SRMS}\left[\omega C - (1/\omega L)\left\{1 - (2/\pi)\alpha' - (1/\pi)\sin 2\alpha'\right\}\right] \qquad (4.13)$$

By controlling the fundamental component of TCR current, it can be seen from eqn. (4.12) that the static reactor compensator draws either net capacitive or inductive current from the ac supply depending upon whether the current $I_{SF}(\alpha)$ is positive or negative respectively.

The control process is illustrated in Fig. 4.8 . The controlled inductor current, $i_{TCR}(\alpha)$, the fixed capacitor current, i_C , and the total current drawn from the ac supply, $i_S(\alpha)$, with its fundamental component, $i_{SF}(\alpha)$ are shown together with the applied voltage, v_S as α' is increased from 0° to 90° gradually. The inductive reactance, ωL has been assumed to be smaller than the

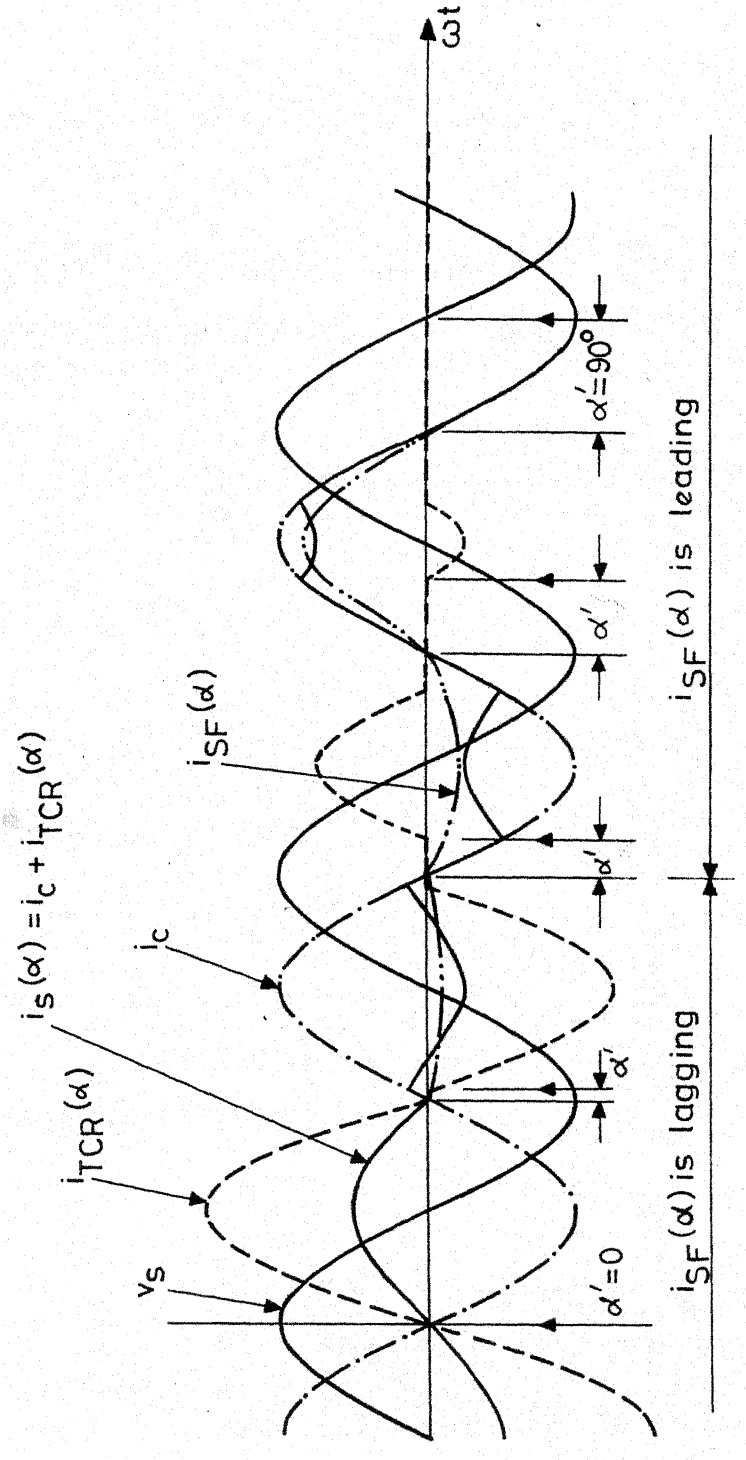

Fig 4.8 Associated waveforms for TCR compensator illustrating control process.

capacitive reactance, $1/\omega C$ in this illustration so as to achieve range of control in both the inductive and capacitive domains. As is evident, the effective reactance and the compensating current can be adjusted at discrete instants of time, not more often than once in each half-cycle. However, it should be noted that the current can be changed from maximum leading to maximum lagging in one half-cycle. So, in practice, the thyristor-controlled reactor scheme can be made to achieve a very fast dynamic response using fast measuring circuits and control devices.

Control approaches: For control of reactive power in the thyristor-controlled inductor scheme, α' has to be computed and controlled accordingly. For computing α', three basic control approaches are generally employed which are outlined in the following paragraphs.

The first one is of direct computational type which is called "feed forward" control. This control approach is based on the fundamental assumption that the load is in the steady state between any two consecutive instants of time at which the current in the compensator is changed. Thus, between these time instants the relevant load currents (or powers, or impedances) can be sensed and, from these, the required compensating currents can be computed using appropriate steady state relations.

In 3-phase systems, the processing of each of the three steady state equations for the three phases, expressing the required compensating current in terms of quantities characterizing the load (currents, power or impedances), is carried out over time intervals which are mutually displaced by one third of the period of the ac system voltage. The three compensating currents are measured independent of each other and the required firing angle, α' is determined using the relation (4.13) . Thus, the feedforward control scheme requires two main functional elements as illustrated by the block diagram of Fig. 4.9 : one to compute the desired inductor current and the other to determine the firing angle corresponding to the desired inductor current.

The second control approach utilizes feedback concept for the control of compensating power. Though this approach is mainly used for regulating the terminal voltage of a transmission line network [16, 18], it can also be used for load compensation. The basic principle is to control the TCR with an appropriate error signal. The error signal represents the difference between a chosen reference and a corresponding parametric value of the variable to be controlled (voltage or power factor) , A change in the error signal results in an opposing change

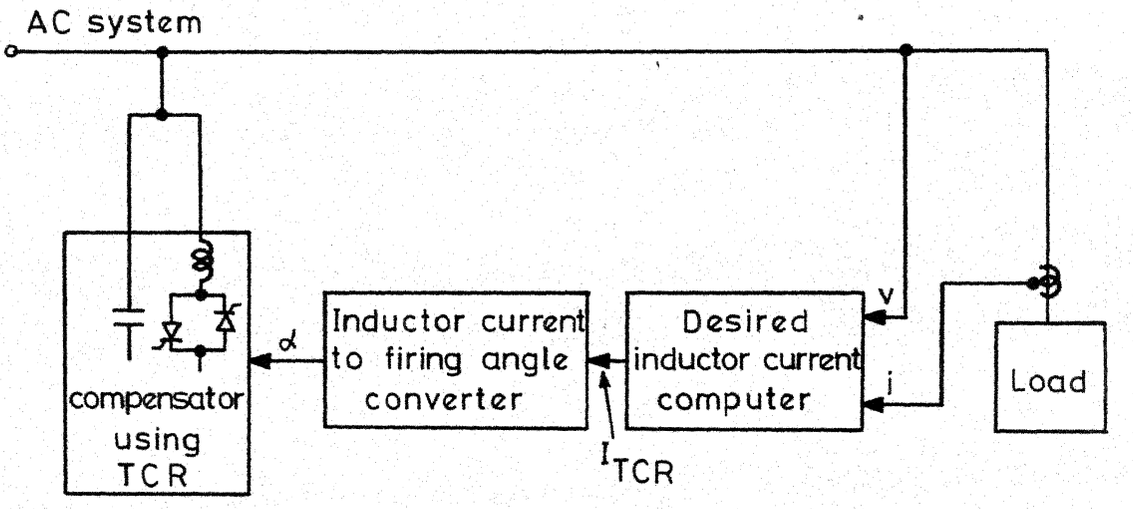

Fig. 4.9 Major functional elements in a general feedforward control scheme

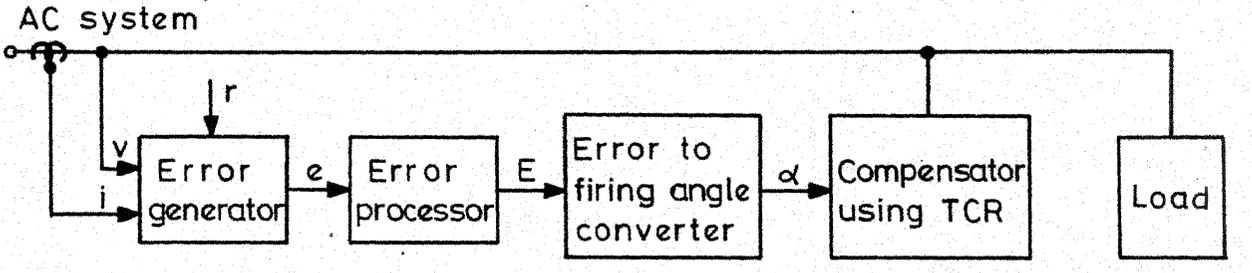

Fig. 4.10 Major functional elements in a general feedback control scheme.

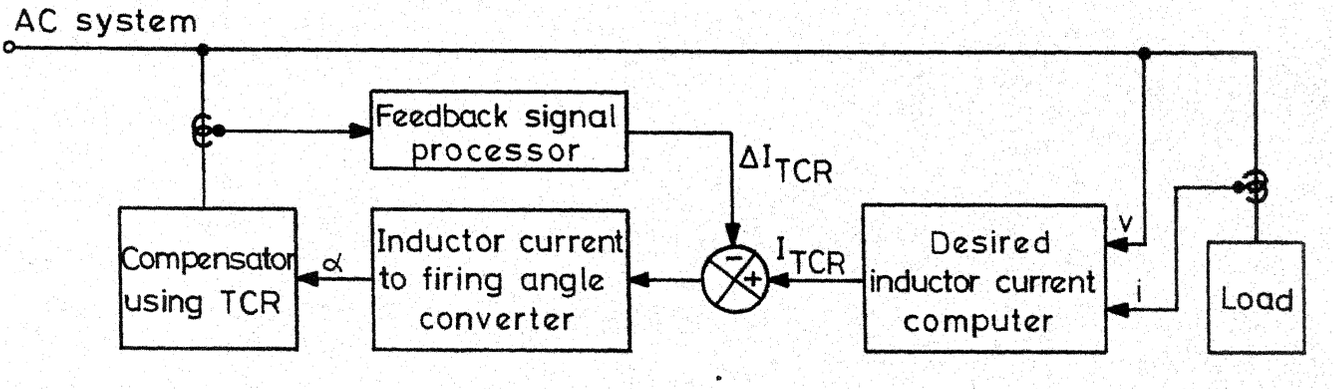

Fig. 4.11 Major functional elements in an overall feedforward control scheme using negative feedback.

in the effective susceptance value of the TCR. This tends to keep the error signal close to zero. The block diagram of a typical feedback control scheme is shown in Fig. 4.10. There are three main functional elements in the feedback loop. The function of the error generator is two-fold. First, it derives a parametric value of the variable, x, to be controlled (e.g., voltage components, reactive power etc.) from the input signals which are the line currents and voltages of the system. Secondly, it generates an error signal, e, by comparing the derived parametric value of the variable with the reference signal, r. The output signal, E of the error processor is proportional to the error signal, e, and the derivative and/or integral of the error signal may be incorporated to get better control [16]. The Error to Firing Angle Converter converts E to the desired firing angle of the thyristor.

The feedforward and feedback control approaches are complementary. The former is inherently stable and fast whereas the latter can be made very accurate. The third control approach combines the good features of both feedforward and feedback control. For example, the accuracy of the desired inductor current to firing angle converter can be improved and made independent of the circuit parameters by providing a negative feedback from the

actual inductor current as shown in Fig. 4.11 . The output of the feedback signal processor, ΔI_{TCR} represents the deviation of the actual inductor current from the desired value.

4.4 CONCLUSIONS

It is possible to change the current flow through the static shunt compensator using thyristor-controlled inductor from maximum leading to maximum lagging in one half cycle of the supply frequency. Such a fast response is not possible with other types of compensators. Therefore, the thyristor-controlled compensator is finding widespread application not only in industrial power systems for load compensation but also in the utility systems for transmission line voltage regulation. In the next chapter, the details of a single-phase thyristor-controlled static shunt compensator have been presented. The experimental results regarding steady state and dynamic response of the same are also discussed in detail.

CHAPTER V

SINGLE-PHASE THYRISTOR PHASE-CONTROLLED REACTIVE POWER COMPENSATOR

5.1 INTRODUCTION

In chapter IV the basic principles of static reactive shunt compensator employing thyristor controlled reactor (TCR) for load compensation have been explained in detail. In this chapter, a static reactive shunt compensator has been practically realized for improvement of power factor of a single-phase load on those principles. Simple but novel control circuit has been developed for this purpose. Fundamentally, the information regarding reactive load current must be known in order to improve the supply power factor. The feedforward or computational type control approach [18] is adopted. The details of experimental set-up including control circuits are explained. The experimental results showing supply power factor with and without the TCR compensator are presented. Moreover, the dynamic response of the TCR regulator whenever load is changed is presented by oscillograms (traced from storage oscilloscope) obtained from the experimental set-up.

The experimental results show that the power

factor is improved substantially and the regulator requires only one cycle to implement the desired improvement in power factor from the instant the load is changed. Furthermore, the experimental results showing the dynamic response of the TCR regulator point out that there is scope for improvement in the control circuit.

5.2 PRACTICAL CONTROL APPROACH USING FEEDFORWARD SCHEME

The block diagram of the control scheme based on the main functional block diagram of Fig. 4.9 is shown in Fig. 5.1 . The instantaneous values of system voltage, V_S, load current, i_L, and capacitor current, i_C, are measured and fed to the signal processing unit which basically consists of a Reactive Current Detector and a difference amplifier. The output of the signal processing unit is the difference between the rms value of the capacitor current, I_C , and the rms value of the reactive component of the load current, $I_L \sin \theta$. This difference also gives the fundamental component of the desired TCR current, I_{TCRF}. The "Inductor current to firing angle converter" block of Fig. 4.9 essentially consists of a function circuit and a comparator as shown in Fig. 5.1 . The function circuit generates the function relating fundamental rms TCR current, I_{TCRF}, with firing angle, α', in real time. Referring to

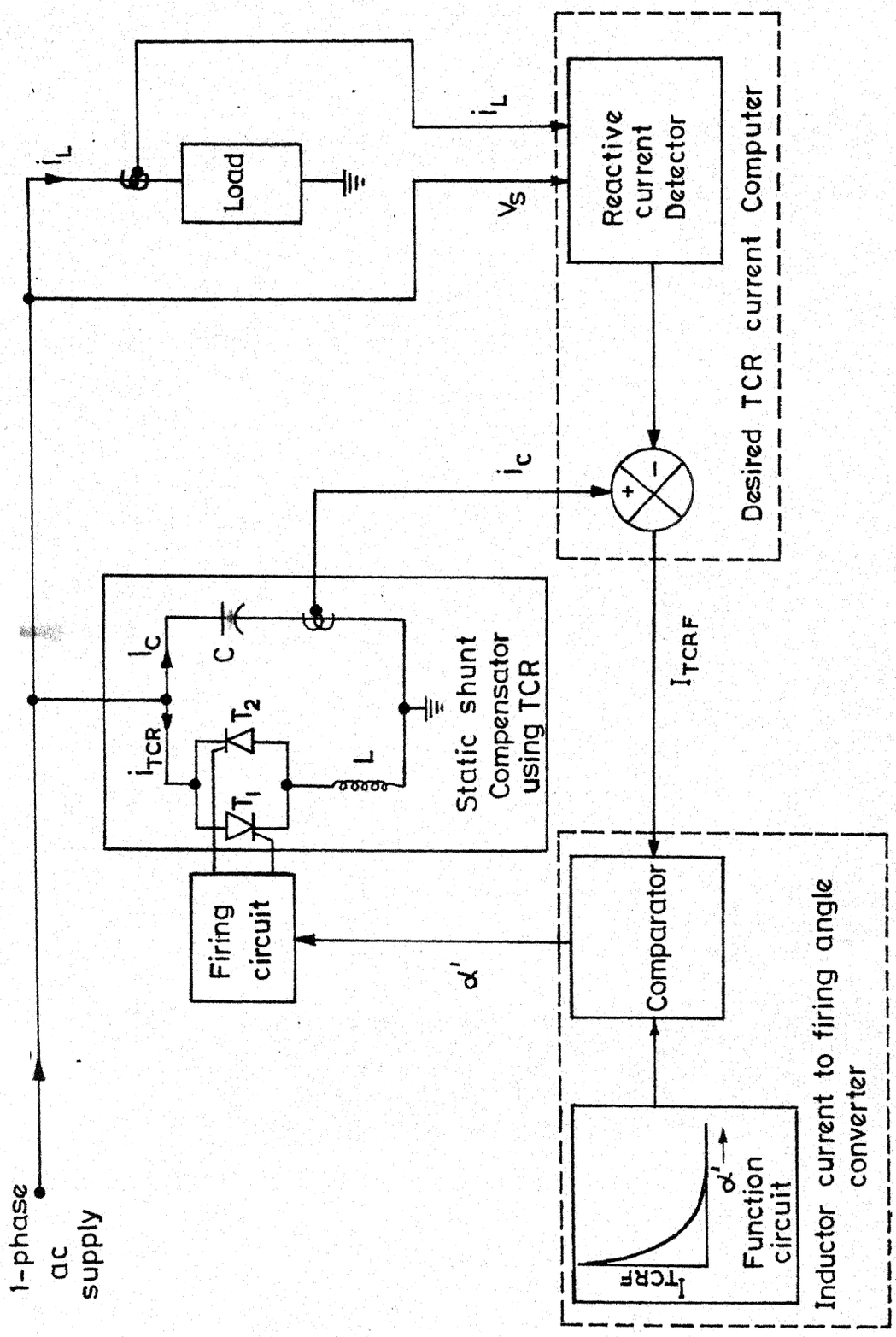

Fig. 5.1 Block diagram of the control scheme.

section 4.3.2 , we have,

$$I_{TCRF}(\alpha) = (V_{SRMS}/\omega L)\left[1 - (2/\pi)\alpha' - (1/\pi)\sin 2\alpha'\right] \quad (5.1)$$

The desired TCR current, I_{TCRF}, is compared with the output of the function generator to get information about the firing angle, α' , in real time. This information is finally passed on to the 'Firing Circuit' block to produce the gate pulses at the desired instants for the thyristors, T_1 and T_2 , connected back to back in series with the reactor, L.

The different waveforms and processed control signals illustrating the control process is depicted in Fig. 5.2 taking the system voltage as the time reference. Let us consider, for example, the kth steady state interval. The instantaneous values of the load current and the capacitor current are measured and the rms values of I_C and $I_L \sin\theta$ are computed during the kth steady-state interval of computation where k represents the number of supply cycles. The difference between these two signals which gives the value of the required TCR current, I_{TCRF} , is also computed during this interval. During the kth firing interval the function relating fundamental rms TCR current with the firing angle, α' is generated and this is compared with the desired I_{TCRF} . Thus, the firing

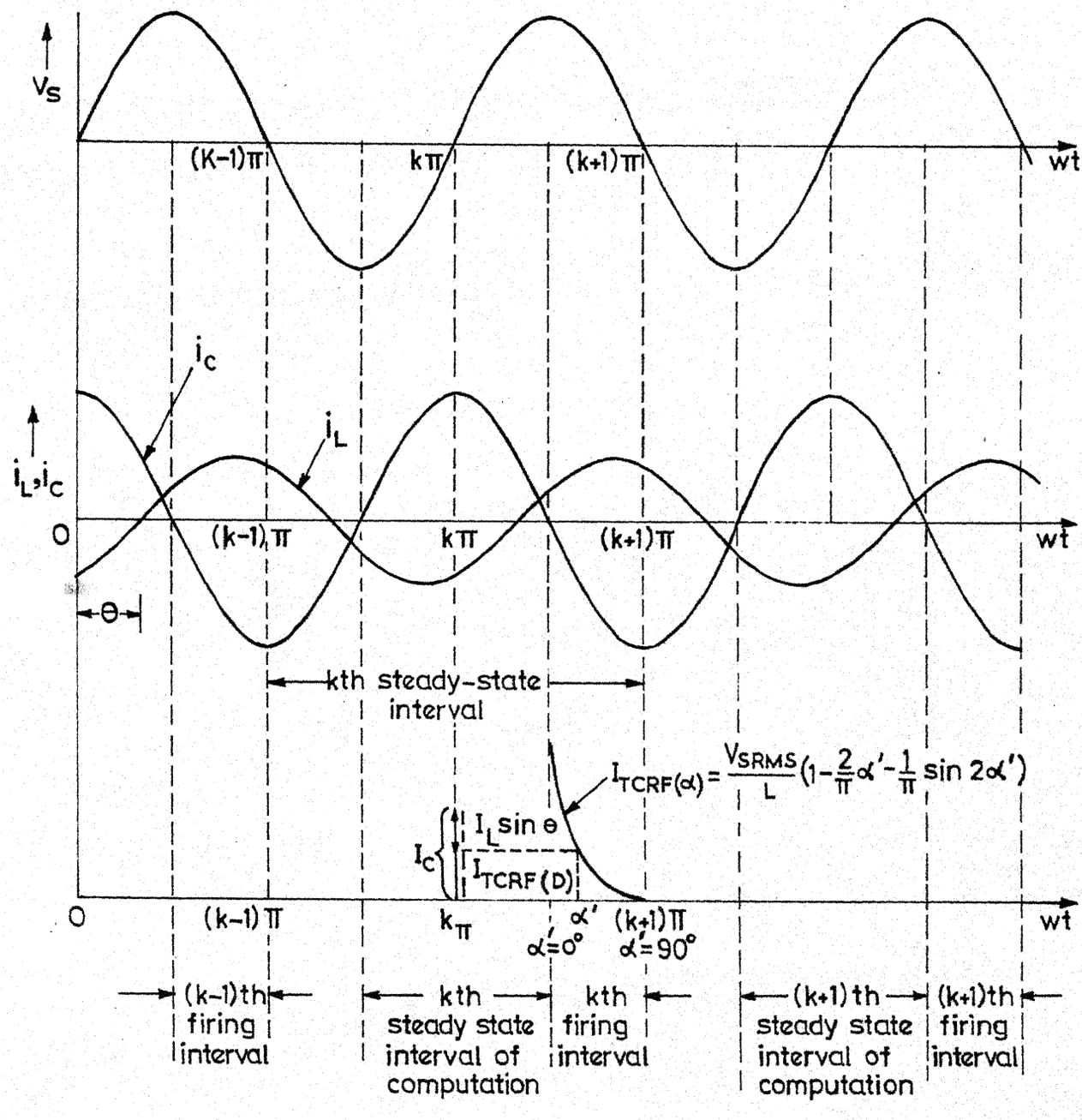

Fig.5.2 Voltage and current waveforms and control signals to describe the control process.

angle, α', is determined in real time and T_1 is triggered accordingly in the kth firing interval. The thyristor T_2 is triggered just half a time period after T_1 is triggered. The TCR current, thus, can be controlled in each cycle of the supply frequency.

5.3 CONTROL CIRCUIT

The control circuits used in different blocks of Fig. 5.1 are explained in this section. The instantaneous values of the load current and the capacitor current are measured using sensing resistors. Voltage followers using opamps are provided to present high input impedance to the power circuit. The supply voltage is sensed using a potential divider. These signals are required to produce the desired TCR current. Fig. 5.3 (a) shows complete details of the TCR Current Computer. The desired TCR Current Computer is designed assuming that the load current and the capacitor current are purely sinusoidal. With this assumption the reactive component of the load current is easily computed by using sample and hold technique. The load current is first inverted using an inverting amplifier and fed to the sample and hold circuit. The output tracks the negative load current during the negative half cycle of the supply voltage and its value at the voltage zero, $I_{Lm}\sin\theta$ (I_{Lm} and θ being the peak value

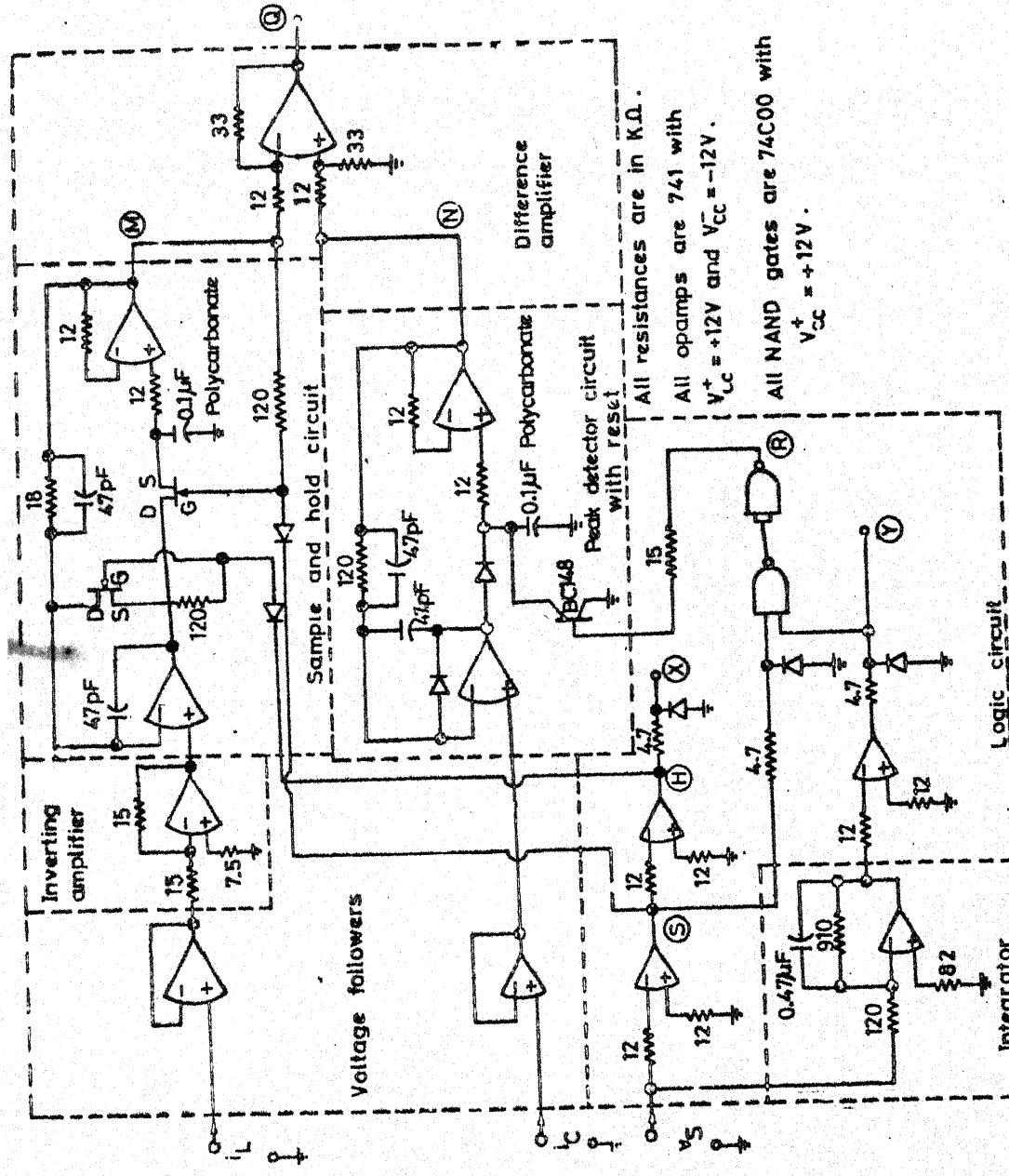

Fig. 5.3 (a) Circuit diagram for desired TCR current computer.

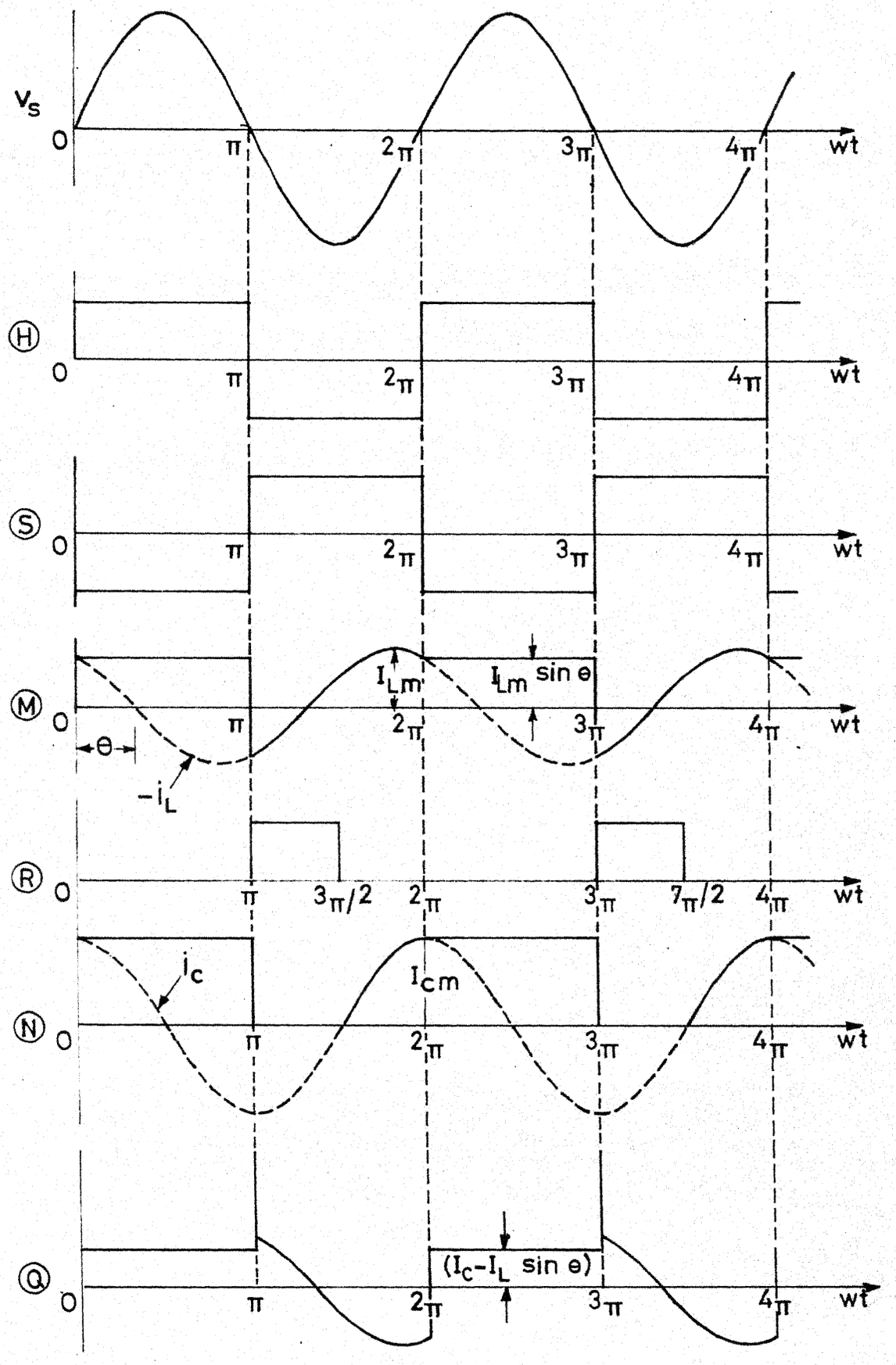

Fig. 5.3(b) Waveforms at different points of the desired TCR current computer circuit.

and the phase angle respectively of the load current) is held during the positive half cycle. The output waveforms of different stages of Fig. 5.3 (a) are shown in Fig. 5.3 (b). For example, the waveform (H) of Fig. 5.3 (b) shows the output of the sample and hold circuit at the point marked (H) . A non-inverting two-opamp sample and hold circuit [19, 20] is used. The sample and hold signals fed to the gates of the FET switches are obtained at point (S) and (H) . These are derived from the supply voltage. The rms value of the load current , $I_L \sin\theta$, is subsequently obtained by multiplying the quantity $I_{Lm} \sin\theta$ with the form factor of a sine wave (0.707). In a similar way, the rms value of the capacitor current, I_C , is obtained by first measuring the peak value, I_{Cm} , and then multiplying with the form factor. A peak detector circuit with reset [20] as shown in Fig. 5.3 (a) is used to determine the peak value. The waveform (N) (Fig. 5.3 (b)) shows the output of peak detector. Since the capacitor current may vary with the fluctuations in the supply voltage, the circuit is reset at the end of each cycle so that actual peak value is obtained in each cycle. The reset takes place when the transistor across the "memory" capacitor is driven into saturation by providing the reset pulse obtained at the point (R) of the

logic circuit (Fig. 5.3 (b)) to the base of the transistor. The output of the sample and hold circuit, $I_{Lm}\sin\theta$, and that of the peak detector with reset circuit, I_{Cm} , are given to the inverting and non-inverting inputs of a difference amplifier [20] respectively. The difference amplifier is designed with a gain equal to the form factor (0.707) of a sine wave so that the difference between the rms value of the capacitor current and that of the reactive component of the load current, $(I_C - I_L\sin\theta)$, is obtained at its output during the positive half cycles of the supply voltage. The waveform (Q) (Fig. 5.3 (b)) illustrates the output of difference amplifier at the point marked (Q) in Fig. 5.3 (a).

The function circuit for generating the functional relationship between I_{TCRF} and α' in real time is shown in Fig. 5.4 (a) and the waveforms at different stages are illustrated in Fig. 5.4 (b). As seen from the right hand side of eqn. (5.1) , the function consists of a constant term, 1 , a ramp term, $(2/\pi)\alpha'$, and a sine term, $(1/\pi)\sin 2\alpha'$ .Since $\alpha' = 0$ when the supply voltage reaches its peak value, it implies that to generate the function in real time, a ramp has to be generated such that it starts at $\alpha' = 0°$ and reaches its peak value of $2/\pi$ at $\alpha' = 90°$. Also, a sine function has to be generated

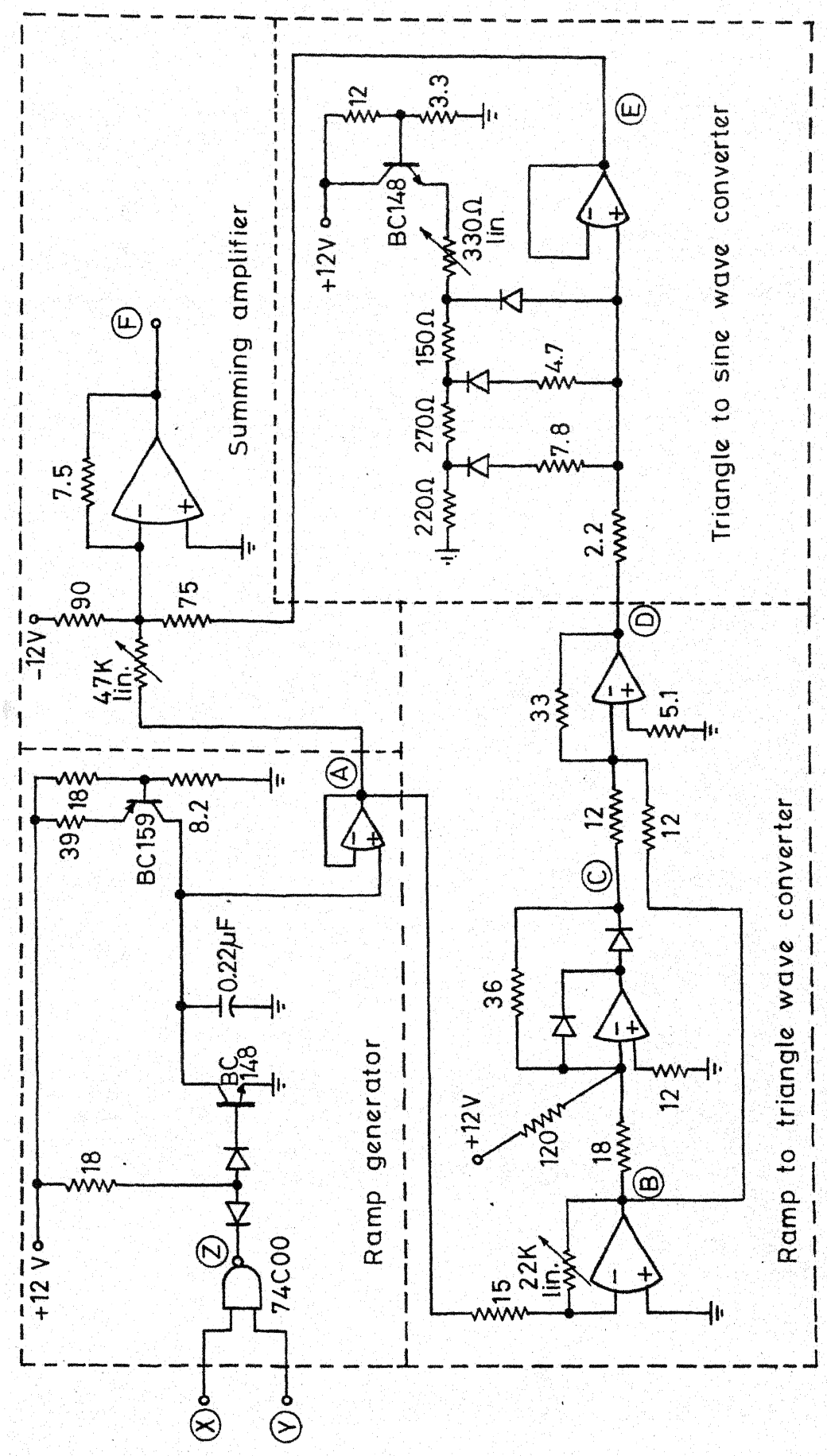

All resistances are in KΩ unless otherwise stated.

All opamps are 741 with $V_{cc}^{+} = +12V$ and $V_{cc}^{-} = -12V$.

Fig. 5.4 (a) Circuit diagram for the function circuit.

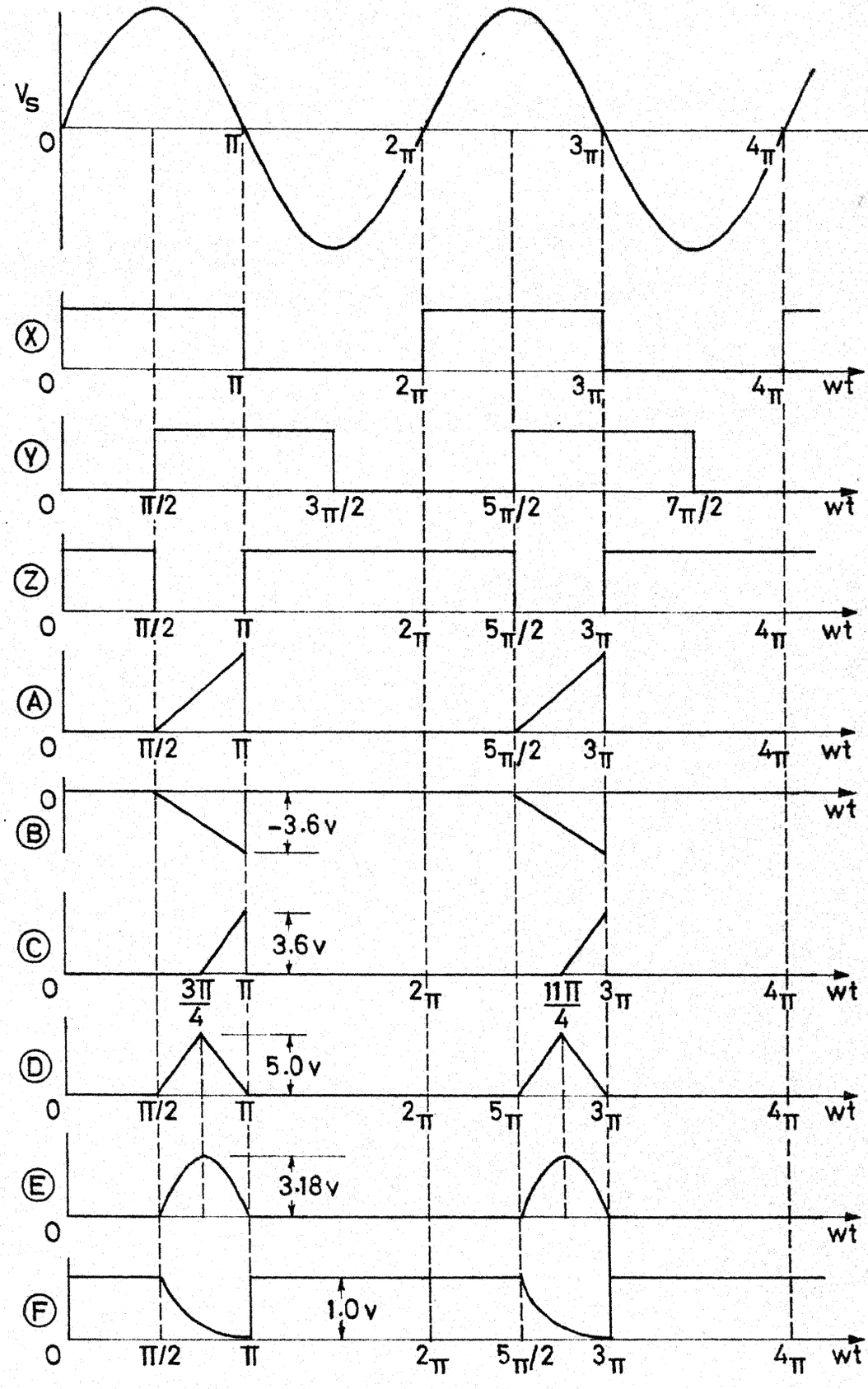

Fig. 5.4(b) Waveforms at different points of the function circuit

which starts at $\alpha' = 0°$, reaches its positive peak value of $1/\pi$ at $\alpha' = 45°$ and again becomes zero at $\alpha' = 90°$. With these considerations in mind, the function circuit is realized as described below.

The logic signals derived at points (X) and (Y) of the circuit shown in Fig. 5.3 (a) are fed to a NAND gate to get the pulse at (Z) which serves as the timing pulse for discharging the capacitor in the ramp generator as shown in Fig. 5.4 (a) . A linear ramp output is obtained at the point marked (A) .

The desired sine function is obtained by first converting the ramp to triangular wave and then the triangle to sine wave. A current-biased zero-bound circuit [20] is used for converting the ramp to triangular wave. These waveforms are illustrated by (B) , (C) and (D) of Fig. 5.4 (b). A simple triangle to sine converter using the principle of piece-wise approximation is used [21] . The circuit is designed for three break points as shown in Fig. 5.4 (a). The waveform (E) (Fig. 5.4 (b)) corresponds to the output sine wave converter at the point marked (E) (Fig. 5.4 (a)). The outputs of the ramp generater and that of the triangle to sine wave converter along with a dc supply of -12V magnitude are fed to the inverting input of an opamp used as a summing amplifier. The input

resistances are chosen so as to get the desired gains for the three input signals. At the output marked (F) of the summing amplifier, we get a signal, v_F , given by

$$v_F = 1 - (2/\pi)\alpha' - (1/\pi) \sin 2\alpha' \quad , 0 < \alpha' < 90° \tag{5.2}$$

The output at (F) is then fed to a non-inverting amplifier with gain equal to $V_{SRMS}/\omega L$ (assumed constant) where V_{SRMS} is the rms value of the supply voltage and ωL is the fundamental reactance of the thyristor controlled reactor. This is shown in Fig. 5.5 (a) . Thus, at the output (F') of the non-inverting amplifier the desired function given by equation (5.1) is obtained. The waveform at (F') is shown by the chained curve of Fig. 5.5 (b). This is then compared with the desired value of TCR current given by the signal output at (Q) (Fig. 5.3 (b)). An opamp in open-loop mode is used as the comparator. The comparator output at the point (G) provides the information regarding the firing angle. As seen from the waveforms of Fig. 5.5 (b) , the leading edge of the output pulse at (G) fixes the value of α' in real time. This pulse is then fed to a monostable. The monostable is realized by using a TIMER. The output pulse of the monostable has width equal to half a cycle. This pulse-stretching is necessary to ensure reliable

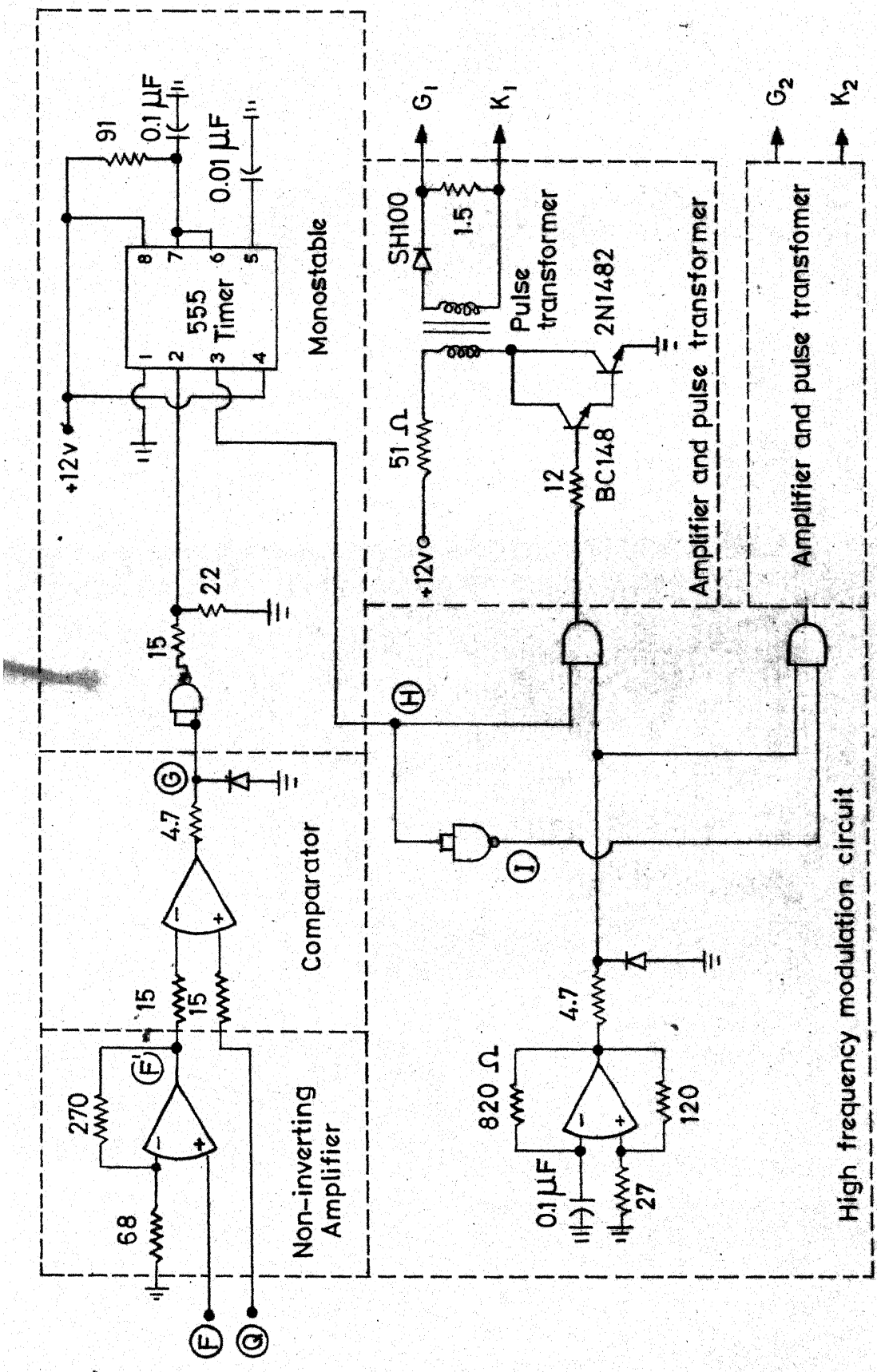

All resistances are in kΩ unless otherwise stated.
All opamps are 741 with $V_{CC}^{+}=+12v$ and $V_{CC}^{-}=-12v$.
NAND gates are 74C00, AND gates are 74C08 with $V_{CC}^{+}=+12v$

Fig. 5.5(a) Circuit diagram for comparator and firing circuit.

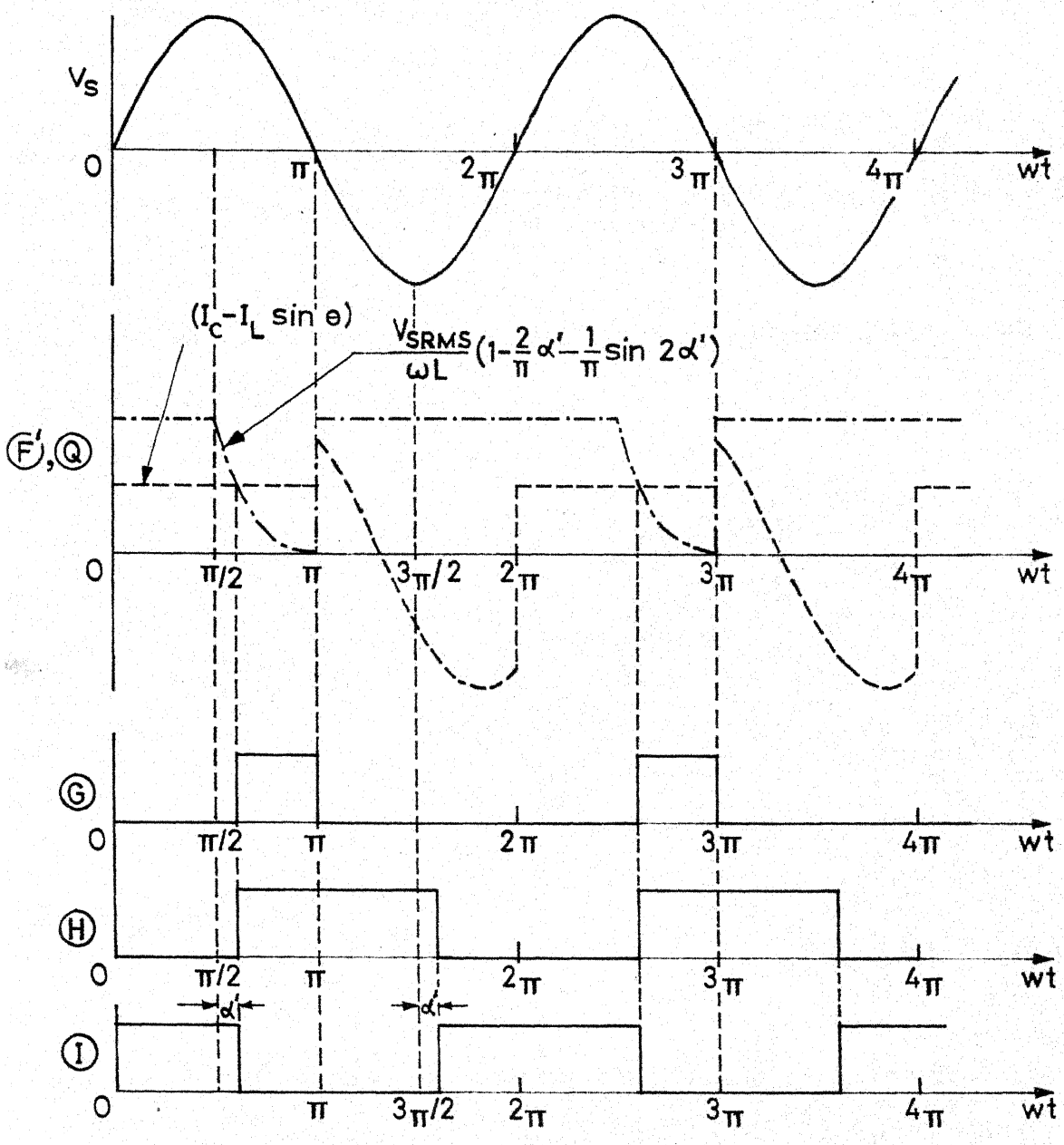

Fig. 5.5(b) Waveforms at different points of comparator and firing circuit.

firing of the thyristors since they are in series with an inductor. The monostable output at (H) is the gate pulse for the thyristor, T_1 while its complement (I) (Fig. 5.5 (b)) is the gate pulse for the thyristor T_2. These gate pulses, however, go through high frequency modulation, amplification stages to achieve reliable triggering. Pulse transformers are also used at the output stage to provide isolation.

5.4 EXPERIMENTAL RESULTS AND DISCUSSIONS

5.4.1 Details of experimental set-up

The response of the static shunt reactive compensator is determined experimentally in the laboratory on an R - L load supplied from a single-phase 230V, 50Hz supply. The load current is varied by varying the load resistance. The reactance of the load inductor is 100 Ω while the load resistance can be varied from 0 to 220 Ω . The load draws a maximum reactive current of 2.3Amp when the load resistance value is zero. This must be compensated by the current drawn by the capacitor. Hence, a capacitor is chosen which draws 2.3Amp from the 230V ac supply. Again, when the load is purely resistive, the TCR current (corresponding to full conduction) should compensate for the full capacitive current. Thus, another inductor having a reactance of 100 Ω is chosen to be used as the TCR .

The design of the inductor is presented in Appendix I.

5.4.2 Steady state response

The power factor of the input current for various values of the load current are calculated by measuring the supply voltage, supply current and the input power. For the same load current, the power factor is determined with and without the compensator. Table 5.1 shows substantial improvement in power factor with the compensator. It is close to unity over a wide range of cariation of load current. For large load current, the current drawn by the TCR is small resulting in large firing angle delay for the controller. Since the harmonic content is high when the triggering angle is large, the power factor is, therefore, not improved significantly for large load currents as seen from Table 5.1 .

Table 5.1

Supply voltage, V_{SRMS} = 231 volts

Load current, I_L (Amps)	Supply current, I_S (Amps)		Input power, W (Watts)		Input power factor $\cos\theta = W/(V_{SRMS} I_S)$	
	Without Compensator	With Comptr.	Without Comptr.	With Comptr.	Without Comptr.	With Comptr.
1.1	1.1	1.02	205	225	0.8075	0.955
1.5	1.5	1.08	237.5	250	0.6860	1.0
1.7	1.7	1.09	235	250	0.5980	0.993
1.8	1.8	1.07	230	245	0.5535	0.991
1.9	1.9	1.05	220	240	0.5020	0.990
2.1	2.1	0.90	175	195	0.3605	0.937
2.2	2.2	0.77	130	150	0.2555	0.843
2.3	2.3	0.28	22.5	30	0.0423	0.464

5.4.3 Transient response

Whenever the load current is changed, the thyristor controlled reactor regulator immediately responds to the load changes and tends to maintain the supply power factor at unity. The response of the regulator is presented in the form of oscillographic results both for an increase and decrease in the load current. Depending upon the load impedance angle before load change and also the instant in the ac supply cycle at which the load change is initiated, it may take a few cycles for the load current to settle down to the steady operating point corresponding to the new load condition. This is also confirmed by the oscillograms obtained from the experimental set-up. However, the regulator corrects the firing angle at the end of each cycle from the instant the load change is initiated. In order to study the transient response of the regulator, it is appropriate to present ac transient analysis. Fig. 5.6 (a) shows a R - L load fed by an ac supply. The load inductor has a winding resistance of R_L ohms. In what follows, the transient process of the thyristor regulator is explained when the load resistance is completely cut-off. Initially, the switch is in the open position. Assuming that steady-state has been reached, the load current, i_L, is given by

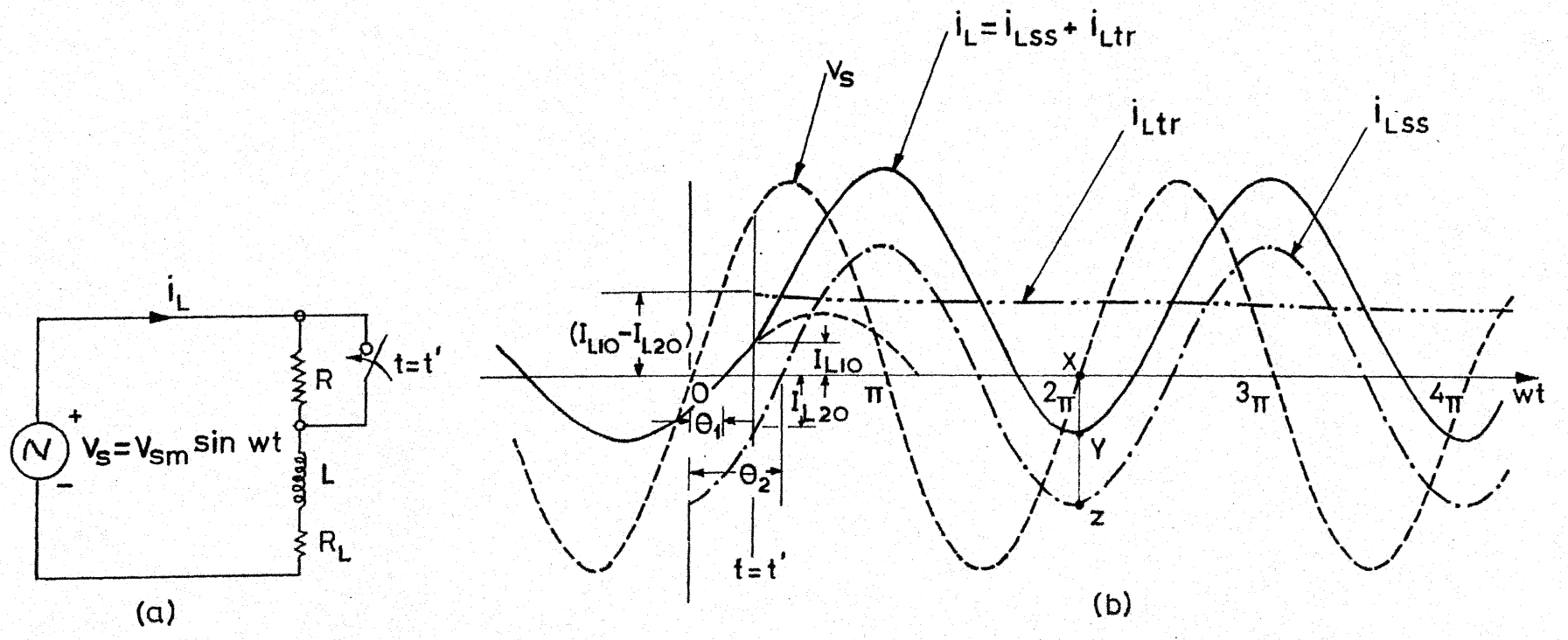

Fig.5.6 Transient process in the load current

(a) Circuit diagram

(b) Waveforms

$$i_L(\omega t) = (V_{Sm}/Z_1) \sin (\omega t - \theta_1) \qquad (5.3)$$

where

$$Z_1 = \left[(R + R_L)^2 + (\omega L)^2 \right]^{1/2}$$

$$\theta_1 = \tan^{-1} \left[\omega L/(R + R_L) \right]$$

Let the switch be closed at, say, $t = t'$ short-circuiting the load resistance, R. The resulting load current after the switching instant is given by

$$i_L(\omega t) = (V_{Sm}/Z_2) \sin (\omega t - \theta_2) + A \cdot \exp (-R_L t/L) \qquad t \geq t' \qquad (5.4)$$

where

$$Z_2 = \left[R_L^2 + (\omega L)^2 \right]^{1/2}$$

$$\theta_2 = \tan^{-1} (\omega L/R_L)$$

The first term on the right hand side of eqn. (5.4) is the steady-state component, i_{Lss}, and the second term is the transient component, i_{Ltr}. The coefficient A is a constant and can be evaluated from the initial condition at $t = t'$. The current at the instant $t = t'$ can be obtained from eqn. (5.3). Let is be I_{L10}. Substituting this in eqn. (5.4), we obtain,

$$I_{L10} = (V_{Sm}/Z_2) \sin (\omega t' - \theta_2) + A \cdot \exp (-R_L t'/L)$$

$$= I_{L20} + A \cdot \exp (-R_L t'/L) \qquad \text{(say)}$$

Hence,

$$A = (I_{L10} - I_{L20}) \cdot \exp(-R_L t'/L)$$

Substituting the value of A in eqn. (5.4), we obtain,

$$i_L(\omega t) = (V_{Sm}/Z_2) \sin(\omega t - \theta_2) + (I_{L10} - I_{L20}) \cdot \exp\left[-R_L(t - t')/L\right] \qquad t \geq t' \qquad (5.5)$$

For qualitative explanation, the waveforms of steady state (i_{Lss}), transient (i_{Ltr}) and total (i_L) load currents are shown in Fig. 5.6(b) ; the suply voltage, is taken as the reference; some arbitrary values are chosen for θ_1, θ_2 and t'. However, the load impedance angle, θ_2, will be almost equal to 90° since R_L is small. These waveforms are then referred while discussing the operation of the controller. The reactive component of the current is measured at the instant $\omega t = 2\pi$. As seen from Fig. 5.6 (b), the reactive component, $I_{Lm}\sin\theta$, is given by the ordinate XZ in the absence of transient component. Thus, the desired TCR current which is equal to the difference between the capacitor current and the measured reactive component of the load current is very small (the reactances of the capacitor and that of the load reactor being chosen equal). This results in large firing angle, α'

approaching nearly 90° as may be seen from Fig. 5.5 (b).

However, due to the presence of transient component, i_{Ltr}, the reactive component of load current is given by the ordinate XY. Since the desired TCR current is thus high, it requires a small value of firing angle, α', and therefore, the thyristors are triggered earlier. This action of the TCR regulator is demonstrated by the oscillograms of Fig. 5.7 (a) - (c) . Notice from these wavefroms that the firing angle, α' , increases in successive cycles as the transient component, i_{Ltr}, decays gradually to zero.

The transient component depends on the load impedance angle before switching and also on the instant of switching. Depending on these values, the point Y in the Fig. 5.6 (b) may lie above the horizontal axis and therefore there will be a large positive swing for the load current, i_L. In this particular case, the TCR current, $(I_C - I_L \sin \theta)$, will have a value higher than $V_{SRMS}/\omega L$; and this will not intersect the output characteristic of the function generator as seen from Fig. 5.5 (b). This will, therefore, result in continuous triggering of the thyristor T_1 till the desired TCR current decreases and is within the control range of the regulator. This is demonstrated by the waveforms shown in the oscillograms of Figs. 5.7 (d) - (e) . The trigger pulse to the thyristor T_1 is

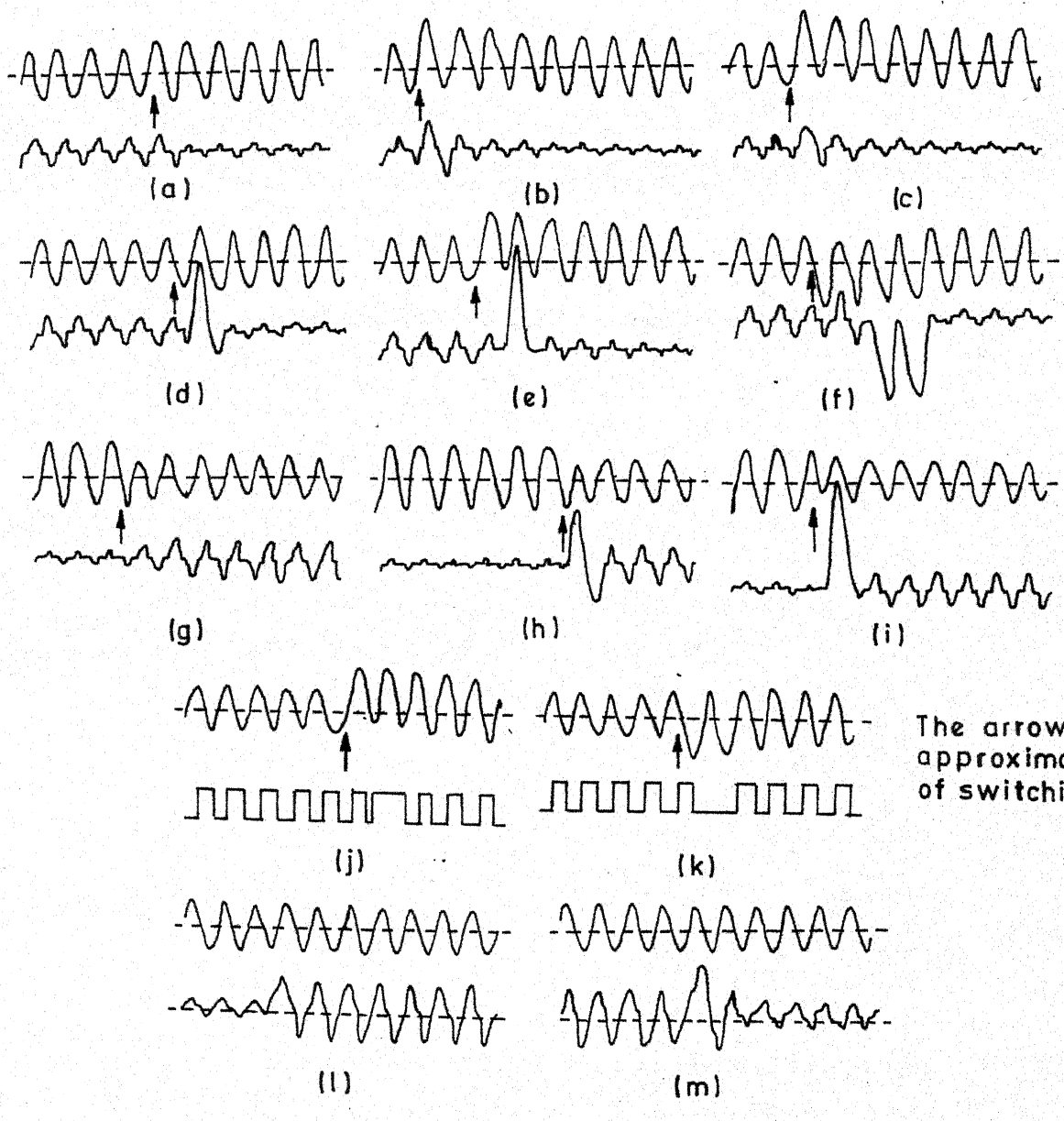

FIG. 5·7 Different waveforms illustrating transient process.
(a) through (i): Upper trace - Load current
Lower trace - TCR current
(j) and (k) Upper trace - Load current
Lower trace - Gate trigger pulse to thyristor T_1
(l) and (m) Upper trace - Supply voltage
Lower trace - Supply current

also obtained under such conditions and is shown in Fig. 5.7 (j) .

Let us consider a situation when the load resistance is cut-off at $\omega t = \pi$. That is, the switch in Fig. 5.6 (a) is closed at the end of positive half cycle. The transient component under this condition will have a high negative component. Since the steady state component remains the same, there will be a larger negative swing of load current at the end of one half cycle. The ordinate XY in Fig. 5.6 (b) may well exceed XZ. In this case, $(I_C - I_L \sin \theta)$, becomes negative and, hence, the thyristor T_1 does not get any firing pulse. Since the gate pulses to the thyristors T_1 and T_2 are complementary, the thyristor T_2 is continuously triggered. This is demonstrated by the waveforms of the oscillogram shown in Fig. 5.7 (f) . And Fig. 5.7 (k) shows load current and firing pulses to the thyristor, T_1 . The control circuit provides gate pulses to the thyristor T_1 after the amplitude of $(I_C - I_L \sin \theta)$ becomes zero and/or positive in subsequent cycles.

The waveforms describing the transient response of the regulator when the load resistance is suddenly introduced are shown in Figs. 5.7 (g) - (i) . The asymmetrical nature of the load current before the steady state

clearly shows the presence of transient component. In this case also, the regulator changes the firing angle, α', in the successive cycles until the transients die down and the load current settles down to the new steady state condition. These waveforms can be analysed in a similar manner.

The waveforms of the supply voltage and the supply current are shown in Fig. 5.7 (l) when the load resistance is shorted and in Fig. 5.7 (m) when the load resistance is introduced suddenly. It may be noted that in steady state the supply current is almost in phase with the supply voltage denoting nearly unity power factor. The distortion in the source current is due to the distortion in the capacitor current and/or the harmonics present in the TCR current.

5.4.4 Suggested modifications for improved control circuit

The experimental study of transient response of the TCR regulator has revealed some limitations of the control circuitry. These can be overcome by incorporating the following modifications in the control circuit.

The asymmetrical nature of the load current, whenever the load is changed, has caused continuous conduction of either T_1 or T_2 for a few cycles. The thyristor

T_1 conducts if there is a large positive swing of transient component in load current. On the other hand, if there is a large negative swing, the thyristor T_2 conducts. As explained in section 5.4.3 , this results in asymmetrical TCR current and possibly in core saturation. This can be eliminated if limits (0 and $V_{SRMS}/\omega L$) are provided for the desired TCR current computer. With this modification in the control circuitry, the firing angle, α' , will always be controlled within the range 0° to 90° for all load changes and the TCR current waveform will always be symmetrical.

In the present control circuitry, the function circuit is designed assuming constant magnitude of supply voltage. This may not provide complete compensation of load reactive power if the system voltage fluctuates. Improvements in the control circuit can be incorporated by continuous measurement of supply voltage in the design of the function characteristic. This, however, requires analog multipliers.

In this control circuit, there is a maximum delay of 20 msecs before the controller can act after necessary measurements whenever the load is changed. This is due to the fact that the firing pulses to T_2 are derived by complementing the gate pulses to T_1 and the function

characteristic is employed only to determine the triggering pulse for T_1 . The maximum delay can be reduced to 10 msecs if T_1 and T_2 are controlled independently by separate function characteristics. This requires duplication of control circuitry and the number of components is increased. In such a scheme, measurements are made in every half cycle and the required changes in the firing angle, α' , are implemented in the successive half cycles.

5.5 CONCLUSIONS

The experimental study of static reactive power compensator has shown that the load reactive power can be compensated and the power factor can be improved significantly over the expected range of load variation. By choosing proper values of the compensating capacitor and the controlled inductor, nearly unity power factor can be achieved over a wide range of load variation. These compensators can be installed by individual consumers for their appliances and by bulk power consumers they can be placed at the service entrance of large industrial centres. Significant savings may accure by their usage. The thyristor controlled reactor compensator provides fast response. With the control circuit developed here, there is a maximum delay of 20 msecs before the controller can act to compensate load reactive power from the instant the

load is charged. By a suitable modification of the control circuitry, the delay time can be reduced to 10 msecs. Such a fast response is not possible with other compensation schemes. This feature makes the static shunt compensator using thyristor phase-controlled reactor very much suitable for power factor improvement particularly in fast varying loads, such as, arc furnaces and rolling mill drives used in steel industries.

CHAPTER VI

CONCLUSIONS

6.1 SUMMARY

The investigations carried out in this thesis on the different converter configurations show that with a slight change in the triggering strategy of fully controlled converter, the power factor is improved substantially both in rectification and inversion operations. Further improvement in power factor may be obtained using ac pulse width modulation technique. But this involves forced commutation of the thyristors, thereby increasing the cost and complexity. Hence, the fully controlled converter with optional freewheel facility looks promising not only for traction locomotives but also for the control of other dc drives in industry. The study has revealed, depending upon the triggering angles, α , ϕ , and load circuit parameters, the fully controlled converter with half-controlled characteristics has four possible discontinuous current modes of operation in rectification while it operates in two discontinuous modes in inversion. The discontinuous current has many adverse effects. The operating diagrams obtained here are quite useful to determine the

possible modes of operation of the converter for a particular application and also to estimate the additional inductance necessary for continuous current operation.

The static reactive power compensators using thyristor phase-controlled reactors and fixed capacitors can efficiently change the power factor in industrial power systems to unity over a wide range of variation in the load reactive power from leading to lagging. They are very effective for fast varying loads owing to their extremely fast response. Economically and technically, they are superior to synchronous compensators. In the recent years they have found wide applications in the utility systems for fast reactive power control to achieve quality voltage regulation.

6.2 SUGGESTIONS FOR FURTHER RESEARCH

The improvement in different performances may be investigated by the series connection of two or more fully controlled converters with optional freewheeling. These performances may be compared with those obtained with the converter configurations studied in this thesis. Closed loop control of dc motor using the converter with optional freewheel may be investigated. Furthermore, the concept of optional freewheeling may be extended to three-phase fully controlled converter circuit and the improvement

in power factor may be studied.

There is also great scope for further work to be done on the static reactive power compensator. Analog multiplication and advanced digital techniques may be incorporated for the measurement of actual load reactive power. Additional feedback control as mentioned in section 4.3.2 may be introduced in the overall feedforward scheme.

Research is already in progress [22] to use the static reactive power compensator employing thyristor controlled reactor for voltage regulation in utility systems. The dynamic and transient responses of the static VAR compensator may be compared with those of a synchronous condenser for load changes and faults in the power system. The stability studies when static VAR compensators are employed may also be carried out. The switching transients on the transmission lines are likely to be reduced with the use of TCR type static VAR compensators. This aspect may also be a topic for further study. These studies can be undertaken on a digital computer or using ac transient network analyser.

LIST OF REFERENCES

(1) S.B. Dewan and A. Straughen ; Power Semiconductor Circuits ; Wiley - Interscience publication, John Wiley and Sons , New York , 1975.

(2) M. Ramamoorty ; An Introduction to Thyristors and Their Applications ; Affiliated East-West Press Pvt. Ltd. publication, New Delhi , 1977.

(3) B.R. Pelly ; Thyristor Phase-Controlled Converters and Cycloconverters ; Wiley-Interscience publication, John Wiley and Sons , New York , 1971.

(4) Electrical Transmission and Distribution Reference Book ; Westinghouse Electric Corporation publication , U.S.A. , 1964.

(5) H. Zander ; "Self-Commutated Rectifier to Improve Line Conditions," Proc. IEE , Vol. 120 , No. 9 , pp. 977-981 , 1973.

(6) W. Farrer and D.F. Andrew ; "Fully Controlled Regenerative Bridges with Half-Controlled Characteristics," ibid Vol. 125 , No. 2, pp. 109-112 , 1978.

(7) S.R. Doradla and P.C. Sen ; "Solid-State Series Motor Drive," IEEE Trans. Ind. Electron. Contr. Instrum. , IECI-22 , No.2 , pp. 164-171 , May 1975.

(8) P.C. Sen and S.R. Doradla ; "Symmetrical and Extinction Angle Control of Solid-State Series Motor Drive," ibid IECI -23, No. 1, Feb. 1976.

(9) K.A. Krishnamurthy ; G.K. Dubey and G.N. Revankar ; "Converter Control with Selective Reduction of Line Harmonics ," ibid Vol. 125 , No. 2 , pp. 141-145, 1978.

(10) P.C. Sen and S.R. Doradla ; "Evaluation of Control Schemes for Thyristor-Controlled DC Motors"," IEEE Trans. Ind. Electron. Contr. Instrum. , IECI - 25, No. 3 , pp. 247-255 , August 1978.

(11) T. Kataoka, K. Mizumachi and S. Miyairi ; " A Pulse-Width Controlled AC to DC converter to Improve Power Factor and Waveform of AC Line Current ," ISPCC-1977 Conference paper.

(12) V. Subbiah and S. Palanichamy ; "Investigations on Operation of Fully Controlled Thyristor Converters," Proc. IEE, Vol. 125 , No. 1 . pp. 58-59, December 1978.

(13) V. Subbiah and S. Palanichamy ; "Mode Identification and Minimum Inductance Estimation for Fully Controlled Thyristor Converters," IEEE Trans. Ind. Electron. Contr. Instrum. , IECI - 26 , No. 1, pp. 49-50 , Feb. 1979.

(14) G. Moltgen ; Line Commutated Thyristor Converters ; Pitman publishing, London, 1972.

(15) L.O. Barthod, H. Becker, J. Dalzell, et al , "Static Shunt Devices for Reactive Power Control," CIGRE Report 31-08 , 1974.

(16) K. Reichert, J. Kauferle and H. Glavitsch, "Controllable Reactor Compensator for More Extensive Utilisation of High Voltage Transmission System," CIGRE Report 31-04, 1974.

(17) H. Becker, et al , "Three-phase Shunt Reactors With Continuously Controlled Reactive Current," CIGRE Report 31-13, 1972.

(18) L. Gyugyi, R.A. Otto, T.H. Putman ; "Principles and Applications of Static Thyristor-Controlled Shunt Compensators," IEEE Trans. on PAS , Vol. 97, No. 5, pp. 1935-1945, Sept./Oct. 1978.

(19) J.G. Greame, G.E. Tobey and L.P. Huelsman; Operational Amplifiers Design and Applications; McGraw-Hill Kogakusha Ltd. publication, Copyright 1971 by Burr-Brown Research Corporation.

(20) John I. Smith ; Modern Operational Circuit Design ; Wiley-Interscience publication, John Wiley and Sons, New York, 1971.

(21) U. Tietze, Ch. Schenk ; Advanced Electronic Circuits; Springer-Verlag Berlin Heidelberg New York publication, 1978.

(22) R.L. Hauth, T. Humann and R.J. Newell ; "Application of a Static VAR System to Regulate System Voltage in Western Nebraska," IEEE Trans. on PAS, Vol. 97, No. 5, pp.1955-1964,Sept./Oct. 1978.

(23) A.K. Sawhney ; A Course in Electrical Machine Design ; Dhanpat Rai & Sons , Jullunder-Delhi publication , 1972 .

APPENDIX I

DESIGN OF REACTOR [23]

An inductor with an air gap is designed to be connected to the supply system as the thyristor controlled reactor (TCR) . The design details are given here.

Voltage rating, V = 250 v ac

Current rating, I = 2.5 Amp

Hence, $VA = 250X2.5 = 625\ VA$

Core

Corresponding to this VA, turns per volt,

$T_e = 2.0$

Flux in the core, $\emptyset_m = 1/(4.44\ f\ T_e)$

$= 1/(4.44X50X2)$ Wb

$= 2.23$ mWb

The maximum flux density, B_m in the core is assumed as $1\ Wb/m^2$.

$\therefore$ Net area of the core,

$A_i = (2.23X10^{-3}/1)\ m^2 = 22.3\ cm^2$

Assuming stacking factor to be 0.9, gross area

of the core, $A_c = 22.3/0.9 \simeq 25.0 \text{ cm}^2$

Taking a square cross-section for the central limb, width of the central limb,

$A = \sqrt{25.0} = 5.0 \text{ cm}$

Winding

Number of turns, $T = V \times T_e$

$= 250X2 = 500$

Taking a current density of 1.5 Amp/mm^2 for the winding, area of conductor required,

$a = 2.5/1.5 \simeq 1.67 \text{ mm}^2$

Diameter of bare conductor (round),

$d = \left[(4/\pi) \times 1.67\right]^{1/2} \simeq 1.46 \text{ mm}$

Referring to the table of available standard synthetic enamelled copper conductors, the nearest standard conductor has :

bare diameter , $d = 1.5$ mm

Diameter with medium covering, $d_1 = 1.605$ mm

$\therefore$ Area of conductor provided,

$a = (\pi/4) \times (1.5)^2 = 1.77 \text{ mm}^2$

Space factor, $S_f = 0.8 (d/d_1)^2$

$= 0.8 (1.5/1.605)^2 = 0.699$

Window area required, $A_w = 1.2\ T\ a/S_f$

$= 1.2X500X1.77/0.699\ mm^2$

$= 15.2\ cm^2$

Stampings

Referring to the table of available E - I stampings, stamping No.43 has the desired dimensions (see Fig. A1) as follows.

A = 2"

B = 6"

C = 5"

D = 1"

E = 1"

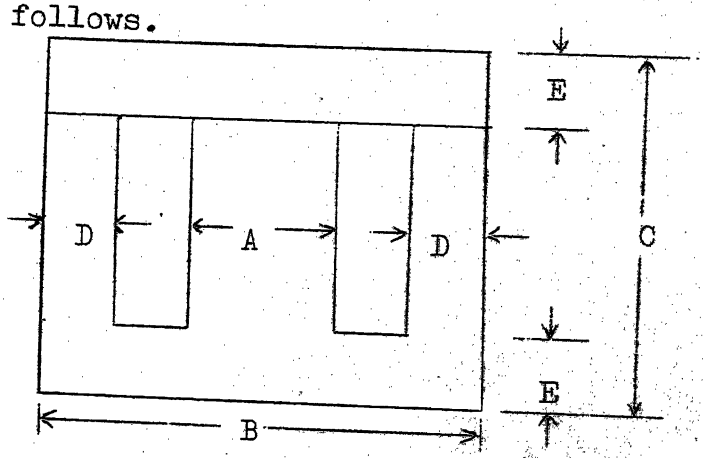

Fig. A1. Stamping Dimensions.

Width of the window,

$W_w = (B - A - 2D)/2 = 1"$

Height of the window, $H_w = C - 2E = 3"$

$\therefore$ Area of window provided, $A_w = 3X1\ inch^2 = 19.35\ cm^2$

Air-gap

From the B - H curve corresponding grade H10 stampings, mmf per metre at a flux density of 1 Wb/m^2 is

$at_i = 69\ AT/m$

Length of flux path in iron,

$l_i = 2\ (C - E) + A + D + W_w = 12'' \simeq 0.3$ m

Mmf per metre required for air-gap,

$at_g = 800000\ B_m/\sqrt{2} = 565000$ AT/m

Number of air-gaps in flux-path, $n_g = 2$

Therefore, impedance of inductor,

$$Z = T^2/\left[(at_i l_i + n_g at_g l_g)\ T_e\right]$$

Also,

$$Z = 250/2.5 = 100$$

Hence,

$$100 = \frac{500^2}{(69 \times 0.3 + 2 \times 565000 l_g) \times 2}$$

which gives

length of air-gap, $l_g = 1.1$ mm

Inductance, $L = Z/(2\pi f) = 100/(100\pi) = 0.318$ H